2018

Synthesis And Characterization Of Polydiene-Grafted Nanoparticles

Zaid Mohammed Abbas Alajeeli
University of South Carolina

SYNTHESIS AND CHARACTERIZATION OF POLYDIENE-GRAFTED NANOPARTICLES

by

Zaid Mohammed Abbas Alajeeli

Bachelor of Science
Al-Nahrain University, 2005

Master of Science
Al-Nahrain University, 2008

Submitted in Partial Fulfillment of the Requirements

For the Degree of Doctor of Philosophy in

Chemistry

College of Arts and Sciences

University of South Carolina

2018

Accepted by:

Brian Benicewicz, Major Professor

Chuanbing Tang, Committee Member

Thomas Vogt, Committee Member

Ehsan Jabbarzadeh, Committee Member

Cheryl L. Addy, Vice Provost and Dean of the Graduate School

DEDICATION

To the great homeland of Iraq, to my dad's soul and the one who changed me.

ACKNOWLEDGEMENTS

I would like to start with this quote by John Ruskin "A great thing can only be done by a great person; and they do it without effort". Many thanks to the greatest person in my PhD path, my advisor, Prof. Brian Benicewicz. For the last five years he was father, friend, leader and amazing teacher. Special thanks and gratitude to my committee member Prof Chuanbing Tang for his great personality, I always remember how many times he walked by my office to ask about me and my country safety situation, that means a lot to me. I would also thank my committee members Prof. Thomas Vogt, and Prof. Ehsan Jabbarzadeh for their encouragement, helpful advice, and honest criticism throughout my doctoral work.

I really like to express my gratitude to everyone I have worked with in the Benicewicz group, I had great time to learn from everyone. Since I arrived, no one called me Zaid because Dr. Tony Neely, Dr. Anand Viswanath, Dr Michel Bell and Dr. Mohammad Mohammadkhani told everyone my name is "Shiekh", thanks for this name. Also, I would love to thank Dr. Kayley Hayat, Dr. Yang Zheng, Dr. Yucheng Huang, Dr. Julia Pribyl, Laura Murdock, Maan Al Ali, Andrew Pingitore, Susan Hipp, Warren Steckle, Dr. Quoqing Qian, Dr. Alex

Gulledge, Dr. Amin Daryaei, Dr. Fei Huang, Dr. Lihui Wang, Karl Golian, Kayla Lantz, Dr. Amrita Sarkar, Md. Anisur Rahman, Meghan Lamm, and Dr. Mitra Ganewatta. A great thanks to our collaborators in Stefik group, Dr. Morgan Stefik and Zack Marsh for their giant efforts in this work.

What makes the Benicewicz group great is collaboration with great people in particular the research groups of Prof. Sanat Kumar at Columbia University and Prof. Linda Schadler at Rensselaer Polytechnic Institute. Therefore, I would thank Andrew Jimenez, Connor Bilchak, Mayank Jhalaria, Marissa Giovino, and Xin Ning. A great acknowledgement to my great friend Massimo Tawfilas at University of Milano-Bicocca for his amazing collaboration in most of my work.

I would love to thank two American families who helped me all the way through my PhD. The Gordners' and Batemans' for their kindness, help and support. Especially, Trey Gordner and Stephen Bateman for every moment we spent together.

Finally, I have to thank my family, without you all I will not be here. Your love, support, encouragement and emotion were everyday with me. Our father should be proud of every one of us.

ABSTRACT

This dissertation presents the design, synthesis, and characterization of polydiene grafted nanoparticles as a way to tailor nanocomposite interfaces and properties via interface design. The polymerization of dienes was done via reversible addition fragmentation chain transfer (RAFT) polymerization. The grafting of polymer chains on the surface of silica nanoparticles can be controlled through the molecular design of the RAFT agents attached to the nanoparticles surface. The properties of the nanocomposites largely depended on the interface between the particles and the polymer matrix.

In the first part of this work, the polymerization of diene monomers was done on 15 nm diameter silica nanoparticles. SI-RAFT polymerization of isoprene and chloroprene on silica NPs was studied in detail and revealed living character for all these polymerizations. Composites of matrix-free grafted NPs were prepared and analyzed to find the effects of chain length on the dispersibility and organization of particles throughout the matrix. A wide range of grafted polydiene brush molecular weights and graft densities were polymerized on SiO_2 NPs to investigate mechanical properties of composites. Multiple

characterizations such as DSC, WAXS, and SAXS were applied to study the interaction of the polydiene brushes on the inorganic fillers. The surface modified particles with diene polymer brushes were capable of creating a well-dispersed state that resulted in improved mechanical properties of matrix-free composites. High loadings of inorganic particles were attained while avoiding particle aggregation and the improvement in mechanical properties correlated with the loading of the core silica loading level.

In the second part, both free and SI-RAFT polymerization of 2,3-dimethyl butadiene (DMB) was studied. The kinetic study of DMB monomer was studied with free and SI-RAFT polymerization and compared to other diene monomers. The SI-RAFT polymerization was done with two different graft densities to represent both low and high-density graft regimes. The dispersion of particles was investigated and showed that for both low and high graft density an acceptable level of dispersion was observed throughout the final composite which was confirmed with TEM and SAXS studies. The resulting polydimethyl butadiene (PDMB) grafted silica nanoparticles were directly crosslinked to obtain matrix-free nanocomposites that showed good nanoparticle dispersion and much improved mechanical properties compared with the unfilled crosslinked matrix.

The third part of this study examined the reversible addition-fragmentation chain transfer polymerization of chloroprene on the surface of 15 nm diameter silica nanoparticles to obtain polychloroprene-grafted-silica nanoparticles which were dispersed in an industrial matrix of polychloroprene to obtain PCP nanocomposites with different silica core loadings. Two graft densities and a wide range of molecular weights were studied to examine the effects of these key parameters on the cured composite properties. The dispersion of the grafted nanoparticles in a commercial PCP matrix were excellent for both high and low graft densities. The mechanical properties were enhanced for all composites compared to unfilled cured matrix and proportionally improved with increasing silica loading and grafted polymer chain length. Stress-strain properties were most improved in composites using nanoparticles with low graft density and high molecular weight grafted chains.

Finally, polyisoprene (PIP) grafted nanoparticles were prepared and studied for use in rubbery nanocomposites. Scale up approaches were successful and detailed mechanical property studies were conducted to evaluate the advantages of these new polymer grafted nanoparticle based rubbery composites. These trans-PIP grafted particles were dispersed in commercial cis-PIP and in-house prepared trans-PIP matrices to obtain PIP nanocomposites with different silica loadings and a single graft density. Miscibility and dispersion of

particles in both matrices were also studied to examine the compatibility of the different isomers. The trans-PIP-g-NPs were relatively well-dispersed in the cis-PIP matrix where the molecular weights of the grafted and matrix polymers were nearly the same (35 kDa-grafted and 40 kDa matrix). However, the mechanical properties of the trans-PIP-g-NPs in the trans-PIP matrix showed better mechanical properties, likely due to the polymer compatibility even though the molecular weights of the grafted and matrix chains (35 kDa-grafted and 52 kDa matrix) were mis-matched and the particles were not dispersed as well in the matrix.

TABLE OF CONTENTS

LIST OF TABLES

LIST OF FIGURES

LIST OF SCHEMES

LIST OF ABBREVIATIONS

AIBN .....Azobisisobutyronitrile

AIBN .....Azobisisobutyronitrile

ATRP ..... Atom Transfer Radical Polymerization

CDTPA.....4-Cyano-4-[(dodecylsulfanylthiocarbonyl) sulfanyl]pentanoic acid

CRP..... Controlled Radical Polymerization

DCP ..... Dicumyl Peroxide

DLS..... Dynamic Light Scattering

DMA..... Dynamic mechanical analysis

DMAP 4-Dimethylaminopyridine

DoPAT ..... 2-(((dodecylthio)carbonothioyl)thio)propanoic acid

DSC .....Differential scanning calorimetry

dTBP..... Di-tert-butyl peroxide

EDS..... Energy-dispersive X-ray spectroscopy

GPC ..... Gel permeation chromatography

HF .....Hydrofluoric acid

MDSS ..... 2-methyl-2[(dodecylsulfanylthiocarbonyl) sulfanyl] propanoic acid

NMP .....Nitroxide-Mediated Polymerization

NMR..... Nuclear Magnetic Resonance

NP..... Nanoparticle

PCP ..... Polychloroprene

PDI ..... Polydispersity Index

PDMB ..... Polydimethylbutadiene

PIP ..... Polyisoprene

RAFT ..... Reversible Addition-Fragmentation Chain Transfer Polymerization

SAXS ..... Small-Angle X-ray Scattering

SI-RAFT ..... Surface-Initiated RAFT

TEM ..... Transmission electron microscopy

Tg ..... Glass Transition Temperature

TGA ..... Thermogravimetric Analysis

THF ..... Tetrahydrofuran

UV-vis ..... Ultraviolet visible spectroscopy

CHAPTER 1

INTRODUCTION

1.1 Introduction

Over the last 30 years processes of controlled radical polymerization (CRP) have been improved and modified to meet the ambitions of research groups. Better control is gained with these kinds of polymerizations due to the ability to control free radical processes.[1–3] CRP techniques allow precise control over polymer molecular weight, polydispersity, molecular architecture, and end group chemistry. The most studied CRP techniques are nitroxide-mediated polymerization (NMP),[4] atom transfer radical polymerization (ATRP),[5] and reversible addition-fragmentation chain transfer polymerization (RAFT) (Figure 1.1).[6,7] ATRP requires a metal catalyst, and NMP requires a high reaction temperature. RAFT is advantageous over the previously mentioned techniques because it can work at low temperatures, without a metal catalyst, and is able to polymerize a wide range of monomers.

For a long time, it has been a challenge to synthesize polymers with a narrow polydispersity index (PDI) through free radical polymerization because of chain transfer reactions and radical termination. Reversible addition-fragmentation chain polymerization (RAFT) is one of the most successful processes in CRP to obtain polymers with low PDIs (<1.1). The RAFT polymerization process was invented in 1998 by a group of researchers in

Melbourne, Australia at the Commonwealth Scientific and Industrial Research Organization (CSIRO). Compared to other CRPs, RAFT is characterized by its simplicity, compatibility with many monomers, without the use of metal catalyst or high temperature.[8] With RAFT polymerization the key component is the chain transfer agent (CTA), e.g., dithioester or trithiocarbonate (Figure 1.2). The CTA's utility comes from participating in equilibrium between active and dormant states. The CTA commonly referred to as a RAFT agent contains Z and R groups that are responsible for controlling the equilibrium of the polymerization.[7]

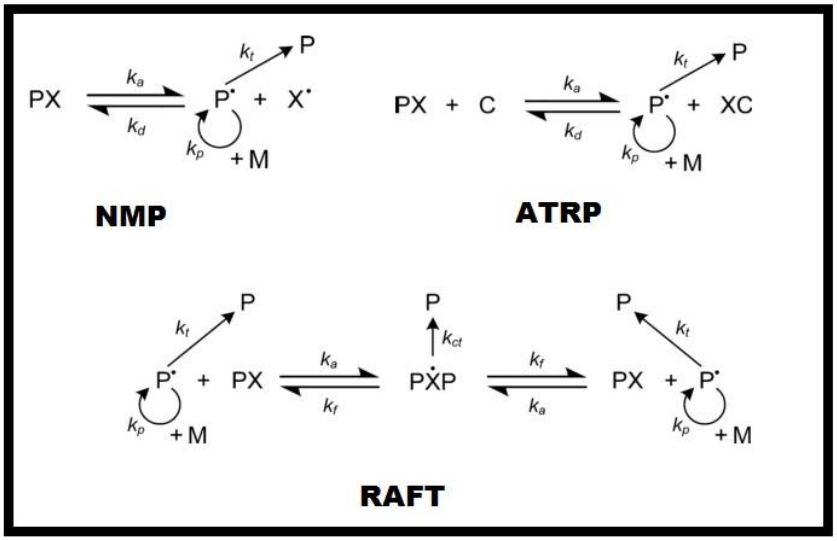

Figure 1.1 Mechanisms of CRPs.[1]

The RAFT general mechanism is shown for dithioester CTA in Figure 1.3. Initiation starts with the homolysis (**1**) of a free radical initiator via traditional initiation methods. The initiator reacts with monomer first (**2**), producing the propagating radical species Pn•. Pn• then reacts with the RAFT CTA during

chain transfer (**3**), causing fragmentation of the dithioester, forming an intermediate and subsequently the new radical species R•(**4**). R• is now a radical species that will re-initiate free monomer and produce the propagating species Pm• (**5**). Chain equilibrium is reached between Pn•, Pm• (**6**) and the intermediate due to the addition of Pm• to a dithioester and subsequent fragmentation. The RAFT CTA remains active at the chain end, allowing for further polymerization as more monomer is added to the solution to create homo or block copolymers and other advanced polymer architectures.[9–15]

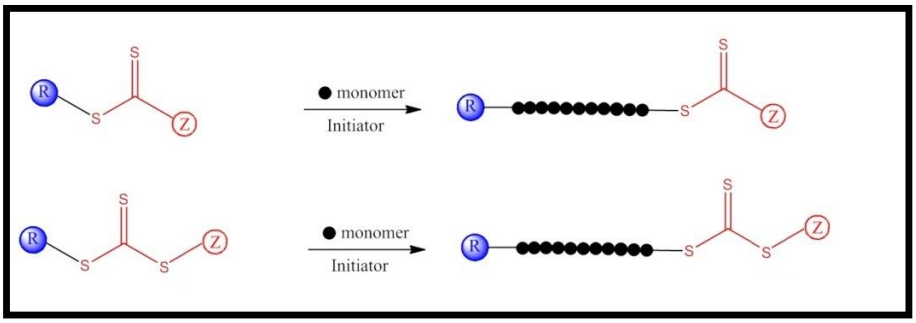

Figure 1.2 Chain Transfer Agents (CTA) dithioester and trithiocarbonate.

The ratio of RAFT agent to initiator in the polymerization has to be high to avoid having a high number of active species which leads to termination between active radical species.[16] A wide range of RAFT agents has been synthesized to fulfill the requirement of different monomer radical stability. The Z and R groups of the RAFT agent are responsible for controlling the equilibrium and the rate of monomer addition to the propagating radical species CTA, and also the rate of CTA fragmentation. The Z group controls the reactivity of CTA

by stabilizing the radical species. The R group has to be an excellent homolytic leaving group with respect to Pn•.[16]

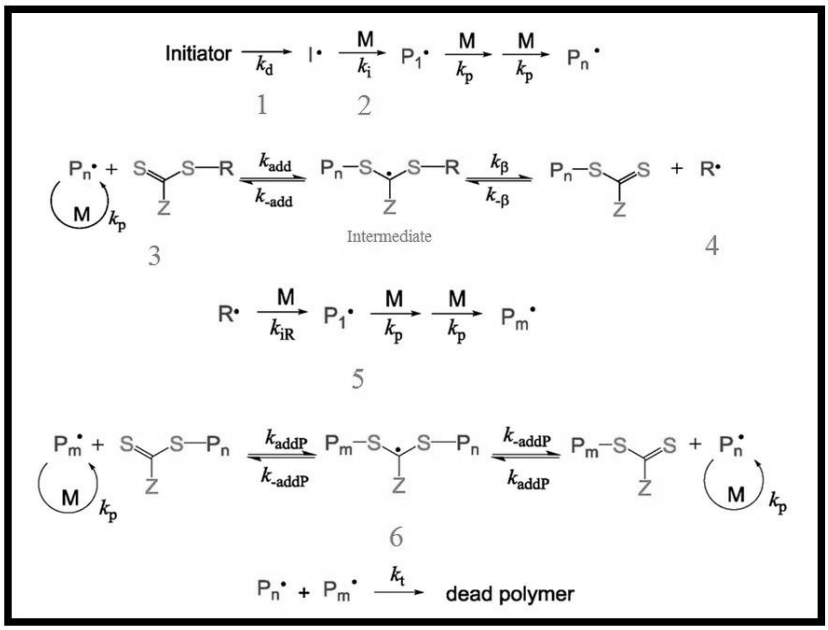

Figure 1.3 Mechanism of RAFT polymerization.[14,15]

1.2. Grafted Surfaces

Polymer grafted nanoparticles have been of interest for many research groups because of their wide variety of applications in surface coatings, separation membranes, insulation systems, drug delivery, organic light-emitting devices, etc. Predominantly bare nanoparticles do not have favorable interactions with the organic medium because of the tendency of agglomeration which is caused by surface tension between nanoparticles and the organic medium (Figure 1.4). Therefore, surface modification with polymer chains can enhance particle dispersion in different matrices. RAFT polymerization is one of the

processes that is used to attach well-defined polymer chains to a substrate surface.[17–24]

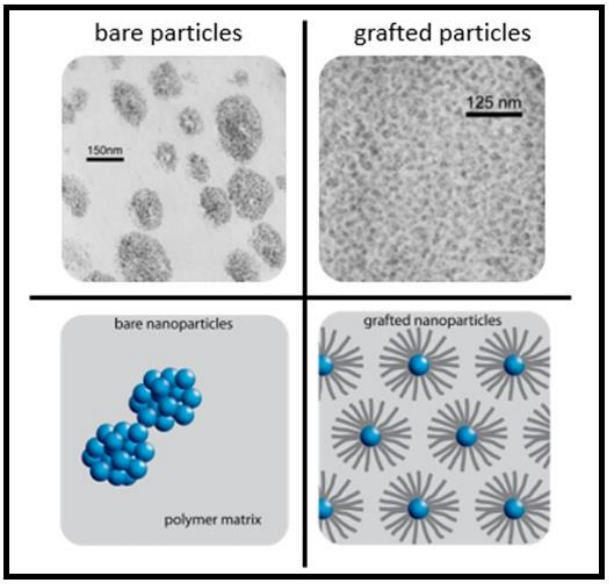

Figure 1.4 Agglomeration of Non-grafted nanoparticles.[25]

Surface modification can be achieved through attachment of polymer chains to a substrate surface through covalent and non-covalent bonds. Non-covalent attachment is called physisorption; covalent attachment is a stronger attachment, so it is more favorable for nanocomposite applications.[26] Covalent attachment uses one of two ways to graft polymers to a surface. "Grafting-to" attaches already prepared polymer chains to surfaces using active sites on those chain ends. "Grafting-from" propagates polymerization from a substrate surface.[21] Grafting-to cannot accomplish high graft density substrates because of the steric interactions that arise from bulky free polymer migrating to an already grafted surface. Grafting-from attaches an initiator or RAFT agent to the surface

of the substrate. Subsequently, the monomer in solution is initiated, and the polymer is grown from the surface.[8] The grafting-from technique results in particles with higher graft density because steric interactions are overcome (Figure 1.5).

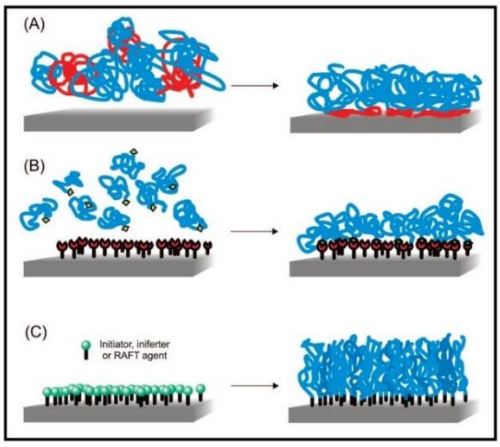

Figure 1.5 A) physisorption, B) grafting-to approach, C) grafting-from approach.[21]

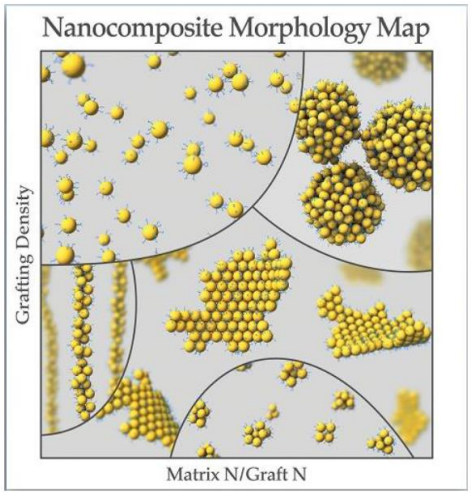

Figure 1.6 Nanocomposite morphology map showing the different nanoparticle dispersion states possible with a variation in graft density (y-axis) and the ratio of matrix chain length to grafted chain length (x-axis). N is defined as the number of repeat units in the polymer chain.[31]

1.3. Polymer Nanocomposite

1.3.1 Nanocomposite

Polymer nanocomposites are used by addition of nanoparticles to polymers and results in materials with improvements in different properties such as physical, chemical, biological, optical, rheological, electrical, thermal, and mechanical.[12,27–30] Physical properties can be affected by nanoscale fillers and change properties and behavior for the entire matrix which provides opportunities in different fields in industry. As mentioned earlier an important aspect of using grafted NPs is to disperse them in a matrix for better properties and there are several ways to disperse them, and the most important way to achieve this is by grafting them with polymer chains that can entangle and be miscible with the matrix and avoid agglomeration.[27] The interface between the matrix and nanoparticles polymer chains depends primarily on the brush chain length and chain density. Even though it is known the high graft density particles are well-dispersed in polymer matrices, in higher grafted chain length/matrix chain length ratios, particles with lower densities could also be miscible. Overall, the miscibility of grafted chains with the matrix chains has been a key challenge for making well-dispersed nanocomposites. Figure 1.6 shows the filler morphologies obtained by Kumar et al.[31] Evenly dispersed

particles were obtained with sufficient polymer coverage. Different polymer chemistries have been carried out on filler surfaces though most polymeric species tend to be derived from chain growth monomers.

1.3.2 Nanocomposites via RAFT polymerization

One way of preparing polymer functionalized nanoparticles is by grafting from the surface of nanomaterials through surface-initiated RAFT polymerization. The grafting with this method could achieve higher graft density and better control of obtaining specific graft densities. The first grafting using the SI- RAFT technique was made by Benicewicz et al. by adding an aminosilane coupling reagent followed by an activated RAFT agent to silica nanoparticle surfaces.[32] Figure 1.7 illustrates the functionalization of nanoparticles by using an activated RAFT agent. Activated RAFT agents contain a modified carboxylic acid that possesses excellent leaving group chemistry. The process proved to be a versatile method for surface modification of silica nanoparticles with effective graft densities of 0.01 – 0.7 ch/nm^2 being achieved. One advantage of SI- RAFT over other types of surface-initiated controlled radical polymerization is that the graft density could be determined prior to polymerization by quantitively measuring the characteristic UV-vis absorption of the RAFT-grafted nanoparticles. The versatility of RAFT has allowed for nanocomposites to be

synthesized for many applications including hybrid materials, optical, electrical, self-healing, and drug delivery.[33–42]

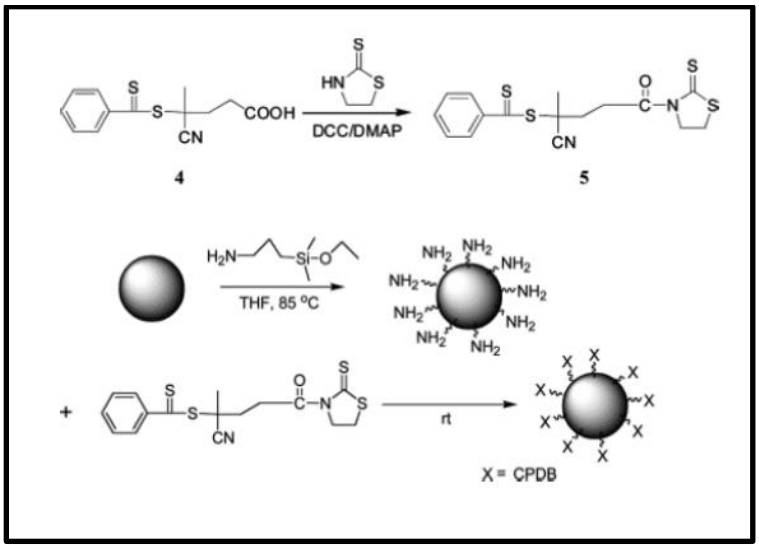

Figure 1.7 Synthesis and attachment of the activated RAFT agent to SiO_2 nanoparticle.[32]

1.4. Polydienes

1.4.1 Polydiene Composites

The term polydiene refers to a general class of polymer materials that are prepared from a 1,3-butadeine monomer core structure. Various substituents on this core structure lead to variety of interesting monomers. Polydienes are attractive materials as valuable elastomers, and its molecular chain contains latent polyvalent functionality contained in their double-bond-rich composition which exhibits interesting physical properties, e.g., low glass transitions (Tg), low degradability, excellent flexibility and high mechanical strength.[42–47] However,

the application of polydienes are limited because of degradation and incompatibility of the rubber with other materials. Thus, polydienes have to be mixed with crosslinkers, fillers and other polymers to overcome the limitations, for example, double bonds in polydiene molecules are used as a functionality for crosslinking. These processes lead to improvements in several properties of rubber composites and to extend the usage of polydienes in many fields such as composites and blends.[48]

Polymer blending has been studied extensively over the past decades in order to achieve a set of desired properties and high performances for specific applications. Inorganic fillers that are used in thermoplastic and rubber industries are important to improve modulus, tensile strength, tear resistance, abrasion resistance and dynamic mechanical properties.[44,49–53] Recently, developments in polydiene composites with improved characteristics are attracting industrial attention, as these composites comprise most of the rubber industry. Rubber composites typically contain a combination of inorganic fillers like carbon black or silica and a flexible polymer to form a flexible rubbery composite. This provides unique materials which exhibit high durability, low degradability and good flexibility. Among different fillers, silica particles have been extensively employed as a filler as they can produce large improvements in composite films in addition to attaining reasonable particle dispersions in an

organic matrix. Meanwhile, the use of a filler such as carbon black can improve toughness and durability.[54]

1.4.2 Polydiene Nanocomposites

Addition of filler into polymeric matrix and blending of the components is a critical aspect to obtaining dispersed particles that result in properties which cannot be achieved from the individual polymer components.[54] Therefore, many studies have been done to investigate the modification of the inorganic fillers such as inorganic filler treatments or polymer grafting.[32,39,56–59] Rubber nanocomposites have already been synthesized through polymer-grafted particles due to the easy attachment and accurate control over the polymer chain attachments. Thus, building on previous work which demonstrated significant improvements for thermoplastic polymers, surface-initiated reversible addition fragmentation chain transfer radical polymerization (SI-RAFT) was proposed to modify silica nanoparticles with butadiene derivative polymers for rubber applications.[8,19,60–62] This approach is designed to corporate specific chemistry to the nanoparticles filler surface which is expected to alter the fundamental interactions between the nanofiller and the matrix and lead to important improvements in the nanocomposite properties. The basic outline for this approach is shown in Figure 1.8.

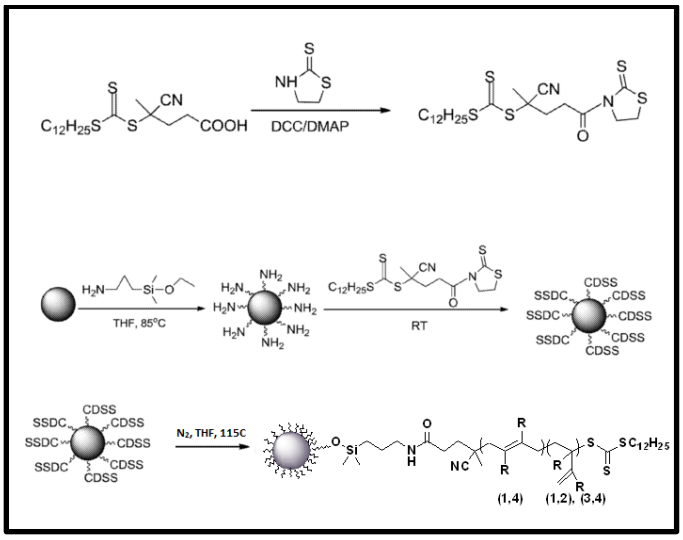

Figure 1.8 Synthesis and attachment of activated RAFT agent to SiO_2 nanoparticle.[61]

1.5 Dissertation Outline

This dissertation focuses on the synthesis, characterization, design and development of polydiene nanocomposite materials and the enhancements of properties afforded by them. To control the interface between the particles and the polymer matrix reversible addition fragmentation chain transfer (RAFT) polymerization was used for the grafting of polymer chains to the surface of silica nanoparticles by attaching the RAFT agents covalently to the inorganic filler. Surface modification was studied with the aim of understanding the structure-property relationships of polymer grafted nanoparticles in nanocomposites. The versatility of this design was demonstrated as it was applied to several different monomers.

Chapter 2 focuses on the SI-RAFT polymerization of isoprene and chloroprene on silica NPs. The kinetics of the free RAFT and SI-RAFT polymerizations were studied. Composites of PIP-g-SiO_2 and PIP-g-SiO_2 NPs were prepared and analyzed to examine the effects of grafted chains on the dispersibility of particles throughout the matrix-free composites. The effects of PIP and PCP brush molecular weight and chain density on the dispersion of silica particles was investigated. The interaction and dispersion states of grafted particles in matrix-free composites was also studied using TEM and SAXS.

Chapter 3 reports on the investigation of new a diene monomer i.e., 2,3-dimethyl butadiene (DMB). To best of our knowledge, there is no report on polymerization of this monomer via RAFT polymerization or nanocomposites made with this polymer. The kinetic studies of DMB polymerization mediated by silica anchored RAFT agent at different graft densities were investigated and compared to the polymerization mediated by free RAFT agent. Comparisons were made to the polymerization of other related dienes. Mechanical properties were investigated for crosslinked samples to study the effect of grafted nanoparticles on the final composite properties. TEM and SAXS were used to investigate the dispersion of silica NPs in the nanocomposite.

Chapter 4 focuses on the reinforcement of industrial PCP by dispersing the grafted PCP nanoparticles made via SI-RAFT polymerization. Two graft densities were used and with a range of grafted molecular weights. Mechanical properties were studied through tensile stress-strain, dynamic mechanical analysis, and strain sweep amplitude DMA to investigate the entanglement of grafted polymer with industrial PCP matrix. The degree of swelling and crosslink density was also studied to compare it to untreated composites. The dispersity of particles and the effect of grafted polymer chain length on the dispersion and interaction with the matrix was investigated.

Finally, Chapter 5 entails a detailed study of grafted nanoparticle dispersion, particularly the dispersion of grafted PIP nanoparticles in two different matrices (cis and trans variation), and its influence on dispersion and properties. One chain density and molecular weight was used with different silica loadings in the matrix. SAXS and TEM studies clearly showed that dispersion of nanoparticles was affected by the silica loading and miscibility of the grafted polymer with the matrix polymer. The effect of these variables was shown in mechanical properties.

Chapter 6 summarizes the conclusions from this work and suggests some directions for future work.

1.6 References

(1) Ilgach, D. M.; Meleshko, T. K.; Yakimansky, A. V. *Polym. Sci. Ser. C* **2015**, *57* (1), 3–19.

(2) Vazaios, A.; Lohse, D. J.; Hadjichristidis, N. *Macromolecules* **2005**, *38* (13), 5468–5474.

(3) Ishizone, T.; Han, S.; Okuyama, S.; Nakahama, S. *Macromolecules* **2003**, *36* (1), 42–49.

(4) Hawker, C. J.; Bosman, A. W.; Harth, E. *Chem. Rev.* **2001**, *101* (12), 3661–3688.

(5) Wang, J. S.; Matyjaszewski, K. *J. Am. Chem. Soc.* **1995**, *117* (20), 5614–5615.

(6) Moad, G.; Rizzardo, E.; Thang, S. H. *Aust. J. Chem.* **2005**, *58* (6), 379–410.

(7) Chiefari, J.; Chong, Y. K.; Ercole, F.; Krstina, J.; Jeffery, J.; Le, T. P. T.; Mayadunne, R. T. A.; Meijs, G. F.; Moad, C. L.; Moad, G.; Rizzardo, E.; Thang, S. H. *Macromolecules* **1998**, *31* (16), 5559–5562.

(8) Li, C.; Benicewicz, B. C. *Macromolecules* **2005**, *38* (14), 5929–5936.

(9) Keddie, D. J.; Moad, G.; Rizzardo, E.; Thang, S. H. *Macromolecules* **2012**, *45* (13), 5321–5342.

(10) Harvison, M. A.; Roth, P. J.; Davis, T. P.; Lowe, A. B. *Aust. J. Chem*. **2011**, *64* (8), 992–1006.

(11) Moad, G.; Rizzardo, E.; Thang, S. H. *Polym. Int*. **2011**, *60* (1), 9–25.

(12) Gregory, A.; Stenzel, M. H. *Prog. Polym. Sci*. **2012**, *37* (1), 38–105.

(13) Roth, P. J.; Boyer, C.; Lowe, A. B.; Davis, T. P. *Macromol. Rapid Commun*. **2011**, *32* (15), 1123–1143.

(14) Moad, G.; Chong, Y. K.; Mulder, R.; Rizzardo, E.; Thang, S. H. *ACS Symp. Ser*. **2009**, *1024*, 3–18.

(15) Moad, G. *In ACS Symposium Series 1187*; **2015**; pp 211–246.

(16) Moad, G.; Rizzardo, E.; Thang, S. H. *Aust. J. Chem*. **2006**, *59* (10), 669–692.

(17) Zhao, Y.; Perrier, S. *Macromolecules* **2007**, *40* (25), 9116–9124.

(18) Wang, Y. Y.; Hsieh, T. E.; Chen, I. C.; Chen, C. *H. IEEE Trans. Adv. Packag*. **2007**, *30* (3), 421–427.

(19) Moll, J. F.; Akcora, P.; Rungta, A.; Gong, S.; Colby, R. H.; Benicewicz, B. C.; Kumar, S. K. *Macromolecules* **2011**, *44* (18), 7473–7477.

(20) Zou, H.; Wu, S.; Shen, *J. Chem. Rev*. **2008**, *108* (9), 3893–3957.

(21) Barbey, R.; Lavanant, L.; Paripovic, D.; Schuwer, N.; Sugnaux, C.; Tugulu, S.; Klok, H.-*A. Chem. Rev.* **2009**, *109*, 5437–5527.

(22) Liu, C. H.; Pan, C. Y. *Polymer (Guildf).* **2007**, *48* (13), 3679–3685.

(23) Wang, L.; Chen, Y. P.; Miller, K. P.; Cash, B. M.; Jones, S.; Glenn, S.; Benicewicz, B. C.; Decho, A. W. *Chem. Commun*. **2014**, *50* (81), 12030–12033.

(24) Li, C.; Han, J.; Ryu, C. Y.; Benicewicz, B. C. *Macromolecules* **2006**, *39* (9), 3175–3183.

(25) Benicewicz, B.; Kumar, S.; Schadler, L. et al. *J. Polym. Sci., Part B: Polym. Phys*. **2006**, *44*, 2944–2950

(26) Gläsel, H.-J.; Bauer, F.; Ernst, H. *Macromol. Chem. Phys*. **2000**, *201* (18), 2765–2770.

(27) Schadler, L. S.; Kumar, S. K.; Benicewicz, B. C.; Lewis, S. L.; Harton, S. E. *MRS Bull*. **2007**, *32* (4), 335–340.

(28) Li, Y.; Tao, P.; Viswanath, A.; Benicewicz, B. C.; Schadler, L. S. *Langmuir* **2013**, *29* (4), 1211–1220.

(29) Krishnamoorti, R. *MRS Bull*. **2007**, *32* (4), 341–347.

(30) Winey, K. I.; Vaia, R. A. *MRS Bull*. **2007**, *32* (04), 314–322.

(31) Kumar, S. K.; Jouault, N.; Benicewicz, B.; Neely, T. *Macromolecules* **2013**, *46* (9), 3199–3214.

(32) Li, C.; Han, J.; Ryu, C. Y.; Benicewicz, B. C. *Macromolecules* **2006**, *39*, 3175–3183.

(33) Viswanath, A.; Shen, Y.; Green, A. N.; Tan, R.; Greytak, A. B.; Benicewicz, B. C. *Macromolecules,* **2014**, *47*, 8137–8144.

(34) Zheng, Y.; Wang, L.; Lu, L.; Wang, Q.; Benicewicz, B. C. *ACS Omega* **2017**, *2* (7), 3399–3405.

(35) Zheng, Y.; Huang, Y.; Abbas, Z. M.; Benicewicz, B. C. *Polym. Chem*. **2017**, 370–374.

(36) Khani, M. M.; Abbas, Z. M.; Benicewicz, B. C. *J. Polym. Sci. Part A Polym. Chem.* **2017**, 1–9.

(37) Zheng, Y.; Abbas, Z. M.; Sarkar, A.; Marsh, Z.; Stefik, M.; Benicewicz, B. C. *Polymer (Guildf)*. **2018**, *135*, 193–199.

(38) Huang, Y.; Zheng, Y.; Sarkar, A.; Xu, Y.; Stefik, M.; Benicewicz, B. C. *Macromolecules* **2017**, *50* (12), 4742–4753.

(39) Tao, P.; Viswanath, A.; Li, Y.; Siegel, R. W.; Benicewicz, B. C.; Schadler, L. S. *Polym. (United Kingdom)* **2013**, *54* (6), 1639–1646.

(40) Bell, M.; Krentz, T.; Nelson, J. K.; Schadler, L.; Wu, K.; Breneman, C.; Zhao, S.; Hillborg, H.; Benicewicz, B. *J. Colloid Interface Sci.* **2017**, *495*, 130–139.

(41) Audouin, F.; Heise, A. *Eur. Polym. J.* **2013**, *49* (5), 1073–1079.

(42) Saunders, K. J. *Organic Polymer Chemistry; Springer*: Dordrecht, **1973**.

(43) Brosse, J. C.; Campistron, I.; Derouet, D.; Hamdaoui, A. E. L.; Houdayer, S.; Reyx, D. *J. Appl. Polym. Sci.* **2000**, *78*, 1461–1477.

(44) Kumnuantip, C.; Sombatsompop, *N. Mater. Lett*. **2003**, *57* (21), 3167–3174.

(45) Salaeh, S. Processing Of Natural Rubber Composites And Blends : Relation Between Structure And Properties, Prince Of Songkla University And University Claude Bernard Lyon, PhD thesis, **2014**.

(46) Hosler, D.; Burkett, S. L.; Tarkanian, M. *J. Science*, **1999**, *284* (5422), 1988–1991.

(47) Heinrich, G.; Kluppel, M.; Vilgis, T. A. *Curr. Opin. Solid State Mater. Sci.* **2002**, *6*, 195–203.

(48) Moaddab, A.; Kalaee, M.; Mazinani, S.; Aghajani, A.; Rajab, M. M. *Rubber Chem. Technol*. **2015**, *88* (1), 53–64.

(49) Mutar, M. A. *J. Al-Nahrain Univ*. **2010**, *13* (3), 1–6.

(50) Muter, M. A.; Mugar, Q. K. *J. Nat. Sci. Res*. **2014**, *4* (24), 60–73.

(51) Datta, R. N. *Rubber Curing Systems*; Rapra Technology Limited: Shropshire, **2002**; *Vol. 12.*

(52) *Handbook of Composites from Renewable Materials Volume 6: Polymeric Composites*; Vijay Kumar Thakur, Thakur, M. K., Kessler, M. R., Eds.; John Wiley & Sons Inc, **2017**.

(53) Dannenberg, E. M. *Rubber Chem. Technol*. **1986**, *59* (3), 512–524.

(54) Roland C. M. *Ref. Modul. Mater. Sci. Mater. Eng*. **2016**, 2475–2480.

(55) Kapgate, B. P.; Das, C.; Basu, D.; Das, A.; Heinrich, G. *J. Elastomers Plast*. **2015**, *47* (3), 248–261.

(56) Bansod, N. D.; Kapgate, B. P.; Das, C.; Basu, D.; Debnath, S. C.; Roy, K.; Wiessner, S. *RSC Adv*. **2015**, *5* (66), 53559–53568.

(57) Kapgate, B. P.; Das, C.; Das, A.; Basu, D.; Wiessner, S.; Reuter, U.; Heinrich, G. *J. Appl. Polym. Sci*. **2016**, *133* (30), 1–10.

(58) Kumar, S. K.; Benicewicz, B. C.; Vaia, R. A.; Winey, K. I. *Macromolecules* **2017**, *50* (3), 714–731.

(59) Moad, G. *Polym. Int.* **2017**, *66* (1), 26–41.

(60) Benicewicz, B.; Wang, L.; Mohammadkhani, M. Butadiene-derived polymers grafted nanoparticles and their methods of manufacture and use, U.S. Patent 9, 249, 250, February 6, **2016**.

(61) Akcora, P.; Liu, H.; Kumar, S. K.; Moll, J.; Li, Y.; Benicewicz, B. C.; Schadler, L. S.; Acehan, D.; Panagiotopoulos, A. Z.; Pryamitsyn, V.; Ganesan, V.; Ilavsky, J.; Thiyagarajan, P.; Colby, R. H.; Douglas, *J. F. Nat. Mater*. **2009**, *8* (4), 354–359.

CHAPTER 2

PREPARATION OF DIENE POLYMERS GRAFTED ON SILICA NANOPARTICLES AND THEIR MATRIX-FREE NANOCOMPOSITES

2.1 Abstract

The grafting of polydienes to the surface of silica nanoparticles has been studied and developed by the RAFT polymerization process. This process has been shown to be applicable for preparing grafted polydienes to the inorganic fillers that are important for the investigation of surface interactions between fillers and rubber materials. The resulting polydiene-grafted silica nanoparticles were directly crosslinked to obtain matrix-free nanocomposites which showed acceptable nanoparticle dispersion and good mechanical properties compared with unfilled crosslinked polydiene rubbers. The dispersion of particles was investigated by transmission electron microscopy (TEM), and small-angle X-ray scattering (SAXS).

2.2 Introduction

The grafting of polymers to inorganic surfaces is one of the most interesting topics due to their applications in nanocomposites, sensors, coatings, optoelectronics, and bio applications.[1-4] Surface-initiated polymerization using the RAFT technique has proven to be a powerful method for the preparation of polymer-grafted particles due to the easy attachment and precise control over the grafting densities of RAFT agents as well as the controlled molecular weights and narrow molecular weight distribution of the grafted polymer chains.[5,6]

Many types of research have been done on polydienes and their properties. The molecular chain consists of latent polyvalent functionality contained in their double-bond-rich composition which exhibits interesting physical properties, low glass transitions (Tg), low degradability, excellent flexibility and high mechanical strength.[7-10] The applications of polydienes are limited due to degradation and phase separation between rubber and other materials. For this reason, polydienes have to be mixed with crosslinkers, fillers and other polymers to overcome this problem, for example, double bonds in polydiene molecules are used as a site for crosslinking. These processes lead to improved properties of rubber composites and extend the usage of polydienes in many fields such as composites and blends.[11,12]

Polyisoprene (PIP) and Polychloroprene (PCP) are well-known polydienes with good material characteristics that are used in industry. Polyisoprene is one of the most important classes of rubber materials due to its value in the tire industry.[13-15] Polymerization of isoprene has been done by anionic, cationic, and radical polymerizations.[16-21] Anionic polymerization is the most widely used technique in industry to produce a well-controlled polymer with narrow polydispersity, but it is susceptible and not compatible with electrophilic and acidic functional groups and is challenging in the presence of contaminants.

Moreover, polychloroprene exhibits excellent resistance to oil, grease and wax, has a wide operating temperature range, and is resistant to ozone and harsh weather conditions compared to other rubbery materials and was discovered by Dupont (1931) and has been widely used in the rubber industry.[22] The applications of polychloroprene range from adhesives and sealants to hoses and automotive parts. To synthesize PCPs, uncontrolled free radical emulsion polymerization is commonly used with thio-based chain transfer agents to limit molecular weight.[23]

There has been some work on controlled radical polymerization (CRP) of isoprene by RAFT and nitroxide-mediated polymerization (NMP). Perrier et al. and also Wooley et al. have independently reported RAFT polymerization of isoprene in bulk using a high temperature stable trithiocarbonate RAFT agent.[24,25] It is important to mention that CRP techniques have not been used for the surface polymerization of dienes. Thus, we propose here an in-depth investigation of the surface-initiated RAFT polymerization of isoprene and chloroprene on silica nanoparticle surfaces and a careful study of the polymerization kinetics at different graft densities. The improvement of nanocomposite properties requires that nanoparticles be well dispersed in the matrix instead of agglomerating. Grafting filler nanoparticles with the same polymer chains as the matrix has been demonstrated to be an effective way to

improve nanoparticle dispersion. The resulting grafted silica nanoparticles were directly crosslinked to create matrix-free nanocomposites that showed improved mechanical properties as compared to unfilled crosslinked polydiene matrix.

2.3 Materials and Methods

Materials. 3,4-Dichloro-1-butene was purchased from TCI chemicals. The RAFT agent 2- (((dodecylthio)carbonothioyl)thio)propanoic acid (DoPAT) (97%) and 2-methyl-2-[(dodecylsulfanylthiocarbonyl) sulfanyl]propanoic acid (MDSS) (97%) were purchased from Strem Chemicals and used as received. Spherical SiO_2 nanoparticles dispersed in methyl ethyl ketone (MEK-ST) with a diameter of 14 ± 4 nm were purchased from Nissan Chemical Co. Tetrabutylammonium bromide (PTC) was purchased from Chem-Impex International. Tetrahydrofuran (THF) (HPLC grade) was purchased from Fisher, 2.2'-Azobisisobutyronitrile (AIBN) was purified by recrystallization from methanol and dissolved in THF to make 10 mM solutions. dicumyl peroxide (Acros, 99%), Dimethylmethoxy-n-octylsilane (Gelest, 95%), and 3-aminopropyldimethylethoxysilane (Gelest, 95%) were used as received. All other reagents were used as received.

Characterization

^{1}H NMR (Bruker Avance III-HD 400 MHz) were conducted using $CDCl_3$ as a solvent. Molecular weights (Mn) and dispersities ($Đ$) were determined using

a Varian 290 LC gel permeation chromatography (GPC) with a 390 LC multidetector unit, and three Styragel columns. The columns consisted of HR1, HR3, and HR4 in the effective molecular weight ranges of 100-5000, 500-30000, and 5000-500000, respectively. THF was used as eluent at 30°C and the flow rate was adjusted to 1.0mL/min. Molecular weights were calibrated with poly(styrene) standards obtained from Polymer Laboratories. The transmission electron microscopy (TEM) was performed on a Hitachi H8000 TEM at an accelerating voltage of 200 KV. The samples were prepared by cryo-sectioning of crosslinked samples of the grafted nanoparticle and placed on copper grids. Small angle X-ray scattering experiments were conducted using a SAXSLab Ganesha instrument at the South Carolina SAXS Collaborative. A Xeons GeniX3D microfocus source was used with a Cu target to generate a monochromic beam with a 0.154 nm wavelength. The instrument was calibrated using a silver behenate reference with the first order scattering vector q*=1.076 nm^{-1}, where $q=4\pi\lambda^{-1}$ sin q with a total scattering angle of 2q. Dynamic Light Scattering (DLS) characterizations were conducted using Zetasizer Nano ZS90 from Malvern. Infrared spectra were obtained using a BioRad Excalibur FTS3000 spectrometer. Thermogravimetric analysis (TGA) measurements were carried out on a TA Q5000 thermogravimetric analyzer (TA Instruments). All the samples were preheated to 100^{o} C and kept at this temperature for 10 min to

remove residual solvents. After cooling to 40° C, the samples were heated to 800° C with a heating rate of 10° C/min in a nitrogen atmosphere. Dynamic mechanical analysis (DMA) was performed with an Eplexor 2000N dynamic measurement system (TA, ARES-RSA3) using a constant frequency of 10 Hz in a temperature range -100° C to 100° C. The analysis was done in tension mode. For the measurement of the complex modulus, E*, a static load of 1% pre-strain was applied and the samples oscillated to a dynamic load of 0.5% strain. Measurements were done with a heating rate of 3° C/min under nitrogen flow. Tensile tests of samples were carried out using an Instron 5543A material testing machine with crosshead speed 20 mm/min (ASTM D412, ISO 527). Samples were cut into standard dumbbell shapes with neck cross-section dimensions of 5 x 22 mm with 0.4mm thickness. At least five measurements were recorded, and the average values were reported.

Experimental

Synthesis of Chloroprene Monomer. For the synthesis of chloroprene monomer, NaOH (16 g, 0.404 mol) and PTC (4.35 g, 0.0134 mol) in 65 ml of water were charged to a 250 mL three-necked round bottom flask. A condenser was fitted, and the mixture was stirred and heated. At 55° C, 3,4-dichloro-1-butene (25 g, 0.2 mol) was added dropwise over five minutes. Heating continued and at 62° C the

product distilled as a hazy liquid; 60–75° C was maintained for two hours. Drying over $MgSO_4$ yielded a clear, colorless liquid. Chloroprene monomer is self-polymerizing under ambient conditions, so it is an unstable monomer. Therefore, it was stabilized by adding 0.1% (w/w) phenothiazine stabilizer to the dried product and the solution purged with nitrogen. Yield 74%. ^{1}H NMR (400 MHz, $CDCl_3$) δ 5.22-5.25 (2H, d, C**H**$_2$=CH), 5.31-5.34 (2H, d, C**H**$_2$=CCl), 6.31-6.40 (1H, q, CCl-C**H**,), (Figure 2.1) (Scheme 2.1). HRMS (EI) (m/z) calcd for C_4H_5Cl: 88.0080; found: 88.0110.[26]

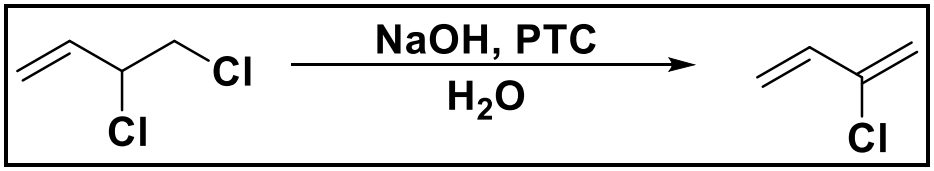

Scheme 2.1 Synthesis of chloroprene monomer.

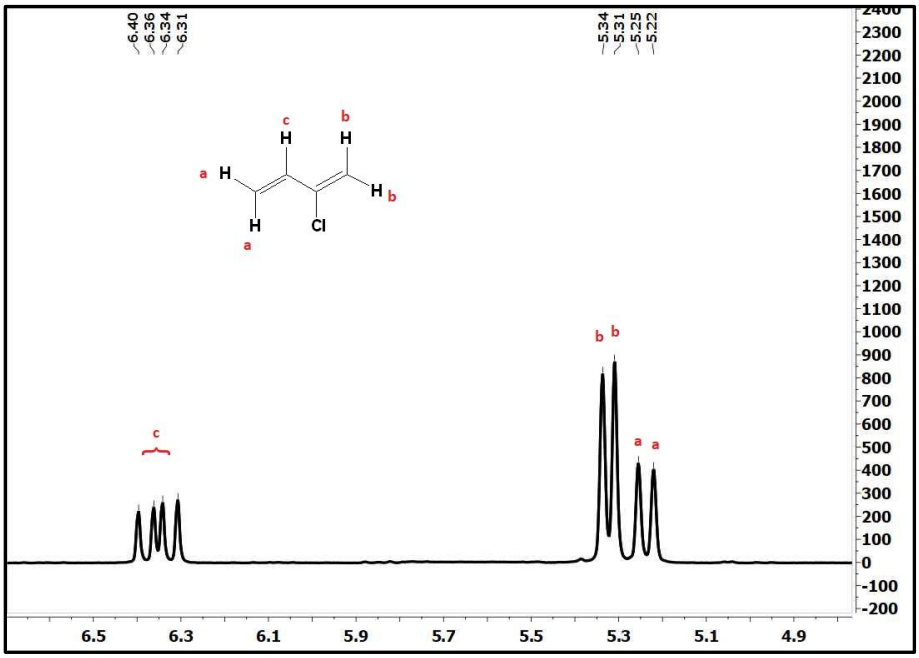

Figure 2.1 ^{1}H NMR (400 MHz, CDCl3) spectrum of chloroprene monomer

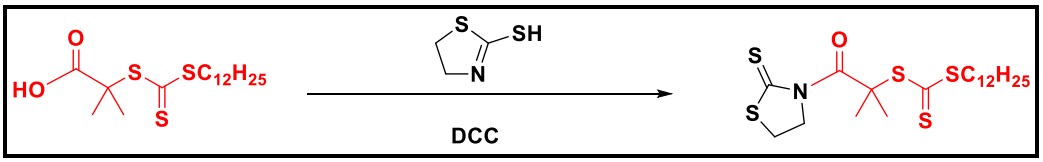

Scheme 2.2 Activation of 2-Methyl-2-[(dodecylsulfanylthiocarbonyl) sulfanyl]propanoic acid (MDSS)

Activation of 2-Methyl-2-[(dodecylsulfanylthiocarbonyl) sulfanyl]propanoic Acid (MDSS). The procedure for the activation of MDSS is given below, similar to that previously reported.[3] MDSS (2 g, 5.49 mmol), N,N'-dicyclohexylcarbodiimide (1.24 g, 6.03 mmol) and 2-mercaptothiazoline (0.718 g, 6.03 mmol) were dissolved in dichloromethane (40 mL) in a 100 mL r.b. flask under a nitrogen stream. After 10 min at r.t., a solution of 4-dimethylaminopyridine (0.067 g, 0.549 mmol) dissolved in dichloromethane (2 mL) was added to the mixture and the nitrogen flow was removed. After 5 h at r.t., the mixture was filtered, and the solvent evaporated using a rotary evaporator. The product was purified by column purification using a silica column with 5:4 ethyl acetate:hexane. Yields are usually greater than 80%, m.p. 34-34°C, ^{1}H NMR (400 MHz, $CDCl_3$) δ 3.21 (2H, t, S-C**H**$_2$-$(CH2)_{10}$-CH_3), 1.6 (6H, s, C-$(CH_3)_2$), 1.19-1.31 (16H, t, -$(CH_2)_8$-CH_3), 1.58 (2H, m, C**H**$_2$-$(CH_2)_8$-CH_3), 2.06 (2H, m, -C**H**$_2$-CH_2-$(CH_2)_8$-CH_3) 0.81 (3H, t, SCH_2-$(CH2)_{10}$-C**H**$_3$), 3.51 (2H, t, N-C**H**$_2$-CH_2-S), 3.91 (2H, t, S-C**H**$_2$-CH_2-N), (Figure 2.2) (Scheme 2.2), GS-MS: 464.11, Elemental Analysis: calcd, C, 51.57; H, 7.57; N, 3.01; O, 3.43; S, 34.41, found, C, 53.08; H, 7.68; N, 2.67; O, 3.76; S, 32.41.[27]

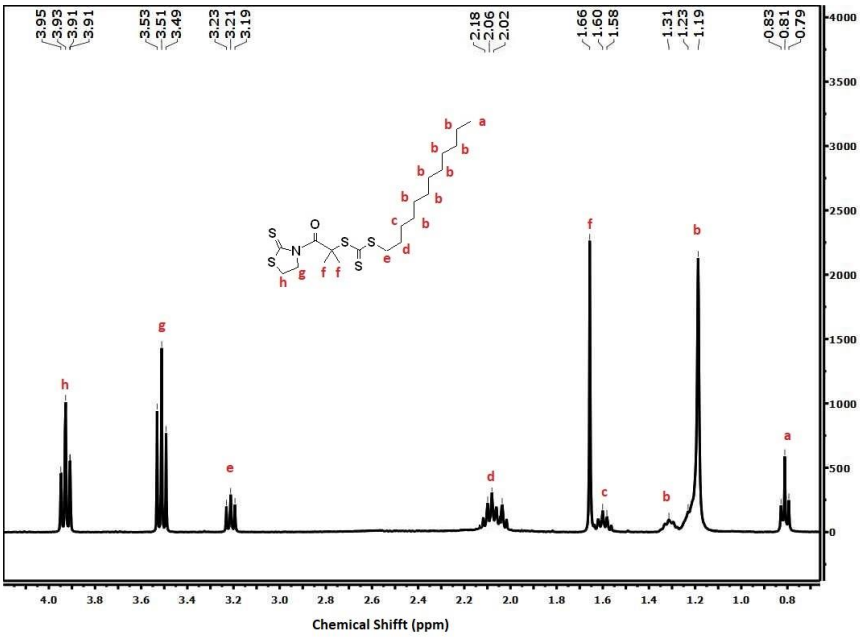

Figure 2.2 ^{1}H NMR (400 MHz, CDCl3) spectrum of activated-MDSS

Activation of 2-(((dodecylthio)carbonothioyl)thio)propanoic Acid (DoPAT). The procedure for the activation of DoPAT is given below. DoPAT (2 g, 5.72 mmol), N,N′-dicyclohexylcarbodiimide (1.30 g, 6.30 mmol) and 2-mercaptothiazoline (0.751 g, 6.30 mmol) were dissolved in dichloromethane (40 mL) in a 100 mL round bottom flask under a nitrogen stream. After 10 min at r.t., a solution of 4-dimethylaminopyridine (0.0697 g, 0.572 mmol) dissolved in dichloromethane (2 mL) was added to the mixture and the nitrogen flow was removed. After 5 h at r.t., the mixture was filtered, and the solvent evaporated using a rotary evaporator. The product was purified by column purification using a silica column with 5:4 ethyl acetate:hexane. Yields were greater than 90%, m.p. 52-54°C. ^{1}H NMR (400 MHz, $CDCl_3$) δ 3.28 (2H, t, S-C**H**$_2$-$(CH2)_{10}$-CH_3), 1.63 (3H, s, C-$(C\mathbf{H}_3)_2$), 1.12-1.33 (16H, t, -$(C\mathbf{H}_2)_8$-CH_3), 1.58 (2H, m, -C**H**$_2$-$(CH_2)_8$-CH_3),

2.09 (2H, m, -C**H**$_2$-CH$_2$-(CH$_2$)$_8$-CH$_3$) 0.82 (3H, t, SCH$_2$-(CH2)$_{10}$-C**H**$_3$), 3.51 (3H, t, -S-C**H**(CH$_3$)-CO-N-C**H**$_2$-CH$_2$-S), 3.93 (2H, t, S-C**H**$_2$-CH$_2$-N), (Figure 2.3) (Scheme 2.3) GS-MS: 450.92, HRMS (EI) (m/z) calcd. for C_4H_5Cl: 451.1166; found: 451.1182. [28]

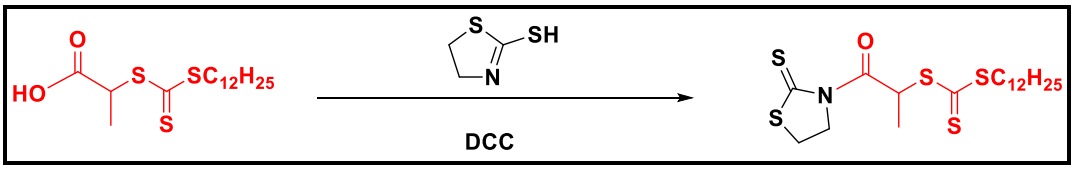

Scheme 2.3 Activation of 2-(((dodecylthio)carbonothioyl)thio)propanoic acid (DoPAT)

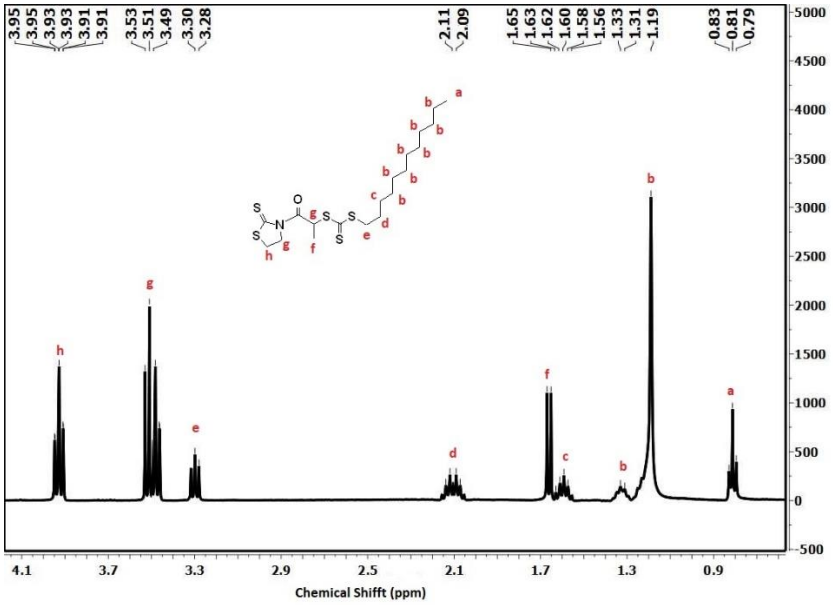

Figure 2.3 ^{1}H NMR (400 MHz, CDCl3) spectrum of activated-DoPAT

Free Polymerization of Isoprene Via RAFT Polymerization by DoPAT. Isoprene (2g, 30 mmol), DoPAT (35 mg, 0.1 mmol), dicumyl peroxide (2.7 mg, 0.01mol) (from 10 mM stock solution of DCP), and THF (2.8 mL) with a polymerization ratio [monomer]: [CTA]:[initiator] 300:1:0.1 were added to a

Schlenk tube. The mixture was degassed by three freeze-pump-thaw cycles, filled with nitrogen, and then the Schlenk tube was placed in a 115° C oil bath (be sure to fill the only a fifth of the tube due to high pressure). The polymerization was stopped by quenching in ice water. Molecular weights were measured using gel permeation chromatography (GPC) in THF which was calibrated with polystyrene standards. A wide range of molecular weights can be polymerized by varying the polymerization feed ratio.

Free Polymerization of Chloroprene Via RAFT Polymerization by MDSS. Chloroprene (0.25 g), MDSS (5.16 mg), AIBN (141ml from 10 mM stock solution) and THF (1 ml) with a polymerization ratio [monomer]: [CTA]:[initiator] 400:1:0.1 were added and mixed thoroughly in a Schlenk flask. The mixture was degassed by three freeze-pump-thaw cycles, filled with nitrogen, and the Schlenk flask was placed in an oil bath at 60° C. The polymerization was stopped by quenching in ice water. Molecular weights were measured using gel permeation chromatography (GPC) in THF which was calibrated with polystyrene standards. Different molecular weights can be achieved by varying the polymerization ratio.

Preparation of DoPAT-Functionalized Silica Nanoparticles. A solution (20 mL) of colloidal silica particles (30 wt % in methyl isobutyl ketone) was added to a

two-neck round bottom flask and diluted with 110 mL of THF. Dimethylmethoxy-n-octylsilane (0.1 mL) was added to improve dispersibility along with 3-aminopropyldimethylethoxysilane (0.7 mL, 5 mmol) and the mixture was refluxed for 5 h under nitrogen protection. The reaction was cooled to room temperature and precipitated in a large amount of hexanes (300 mL). The particles were recovered by centrifugation and dispersed in THF using sonication, then precipitated in hexanes again. The amine-functionalized particles were dispersed in 40 mL of THF for further reaction. Then 2.5 g (5.5 mmol) of activated DoPAT was prepared similarly to a procedure described previously and added dropwise to a THF solution of the amine-functionalized silica nanoparticles (40 mL, 6 g) at room temperature. After complete addition, the solution was stirred overnight. The reaction mixture was precipitated into a large amount of methanol (400 mL). The particles were recovered by centrifugation at 3000 rpm for 5 min. The particles were redispersed in 30 mL THF and precipitated in methanol. This dissolution-precipitation procedure was repeated two more times until the supernatant layer after centrifugation was colorless. The yellow DoPAT- functionalized silica nanoparticles were dried at room temperature and analyzed using UV-Vis spectroscopy to determine the chain density using a calibration curve constructed from standard solutions of free DoPAT. The RAFT agent density of the particles was calculated to be 100

mmol/g of grafted NPs (0.42 chains/nm^2). Different graft densities were achieved by adding different amounts of 3-aminopropyldimethylethoxysilane in the first step as described previously.

Preparation of MDSS-Functionalized Silica Nanoparticles. A solution (20 mL) of colloidal silica particles (30 wt % in methyl isobutyl ketone) was added to a two-neck round bottom flask and diluted with 110 mL of THF. Dimethylmethoxy-n-octylsilane (0.1 mL) was added to improve dispersibility along with 3-aminopropyldimethylethoxysilane (0.7 mL, 5mmol) and the mixture was refluxed for 5h under nitrogen protection. The reaction was then cooled to room temperature and precipitated in a large amount of hexanes (300 mL). The reaction was cooled to room temperature and precipitated in a large amount of hexanes (500 mL). The particles were recovered by centrifugation and dispersed in THF using sonication and precipitated in hexanes again. The amine-functionalized particles were redispersed in 35 mL of THF for further reaction. Then 0.2 g, (0.4 mmol) of activated MDSS was prepared as described above and added dropwise to a THF solution of the amine functionalized silica nanoparticles (40 mL, 6 g) at room temperature. After complete addition, the solution was stirred overnight. The reaction mixture was precipitated into a large amount of hexanes (400 mL). The nanoparticles were recovered by centrifugation at 5000 rpm for 8 min. The particles were redispersed in 30 mL THF and

precipitated in hexanes. This dissolution-precipitation procedure was repeated two more times until the supernatant layer after centrifugation was colorless. The yellow MDSS-anchored silica nanoparticles were dried at room temperature and analyzed using UV analysis to determine the chain density (ch/nm^2) using a calibration curve constructed from standard solutions of free MDSS. Different graft densities were achieved by adding different amounts of 3-aminopropyldimethylethoxysilane in the first step as described previously.

RAFT Polymerization of Isoprene from DoPAT- Functionalized Silica Nanoparticles. In a typical polymerization, isoprene (1.42 g, 21 mmol), DoPAT-g-silica NPs with surface density of 0.10 mmol/g (0.7g, 70 mmol), THF (2.2 mL), and dicumyl peroxide initiator (7.0 mmol) with a ratio between species of [monomer]: [CTA]:[initiator] 300:1:0.1 were added to a Schlenk tube. The particles were dispersed into the solution via sonication for 1 min and subsequently, the mixture was degassed by three freeze-pump-thaw cycles, filled with nitrogen, and the sealed Schlenk tube was placed in a 115^o C oil bath for the desired time and temperature. The polymerization was stopped by quenching in ice water. NMR spectroscopy was used to determine the conversion of monomer comparing the monomer peak with the ones of internal standard (trioxane). The resultant polymer grafted particles were precipitated into a large amount of

methanol and centrifuged at 8000 rpm for 5 min and the particles were dispersed back into THF.

RAFT Polymerization of Chloroprene from MDSS-Functionalized Silica Nanoparticles. In a typical polymerization, chloroprene (2g), MDSS-g-SiO_2 (0.74 g 0.32 ch/nm^2), AIBN (567ml from 10mMstock solution) and THF (4 ml) with a ratio between species of [monomer]: [CTA]:[initiator] 400:1:0.1, were added and mixed well in a Schlenk flask. The mixture was degassed by three freeze-pump-thaw cycles, filled with nitrogen, and the sealed Schlenk flask was placed in an oil bath at 60° C. Aliquots of the reaction solution were withdrawn from the flask periodically throughout the polymerization. The resulting polychloroprene grafted particles were purified by two rounds of centrifugation to remove excess monomers and free polymers then redispersed in THF.

General Procedure for Cleaving Grafted Polymer from Particles. 20 mg of polydiene grafted silica nanoparticles were dissolved in 2 mL of THF. Aqueous HF (49%, 0.2 mL) was added, and the solution was allowed to stir at room temperature overnight. The solution was poured into a PTFE Petri dish and allowed to stand in a fume hood overnight to evaporate the volatiles. The recovered polymer was subsequentlly used for GPC analyses.

Curing Process of Polydiene Grafted Nanoparticles. Thermogravimetric analysis (TGA) was done before curing matrix-free samples to calculate the exact amount of grafted polymer on the surface of NPs. Then two different ways were used to cure PCP and PIP:

- **Curing Process of Polychloroprene (PCP) Nanocomposites.** A solvent mixing technique was used for curing. All equivalents mentioned here are mass equivalents. Chloroprene polymer (100eq), zinc oxide (5eq), magnesium oxide (2eq), phenyl-a- naphthylamine (2eq), stearic acid (0.5eq), 2-mercaptothiazoline (0.5eq) were mixed well in THF (15 mL for each gram of polymer). The mixtures were then poured into Teflon petri dishes for solvent evaporation under vacuum. The dried samples were hot pressed at 160^{o} for 25 min to obtain vulcanized rubber sheet of 0.2-0.4 mm thickness.[29,30]
- **Curing Process of Polyisoprene (PIP) Nanocomposites**. A solvent mixing technique was used to cure the PIP by adding curing agents. The isoprene polymer (100eq) was cured using dicumyl peroxide (10eq) in THF; all equivalents are PHR (Part per Hundred Rubber). After evaporating the solvent samples were hot pressed at 160^{o} for 25 minutes to obtain vulcanized rubber sheet of 0.4 mm thickness.[31,32]

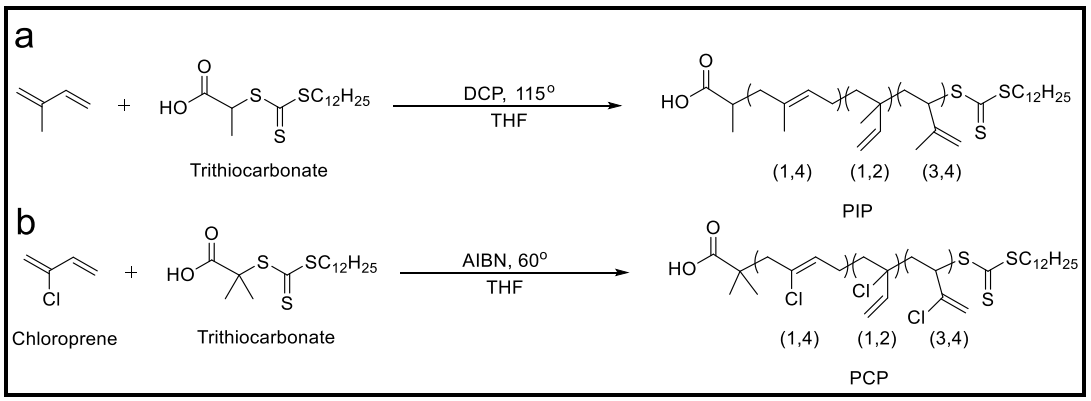

Scheme 2.4 a) Polymerization of isoprene mediated by free DoPAT RAFT agent. b) Polymerization of chloroprene mediated by free MDSS RAFT agent.

2.4 Results and Discussion

Kinetic Study of Free RAFT and SI-RAFT of Isoprene and Chloroprene

We initially started the free RAFT polymerization of isoprene and chloroprene. The ratio between species was kept at [Monomer]/[RAFT]/[Initiator] = 300:1: 0.1 for isoprene and 400:1:0.1 for chloroprene. The reaction was carried out in THF, at 115° C for isoprene and 60° C for chloroprene and the polymerization was monitored over time. The kinetic study for isoprene and chloroprene $\ln(M_0/M_t)$ had a linear relationship versus time and the molecular weight increased with monomer conversion. Both monomers showed some non-linearity at low conversion, which has been referred to as "hybrid behavior" (Figure 2.4, Scheme 2.4, Figure 2.5 and Scheme 2.5).[27,28] This behavior is characterized by an initial molecular weight that us higher than predicted but approaches the calculated molecular weight as conversion increases and is

usually attributed to a low chain transfer constant at the initial stage of polymerization.

The attachment of the RAFT agent onto NP surfaces and the subsequent surface-initiated RAFT polymerization is illustrated in Scheme 2.4. The attachment of the RAFT agent onto silica nanoparticles was measured by UV-vis spectrometry. The RAFT agent used to anchor onto the modified silica nanoparticles was determined quantitatively by comparing the absorption for the RAFT agent anchored to silica nanoparticles to a standard absorption curve made from known amounts of the free RAFT agent. NPs with a wide range of graft densities were used throughout the study (0.005 ch/nm^2 to 0.7 ch/nm^2). In this study, we did not target very high graft density to avoid low ratio of silica to polymer content in the final nanocomposite, which is typically of less interest in practical applications.

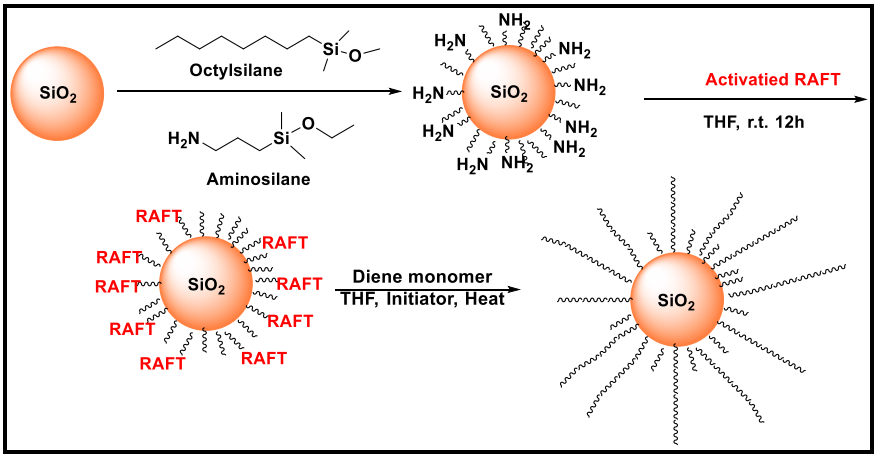

Scheme 2.5 Synthetic of polydiene grafted silica NPs.

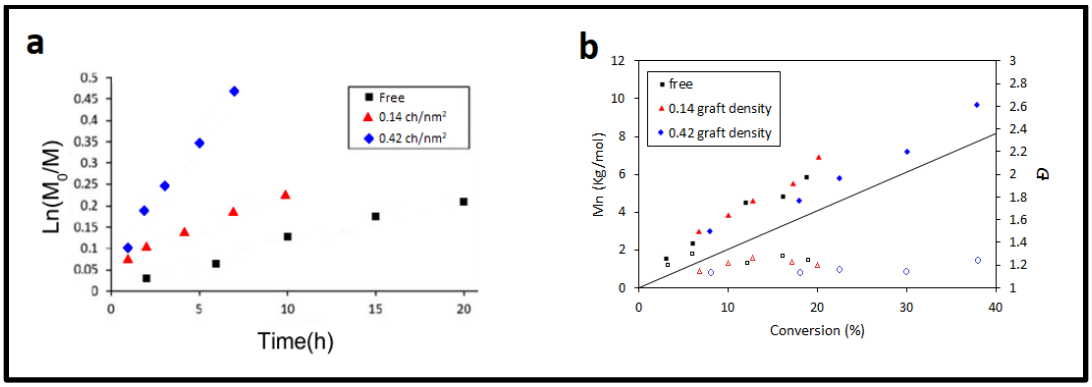

Figure 2.4 a) Pseudo first-order kinetic plots b) dependence of molecular weight (solid line, Mn, theory) on the conversion for the polymerization of isoprene with ratio between species [CP]/[RAFT]/[AIBN] = 300:1:0.1 with free DoPAT; DoPAT grafted particles with 0.14 ch/nm² density; DoPAT grafted particles with 0.42 ch/nm² density.

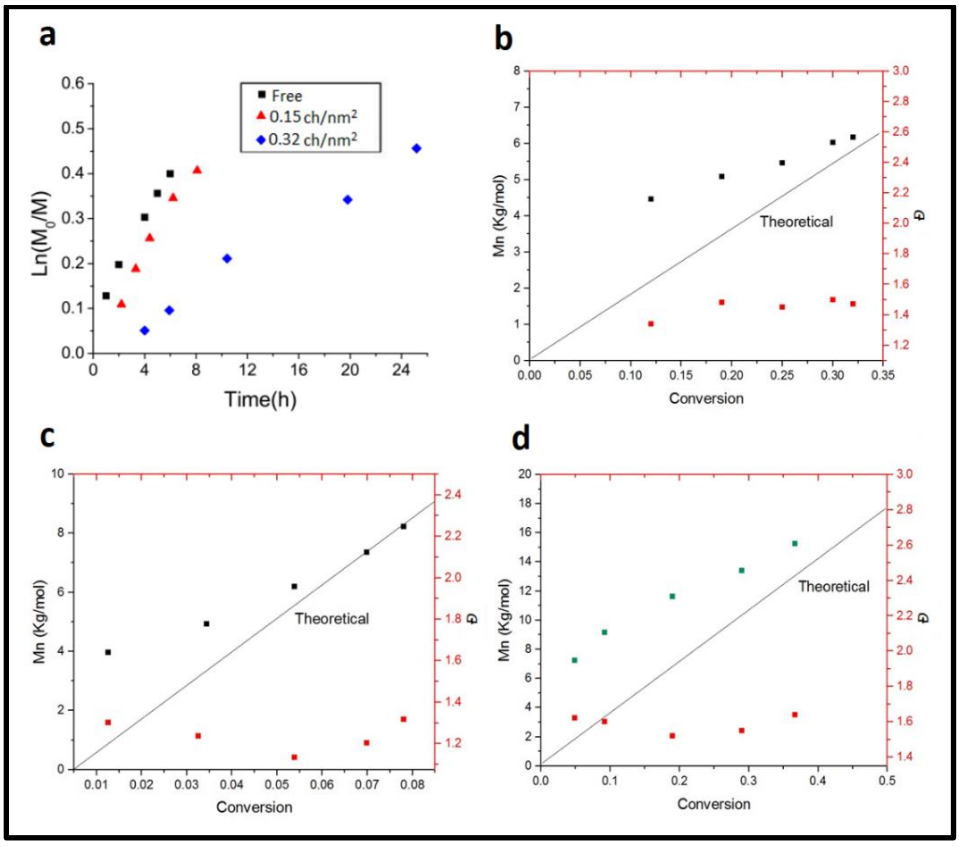

Figure 2.5 a) Pseudo first-order kinetic plots and dependence of molecular weight (solid line, Mn, theory) on the conversion for chloroprene with ratio between species [CP]/[RAFT]/[AIBN] = 400:1:0.1 with: **b)** free MDSS; **c)** MDSS grafted particles with 0.15 ch/nm² density; **d)** MDSS grafted particles with 0.32 ch/nm² density.

Kinetic studies of the SI-RAFT polymerization of both monomers were studied at two different graft densities as well as using free RAFT agent for comparison. Figure 2.4 and Figure 2.5 show that there is a good linear relationship between $\ln(M_0/M_t)$ vs. time versus conversion for the SI-graft polymerization, which indicates a constant radical concentration throughout the reaction and the living character of the polymerizations. Moreover, it is obvious that the free RAFT agent-mediated polymerization was much slower than SI-RAFT polymerization for isoprene and increased with increasing graft density. The results in Figure 2.5 show that these trends were reversed for chloroprene, where the free polymerization kinetics were faster than the SI-RAFT polymerization, and the polymerization become slower with increasing graft density. At this time, the reasons for these trends is unclear, although this study adds more data to understand these relationships as new monomers are evaluated.

Mechanical properties of matrix-free PCP grafted silica nanoparticle composites.

To investigate the mechanical properties of matrix-free polydiene grafted silica nanoparticle composites, we prepared a series of nanocomposites with two graft densities (0.25 and 0.035 ch/nm^2) for polyisoprene composites and one graft

density (0.1 ch/nm^2) for polychloroprene composites, with different molecular weights of the grafted polymer (Table 2.1). The matrix-free nanocomposites were crosslinked as films and cut into dog-bones for tensile testing. Figure 2.6 shows the tensile stress-strain curves of cured nanocomposites, and it was found that the properties of the composites were directly related to the silica content in the nanocomposites. All the matrix-free composites showed improvement in tensile strength for both polyisoprene and polychloroprene compared with unfilled samples.[29] Furthermore, the tensile stress at break increased with silica loading with a corresponding decrease in elongation at break. For matrix-free nanocomposite systems, the increase in molecular weight of the grafted

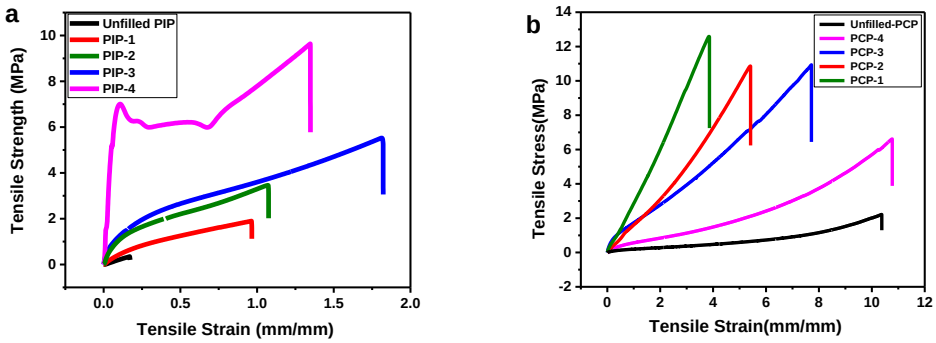

Figure 2.6. Stress-strain curves of crosslinked unfilled and filled composites a) Polyisoprene, b) Polychloroprene.

polymers cause a reduction in silica loading at a fixed graft density. This general trend is consistent with previous literature that tensile strength generally increases continuously with increasing silica loading.[33,34] From experimental

results, increases in grafted molecular weight can lead to increase in the elongation at break due to better entanglement between polymer chains, but lower silica content can also cause a decrease in tensile strength.

Table 2.1 Sample details of matrix-free polydiene grafted silica nanoparticle composites.

Sample Name	Graft Density (ch/nm^2)	Mn (kDa)	Silica content (wt%)	Tensile Strength (MPa)	Elongation at Break (mm/mm)	Graft Density (ch/nm^2)
Unfilled-PIP	--	43k	--	0.32	0.17	--
PIP-1	0.25	19k	34	1.89	0.96	0.25
PIP-2	0.25	41k	20	3.45	1.07	0.25
PIP-3	0.035	51k	48	5.20	1.82	0.035
PIP-4	0.035	38k	73	9.63	1.34	0.035
Unfilled-PCP	--	50k	--	1.8	10.3	--
PCP-1	0.1	47	50	12.9	3.9	0.1
PCP-2	0.1	55	45	11	5.3	0.1
PCP-3	0.1	70	40	11	7.7	0.1
PCP-4	0.1	100	30	6.1	10.9	0.1

The dynamic mechanical behavior was measured at constant strain and frequency for the crosslinked silica nanocomposites. At low temperatures below glass transition temperature, the effect of the silica on E' is observed even though the molecular chain segments are frozen in this region. In the rubbery plateau region above Tg, matrix-free silica composites also had higher storage modulus

relative to the unfilled for both polymers. These data for matrix-free samples showed that the storage modulus increased with increasing silica loading. The glass transition temperature of the matrix-free composites was not affected by silica loading and that is shown in tan delta figures where all the peaks appear at the same temperature. Moreover, the reduction of tan delta peak height increased with silica loading, which may, at least in part, suggest better reinforcing effect and stronger rubber-filler interaction at high silica loading.[9]

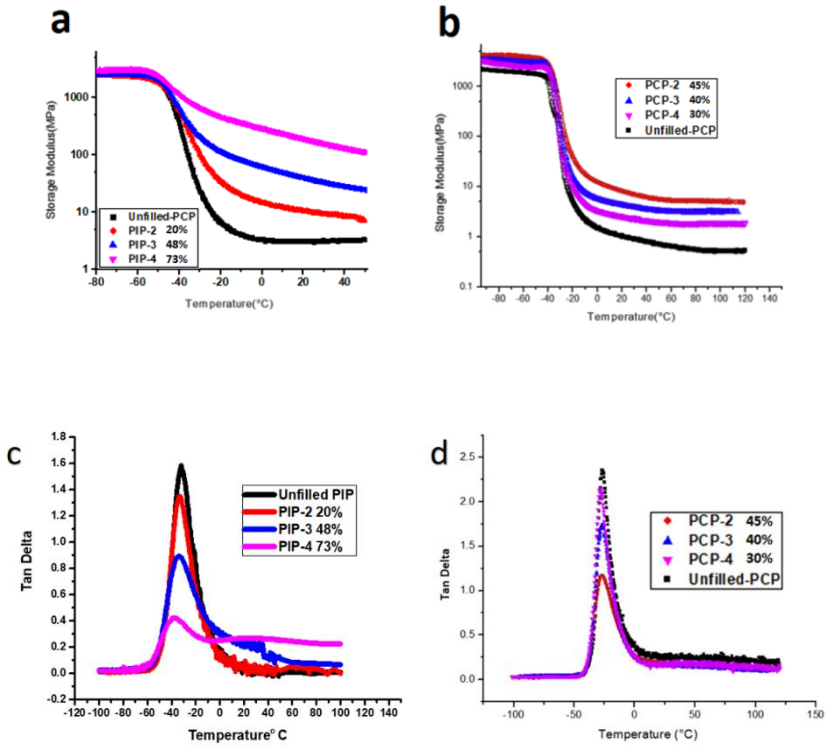

Figure 2.7 Temperature dependence of storage modulus and tan delta of crosslinked unfilled and matrix-free nanocomposites of a,c) Polyisoprene and b,d) Polychloroprene.

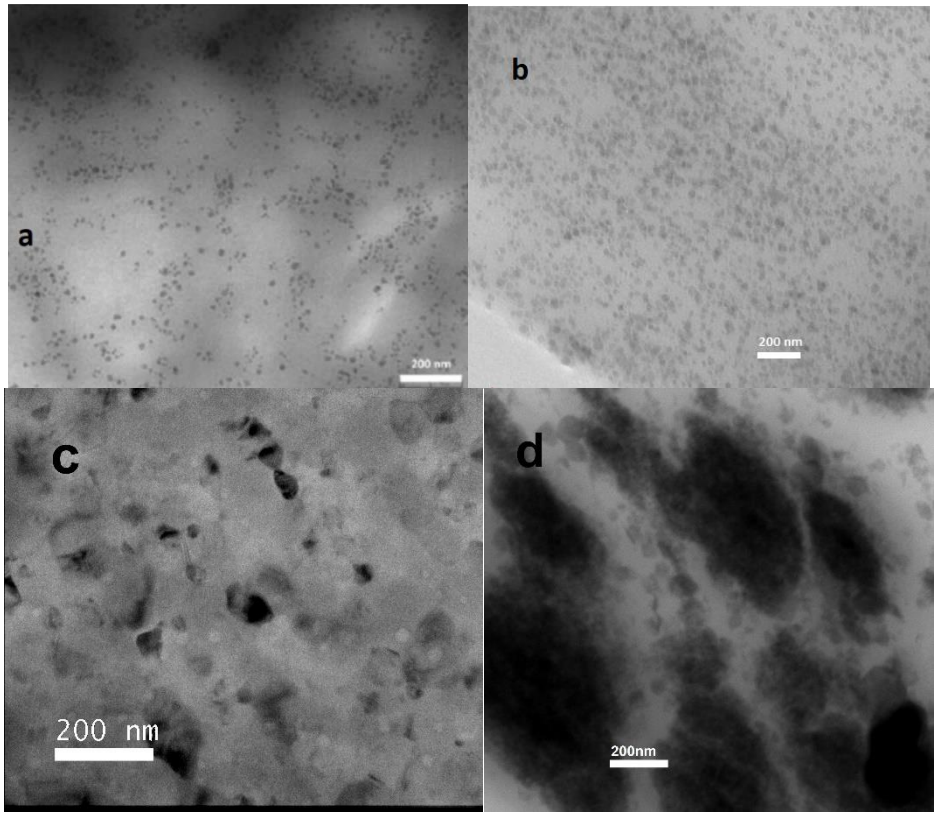

Figure 2.8 TEM micrographs of (a) as prepared PIP-g-SiO_2 NPs Mn 62 Kg/mol) with chain density of 0.1 ch/nm^2 nanocomposite filled with 5% loading NPs, (b) PCP-g-SiO_2 NPs (Mn100 kg/mol) with chain density of 0.1 ch/nm^2 nanocomposite filled with 30% loading NPs, (c) bare silica NPs in PIP matrix filled with 5% loading NPs, (d) bare silica NPs in PCP matrix filled with 30% loading NPs. (scale bars are 200 nm).

As shown in TEM photographs (Figure 2.8) particle dispersion was suitable for both PIP and PCP nanocomposites. There was no significant clustering of particles even at high silica loading of 30% in PCP. In addition, a closer view exhibits no uniform pattern of particle distribution and interparticle spacing, which is most likely due to the significant size disparity of the core silica particles. Small-angle X-ray scattering (SAXS) was used to obtain more information about the investigation of interparticle spacing and particle

dispersion. No agglomeration on was detected from the X-ray scattering pattern at low q. The intensity of all the peaks was relatively weak, indicating a broad distribution of interparticle spacing. The location of the peak did not change much between the samples, which corresponded to a d spacing between 18-23 nm and seems reasonable considering the size of silica core (15 nm) plus the grafted polymers (Figure 2.9).

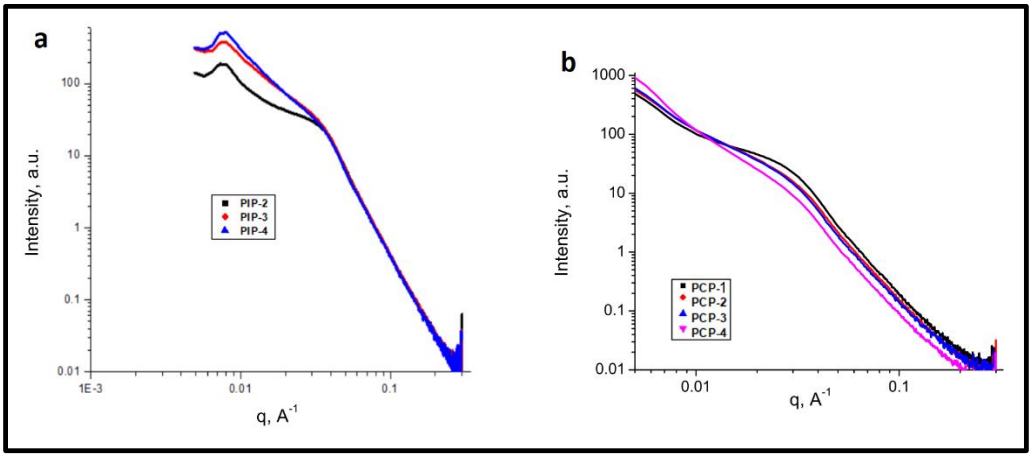

Figure 2.9 Representative small-angle X-ray scattering (SAXS) intensity curves for matrix-free grafted silica nanocomposites.

2.5 Conclusion

In this chapter, we studied the surface-initiated RAFT polymerization of polydiene derivatives grafted onto silica NPs. Trithiocarbonate RAFT agents were anchored onto the surface of silica NPs with controlled graft density, and controlled radical polymerizations were conducted to produce surface grafted polymer of predetermined molecular weight and relatively narrow PDI. The

polymerization kinetics were studied, and it was found that the grafting-from polymerization rate was dependent on the graft density. The polymerization rate of isoprene was faster on particles, but thus trend was reversed for the polymerization rate of chloroprene. Grafted silica NPs were directly crosslinked to form matrix-free nanocomposites that showed uniform particle dispersion and improved mechanical properties compared to unfilled crosslinked films. These durable, sturdy composite materials could be useful in many applications.

2.6 References

(1) R. Gangopadhyay, A. De, *Chem. Mater*. **2000**, *12*, 608–622.

(2) C. Sanchez, B. Lebeau, F. Chaput, J. P. Boilot, *Adv. Mater*. **2003**, *15*, 1969–1994

(3) G. Moad, E. Rizzardo, S. H. Thang, *Aust. J. Chem*. **2005**, *58*, 379–410.

(4) H. Zou, S. Wu, J. Shen, *Chem. Rev*. **2008**, *108*, 3893–3957.

(5) Li, C.; Han, J.; Ryu, C. Y.; Benicewicz, B. C. *Macromolecules* **2006**, *39* (9), 3175–3183.

(6) Li, C.; Benicewicz, B. C. *Macromolecules* **2005**, *38* (14), 5929–5936.

(7) Saunders, K. J. *Organic Polymer Chemistry; Springer*: Dordrecht, **1973**.

(8) Brosse, J. C.; Campistron, I.; Derouet, D.; Hamdaoui, A. E. L.; Houdayer, S.; Reyx, D. *J. Appl. Polym. Sci.* **2000**, *78*, 1461–1477.

(9) Kumnuantip, C.; Sombatsompop, N. *Mater. Lett*. **2003**, *57* (21), 3167–3174.

(10) Salaeh, S. *Processing of Natural Rubber Composites And Blends: Relation Between Structure And Properties*, Prince Of Songkla University And University Claude Bernard Lyon, **2014**.

(11) Hosler, D.; Burkett, S. L.; Tarkanian, M. *J. Science*. **1999**, *284* (5422), 1988–1991.

(12) Heinrich, G.; Kluppel, M.; Vilgis, T. A. *Curr. Opin. Solid State Mater. Sci*. **2002**, *6*, 195–203.

(13) Nazhat, S. N.; Parker, S.; Patel, M. P.; Braden, M. *Biomaterials* **2001**, *22* (17), 2411–2416.

(14) Nazhat, S. N.; Parker, S.; Riggs, P. D.; Braden, M. *Biomaterials* **2001**, *22* (15), 2087–2093.

(15) Hou, S.; Chan, W. K. Preparation of Functionalized Polystyrene-block-polyisoprene Copolymers and Their Luminescence Properties. *Macromolecules* **2002**, *35*, 850-856.

(16) Lu, Z. J.; Huang, X. Y.; Huang, J. L.; Pan, G. Q. *Macromol. Rapid Commun*. **1998**, *19*, 527-531.

(17) Donderer, M.; Langstein, G.; Schafer, M.; Nuyken, O. *Polym. Bull. (Berlin)* **2002**, *47*, 509-516.

(18) Peng, Y.; Wang, J.; Liu, J.; Dai, H.; Cun, L. *Polym. Int*. **1996**, *39*, 63-68.

(19) Kongkaew, A.; Wootthikanokkhan, *J. Polym. Bull. (Berlin)* **1999**, *43*, 327-332.

(20) Wootthikanokkhan, J.; Tongrubbai, B. *J. Appl. Polym. Sci*. **2003**, *88*, 921-927.

(21) Kir, O.; Binder, W. H.; *European Polym. J.* **2013**, *49*, 3078-3088.

(22) Carothers, W. H.; Williams, I.; Collins, A. M.; Kirby, J. E. *J. Am. Chem. Soc*. **1931**, *53* (11), 4203–4225.

(23) Itoyama, K.; Hirashima, N.; Hirano, J.; Kadowaki, T. *Polym. Journal* **1991**, *23* (7), 859–864.

(24) Germack, D. S.; Wooley, K. L.; *J. Polym. Sci., Part A: Polym. Chem.* **2007**, *45*, 4100-4108.

(25) Li, C.; Han, J.; Ryu, C. Y.; Benicewicz, B. C. *Macromolecules* **2006**, *39*, 3175–3183.

(26) Koiry, B. P.; Moukwa, M.; Singha, N. K. *J. Fluor. Chem*. **2013**, *153*, 137–142.

(27) Zheng, Y.; Abbas, Z. M.; Sarkar, A.; Marsh, Z.; Stefik, M.; Benicewicz, B. C. *Polymer (Guildf)*. **2018**, *135*, 193–199.

(28) Khani, M. M.; Abbas, Z. M.; Benicewicz, B. C. *J. Polym. Sci. Part A Polym. Chem*. **2017**, 1–9.

(29) Kapgate, B. P.; Das, C.; Das, A.; Basu, D.; Wiessner, S.; Reuter, U.; Heinrich, G. *J. Appl. Polym. Sci*. **2016**, *133* (30), 1–10.

(30) Chokanandsombat, Y.; Sirisinha, C. *J. Appl. Polym. Sci*. **2013**, *128* (4), 2533–2540.

(31) Rajan, R.; Varghese, S.; George, K. E. *Prog. Rubber, Plast. Recycl. Technol*. **2012**, *28* (4), 201–220.

(32) Boochathum, P.; Prajudtake, W. *Eur. Polym. J.* **2001**, *37*, 417–427.

(33) Sae-Oui, P.; Sirisinha, C.; Thepsuwan, U.; Hatthapanit, K. *Eur. Polym. J.* **2006**, *42* (3), 479–486.

(34) Sae-oui, P.; Sirisinha, C.; Thepsuwan, U.; Hatthapanit, K. *Eur. Polym. J.* **2007**, *43* (1), 185–193.

CHAPTER 3

SI-RAFT POLYMERIZATION OF 2,3-DIMETHYL-1,3-BUTADIENE ON SILICA NANOPARTICLES FOR MATRIX-FREE METHYL RUBBER NANOCOMPOSITES

3.1 Abstract

Reversible addition-fragmentation Chain transfer (RAFT) polymerization of 2,3-dimethyl-1,3-butadiene (DMB) in solution and on the surface of silica nanoparticles was investigated and PDMB-grafted silica nanoparticles (PDMB-*g*-SiO_2 NPs) with different chain densities and molecular weights were prepared. The kinetic studies of DMB polymerization mediated by silica anchored RAFT agents at different graft densities were investigated and compared to the polymerization mediated by the corresponding free RAFT agent. The PDMB-*g*-SiO_2 NPs were cured to prepare rubbery films to obtain matrix-free nanocomposites which exhibited a good dispersion of silica nanoparticles and improved mechanical properties compared to the unfilled crosslinked rubber.

3.2 Introduction

Poly(2,3-dimethyl-1,3-butadiene) (PDMB) also known as methyl isoprene or methyl rubber in industry, is a historically significant rubber which was used by the Germans during WWI as a substitution for natural rubber.[1–3] The early synthesis of the monomer involved conversion of acetone to pinacol in the presence of aluminum oxide as catalyst, then dehydrogenation of pinacol to form the diene.[4,5] The polymerization of DMB has not been widely studied because the resulting rubber is softer than natural and synthetic rubber.[6,7] DMB was the first

monomer to be converted into industrially synthesized rubber, referred to as methyl rubber because it has one more methyl group than isoprene. The industrial process to produce methyl rubber was developed by Hoffmann in 1910 and produced during 1914–1918, but it was not widely used after that due to unfavorable properties like excessive hardness at low temperature and susceptibility to oxidation.[8,9]

The synthesis of PDMB through free radical polymerization is commonly used to produce very high molecular weight polymers with broad molecular weight distribution.[4,10–12] There are few reports on the controlled radical polymerization of DMB which could be because of the lack of control due to steric hindrance on this monomer and the rubber made out of is not suitable for industrial applications.[13,14] Polymerization of DMB by anionic polymerization affords good control over molecular weight and narrow molecular weight distribution, but this method is challenging because of the sensitivity of the reaction towards the presence of contaminants.[15] Thus, to the best of our knowledge, there is no report on RAFT polymerization of DMB.

The most important factor when polymerizing a new monomer via RAFT polymerization is to select the proper RAFT agent and the reaction conditions, because the inappropriate RAFT agent can lead to a reduction control, severe

retardation or inhibition.[16] Therefore, three different RAFT agents were explored for the polymerization of DMB; 2-(((dodecylthio)carbonothioyl)thio)propanoic acid (DoPAT), 2-methyl-2-[(dodecylsulfanylthiocarbonyl) sulfanyl]propanoic acid (MDSS), and 4-cyano-4-[(dodecylsulfanylthiocarbonyl) sulfanyl]pentanoic acid (CDTPA) (Figure 3.1). All three RAFT agents were used in the same conditions, despite that some retardation and poor control was realized in previous studies of RAFT polymerization of diene monomers which has been related to RAFT agent reactivity. Furthermore, it is mentioned in the literature, that the RAFT polymerization process does not affect the polymer microstructure.[17]

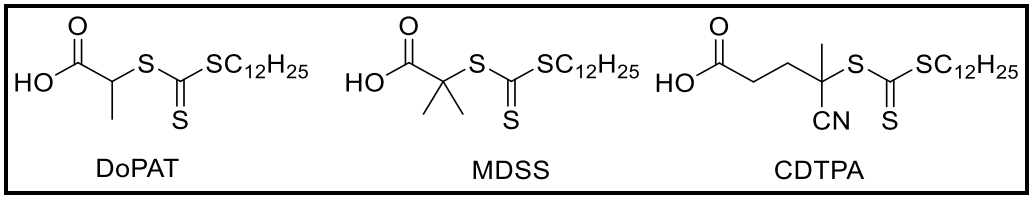

Figure 3.1 Chain transfer agents used for DMB RAFT polymerization.

Nanoparticles have been synthesized and used in reinforcement of different inorganic matrices.[18–22] It is well known that the addition of inorganic fillers into a polymer matrix can improve the thermomechanical properties compared to the neat polymer.[23,24] The formation of clusters (or agglomerates) stemming from phase separation between the polymer matrix and nanofiller can actually diminish property enhancement, so to obtain the targeted improvement,

it is necessary that the nanoparticles be well dispersed in the matrix.[25–27] Nanoparticles which are covalently grafted with polymer chains that are the same as or miscible with the matrix have been extensively studied and proven to be an effective means of controlling the nanoparticle dispersion given that there is sufficient control of the grafted chain molecular weight and graft density.[28,29]

In this work, we report the free and surface-initiated RAFT polymerization of DMB from silica nanoparticles and careful studies of the polymerization kinetics at different graft densities. These results were compared to other dienes that had been studied under the same conditions. The resulting PDMB, neat and grafted on silica nanoparticles, were crosslinked to create matrix-free nanocomposites that showed improved mechanical properties compared to neat DMB.

3.3 Materials and Methods

Materials. DMB monomer was purchased from Alfa Asear. The RAFT agent 4-Cyano-4-(((dodecylthio)carbonothioyl)thio)pentanoic acid (CDPA, >97%) was purchased from Strem Chemicals and used as received. Spherical SiO_2 nanoparticles dispersed in methyl ethyl ketone (MEK-ST) with a diameter of 14 ± 4 nm were purchased from Nissan Chemical Co. Tetrahydrofuran (THF) (HPLC grade, Fisher), dicumyl peroxide (Acros, 99%), n-octyldimethylmethoxysilane

(Gelest, 95%), and 3-aminopropyldimethylethoxysilane (Gelest, 95%) were used as received. All other reagents were used as received.

Anionic polymerization of 2,3-dimethyl-1,3-butadiene. The anionic polymerization of DMB was carried out by the syringe high vacuum technique under dry nitrogen in baked glass.[13] After baking the glasses at 125° C, DMB (60.9 mmol, 5g) was added into Schlenk flask with 5 mL of dry THF as a solvent. The flask was subjected to three cycles of freeze-pump-thaw then filled with dry nitrogen. Then n-Butyllithium in hexane (0.02 mmol, 1.3mg) was added as an initiator by a syringe through the septum while stirring and the reaction was heated at 60° C for 24 hours. The polymerization was terminated by rapidly cooling the reaction mixture in a water bath to room temperature. The resulting PDMB was precipitated into a large amount of methanol and centrifuged at 8,000 rpm for 10 min and redispersed in THF. Different molecular weights were synthesized by varying [monomer: initiator] ratio and time.[30]

RAFT polymerization of 2,3-dimethyl-1,3-butadiene. A 25 mL Schlenk flask, equipped with a magnetic stirrer, was charged with a mixture of DoPAT (10 mg, 28.6 mmol), dicumyl peroxide (DCP) (0.58 mg, 2.15 mmol), DMB (0.94 g, 11.44 mmol) and THF (2 ml). The mixture was degassed by three freeze-pump-thaw cycles, filled with nitrogen, and the sealed Schlenk flask was placed in an oil bath

at 115°C for 20 hours. Termination proceeded by rapidly cooling the reaction mixture in a water bath to room temperature. The resulting PDMB grafted particles were precipitated into a large amount of methanol and centrifuged at 8,000 rpm for 10 min and re-dispersed in THF. The molecular weight of this sample was 7K. Different molecular weights were synthesized by varying [monomer: CTA: initiator] ratio and time.

Synthesis of CPDA-*g*-SiO$_2$. A solution (20 mL) of colloidal silica particles (30 wt % in methyl isobutyl ketone) was added to a two-neck round bottom flask and diluted with 60 mL of THF. Then, n-octyldimethylmethoxysilane (ODMES) (0.4 mL, 1.61 mmol) was added and the mixture was refluxed in a 75°C in oil bath for 12 hours under nitrogen protection. The reaction was cooled to room temperature and precipitated in an excess of hexanes (200 mL). The particles were later recovered by centrifugation and dispersed in THF (50 mL) using sonication and precipitated in hexanes again. 3-Aminopropyldimethyethoxysilane (0.25 ml, 1.33 mmol) were added to ODMES-functionalized particles in THF (50 ml) and the mixture was refluxed in a 75° C oil bath for 3 hours under nitrogen protection. The reaction was cooled to room temperature and precipitated in an excess of hexanes (200 mL). The particles were recollected by centrifugation and dispersed in THF using sonication and precipitated in hexanes again. The amine-functionalized particles were dispersed

in 50 mL of THF for further reaction. Then activated CPDA (0.511 g, 1.13mmol) was prepared and added dropwise to a THF solution of the amine functionalized silica nanoparticles (50 mL, 6 g) at room temperature.[22] After complete addition, the solution was stirred overnight. The reaction mixture was precipitated into an excess of hexanes (400 mL). The particles were recollected by centrifugation at 3000 rpm for 8 min. The particles were redispersed in 30 mL THF and precipitated in hexanes. This dissolution-precipitation procedure was repeated two more times until the supernatant layer after centrifugation was colorless. The yellow CPDA-anchored silica nanoparticles were dried at room temperature and analyzed using UV analysis to determine the chain density using a calibration curve constructed from standard solutions of free CPDA.

Polymerization Procedures of Surface-initiated RAFT of DMB. In a typical polymerization, DMB (0.8g), CPDA-*g*-SiO_2 (0.46g 0.15ch/nm^2), DCP (161ul from 10mM stock solution), THF (2ml) and toluene (1ml) were added and mixed well in a Schlenk tube. The mixture was degassed by three freeze-pump-thaw cycles, filled with nitrogen, and the sealed Schlenk flask was placed in an oil bath at 115°C. The resulting PDMB grafted particles were precipitated into a large amount of methanol and centrifuged at 8,000 rpm for 10 min and redispersed in THF. Different molecular weights can be synthesized by varying the ratio of [monomer: CTA: initiator] and time. After polymerization, grafted polymer

chains were cleaved from the nanoparticles, by the following procedure. PDMB grafted silica particles (20 mg) were dissolved in 2mL of THF. Aqueous HF (49%, 0.2 mL) was added, and the solution was allowed to stir at room temperature overnight. The solution was poured into a PTFE Petri dish and allowed to stand in a fume hood overnight to evaporate the volatiles. The collected PDMB was then subjected to GPC analysis.

Curing process of PDMB grafted particles. The solvent mixing technique was used to cure the PDMB by adding curing agent in THF. PDMB (100 eq) with dicumyl peroxide (10 eq) [all equivalents are PHR (Parts per Hundred Rubber)] was used to cure the rubbery materials. After evaporating the solvent, samples were hot pressed at 160^{o} for 25 minutes to obtain a vulcanized rubber sheet of 0.4 mm thickness.

Characterization Techniques

Molecular weights. Molecular weights (Mn) and dispersities (*Đ*) were determined using a Varian 290 LC gel permeation chromatography (GPC) with a 390 LC multidetector unit, and three Styragel columns. The columns consisted of HR1, HR3, and HR4 in the effective molecular weight ranges of 100-5000, 500-30000, and 5000-500000, respectively. THF was used as eluent at 30°C and the

flow rate was adjusted to 1.0mL/min. Molecular weights were calibrated with poly(styrene) standards obtained from Polymer Laboratories.

Nuclear Magnetic Resonance Spectroscopy. ^{1}H NMR (Bruker Avance III-HD 400 MHz) spectra were recorded using $CDCl_3$ as a solvent.

Transmission Electron Microscopy. The transmission electron microscopy (TEM) was performed on a Hitachi H8000 TEM at an accelerating voltage of 200 KV. The samples were prepared by cryosectioning of the crosslinked samples in a solution of H_2O: DMSO 30:70, then placed on copper grids.

X-ray Scattering (SAXS). X-ray experiments were conducted using a SAXS Lab Ganesha at the South Carolina SAXS Collaborative. A Xenocs GeniX3D microfocus source was used with a Cu target to generate a monochromic beam with a 0.154 nm wavelength. The instrument was calibrated using National Institute of Standards and Technology (NIST) reference material 640c silicon powder with the peak position at $2\theta=28.44^{\circ}$ where 2θ is the total scattering angle. A Pilatus 300 K detector (Dectris) was used to collect the two-dimensional (2D) scattering patterns. All small-angle X-ray Scattering (SAXS) data were acquired with an X-ray flux of ~4.1 M and ~21.4 M photons/s incident upon the samples. All data were acquired by 10-15 minutes measurements. Transmission SAXS was measured normal to sample substrates to observe the purely in-plane

morphology. These 2D images were azimuthally integrated to yield the scattering vector and intensity.

Dynamic Mechanical Analysis. Dynamic mechanical analysis was performed with an Eplexor 2000N dynamic measurement system (TA, ARES-RSA3) using a constant frequency of 10 Hz and the gap is 10mm in a temperature range -50° C to 60° C. The analysis was done in tension mode. For the measurement of the complex modulus, E*, a static load of 1% pre-strain was applied and then the samples oscillated to a dynamic load of 0.5% strain. Measurements were done at a heating rate of 3° C/min under nitrogen flow. Samples were cut into rectangular shapes with dimensions of 4.8*15 mm with 0.4mm thickness. At least two measurements were recorded, and the average values were reported.

Stress-Strain Analysis. Tensile tests of samples were carried out using an Instron 5543A material testing machine with crosshead speed 20 mm/min (ASTM D412, ISO 527). Samples were cut into standard dumbbell shapes with neck cross-section dimensions of 5 x 22 mm with 0.4mm thickness. At least five measurements were recorded, and the average values were reported.

Hardness Test. Hardness of PDMB cured specimens was measured using a durometer with Shore A scale (Cogenix Wallace, Surrey) as per ASTM D2240. Samples were cut into standard square shapes with dimensions of 5*5 mm, and

the sheets having a sufficient thickness of 6mmwere used. At least five measurements were recorded, and the average values were reported.

3.4 Results and Discussion

Polymerization of free Dimethyl Butadiene via RAFT Polymerization

Before performing the SI-RAFT polymerization of DMB, detailed studies of the polymerization of DMB controlled by free RAFT agents were conducted. Three trithiocarbonate RAFT agents MDSS, CDTPA and DoPAT were tested to study which would give the best control over the polymerization. All polymerizations were set-up under the same conditions; 115^{o} C and [600:1:0.1] ratio of monomer to RAFT agent to initiator [M:CTA:Inti]. It was found that CDPTA lacks good control as indicated by the broad dispersity (2.1), likely because of the presence of electron-withdrawing groups on the RAFT agent which lead to higher transfer coefficients. In the literature, multiple side reactions have been identified, e.g., hydrolysis, cycloaddition reactions, and hetero Diels−Alder reaction with diene monomers.[16,31,32] The other two RAFT agents showed good reasonably control, but DoPAT was found to have the best control with the narrowest dispersity (1.21) (Table 3.1 and Scheme 3.1).

Several initiators were also tested in the DoPAT RAFT system at various temperatures and conditions. As shown in (Table 3.2) polymerization was not

observed at temperatures of 70° C or lower. For example, polymerization using 2,2′-Azobis(2-methylpropionitrile) (AIBN) at 70° C did not show any monomer consumption by NMR or polymer growth by GPC. The conversion using AIBN at 95° C for 24 hours was the highest compared to the other initiators, but yielded broad dispersities (1.42) and low molecular weight (6kg/mol) as detected by GPC. Polymerization using di-tert-butyl peroxide (dTBP) at 135° C and benzoyl peroxide (DBPO) at 95° C show similar dispersities and slightly higher molecular weights but all with higher dispersities than DCP. Therefore, DCP used to perform more extensive studies on DMB.

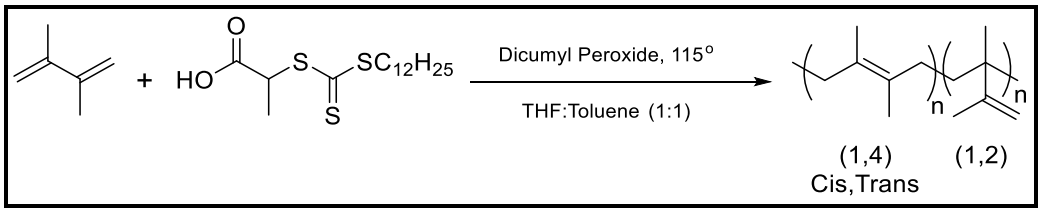

Scheme 3.1 Polymerization of Dimethyl butadiene by free DoPAT RAFT agent.

Table3.1 RAFT Polymerization of DMB using free RAFT agents at 115° C and identical conditions.

Sample	RAFT	Initiator	[M:CAT:I]	Temp °C	Time hr	Conversion %	Mn kg/mol	Đ
1	DoPAT	DCP	600:1:0.1	115	3	8	3.6	1.21
2	MDSS	DCP	600:1:0.1	115	3	6.1	2.1	1.38
3	CDTPA	DCP	600:1:0.1	115	3	9.2	4.2	2.1

Table 3.2 RAFT Polymerization of DMB of free CDPA Using Different Initiators at Various Temperatures and Conditions.

Sample	Initiator	[M:CAT:I]	Temp °C	Time hr	Conversion %	Theoretical Mn	Mn kg/mol	Đ
1	DCP	600:1:0.1	115	24	20	9.8	7.2	1.26
2	AIBN	600:1:0.1	70	24	NR	--	---	---
3	AIBN	600:1:0.1	95	24	27	13.3	6	1.42
4	dTBP	600:1:0.1	135	24	17	8.4	11	1.43
5	DBPO	600:1:0.1	95	24	23	11.4	9.8	1.44
6	DCP	5000:1:0.1	115	40	---	---	50	1.34
7	DCP	7000:1:0.1	115	40	---	---	76.3	1.43
8	nBuLi	1500:1	40	24	---	---	15.8	1.32
9	nBuLi	3000:1	40	24	---	---	26.4	1.42

We studied the microstructure of PDMB polymerized via RAFT by NMR, which has not been reported previously. It was found that the ratio between microstructures was 97% 1,4 addition and 3% 1,2 addition, as shown in Table 3.3, Figure 3.2. The ratio of each component was close to PDMB obtained from free anionic polymerization and did not change across samples of different molecular weights although significant differences were found in the cis/trans ratios. From the NMR spectrum it was easy to determine not only the percent of 1,4 addition cis and trans and 1,2 additions, but also the distribution of dyads and triads of these structural units.[13,15] Analysis of these peaks was made by using the

following relationships relating the probabilities of occurrence of the dyads to those of the triads.

(cc) + (ct) +(tt) =1

(ccc) + (tcc) +(tct) + (ttt) +(ctt) + (ctc) =1

Table 3.3 Overall Microstructure of the Anionic and the RAFT Polymers, and Distribution of Dyads and Triads

Addition	RAFT %	Anionic %
Cis-1,4	41.7	25
Trans-1,4	55.5	72
1,2	2.8	3
Triads		
tct*	22	17
Tcc	33	7
ccc	7	2
ttt	22	42
ctt	8	28
ctc	8	4
Dyads		
tt	38	58
ct	44	35
cc	18	7

*c, 1,4-Cis, t, 1,4-Trans

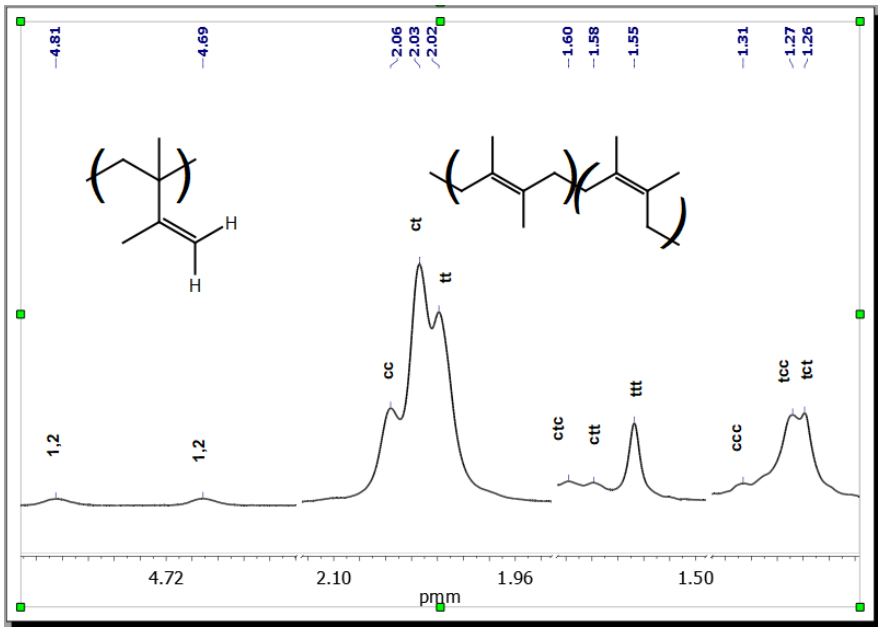

Figure 3.2 400-MHz ^{1}H NMR spectra of poly(2,3-dimethyl-1,3-butadiene)

The free RAFT polymerization of DMB was done with a mole ratio of [monomer]/[CTA]/[initiator] 600:1:0.1 at 115^{o} C under nitrogen gas. The kinetic results for the free RAFT polymerization of DMB are shown in Figure 3.3 (GPC data shown in Figure 3.4 and Table 3.4). Monomer consumption was linear with respect to time which indicates a constant radical concentration throughout the polymerization. The controlled polymerization was evidenced by the linear increase of Mn with respect to monomer conversion. Experimental molecular weights generally agreed with theoretical molecular weights, and molecular weight distributions were generally narrow (~1.21). The control of DoPAT trithiocarbonate RAFT agents agrees with previous studies on diene monomers reported by Benicewicz[21,33] and confirmed that the selected RAFT for the current studies was suitable for high-temperature RAFT polymerizations.

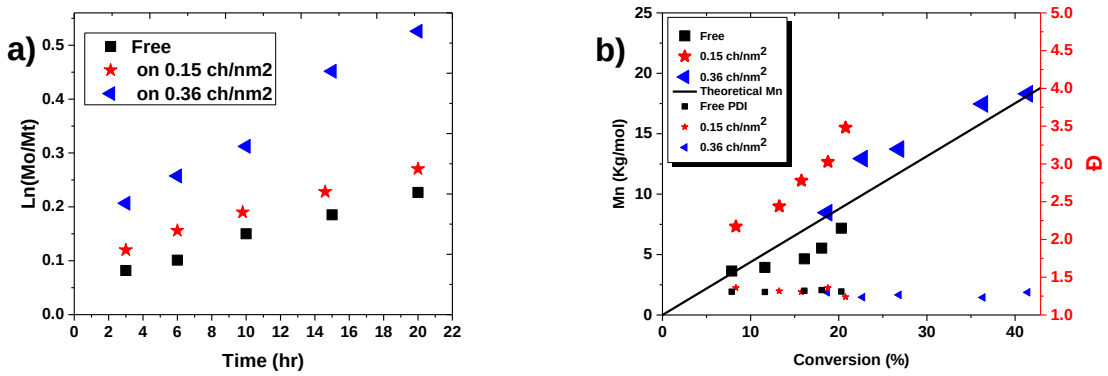

Figure 3.3 (a) First-order kinetic plots and (b) dependence of molecular weight (solid line, Mn, theory) on the conversion for the SI- RAFT polymerization of DMB on silica nanoparticles; high surface density (triangle, 85 mmol/g, 0.36 ch/nm^2); low surface density (star, 34 mmol/g, 0.15 ch/nm^2); free DoPAT, (square). All polymerization were under the same conditions [monomer]:[CTA]:[initiator] 600:1:0.1.

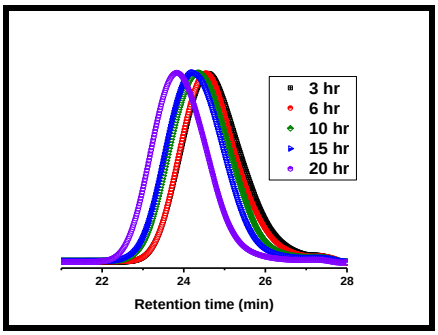

Figure 3.4 GPC traces of PDMB prepared from free RAFT polymerization

Table 3.4 The kinetic results for the free RAFT polymerization of DMB [monomer]:[CTA]:[initiator] 600:1:0.1.

Sample	Ln(M_o/M_t)	Theoretical Mn (kg/mol)	Mn (kg/mol)	PDI	Conversion %
3hr	0.078	3.5	3.6	1.38	7
6hr	0.096	5.7	3.9	1.33	11.6
10hr	0.160	7.9	4.6	1.37	16.1
15hr	0.169	8.9	5.5	1.36	18
20hr	0.203	10	7.2	1.31	20.3

Polymerization of Dimethyl Butadiene via SI-RAFT

The investigation of polymerization kinetics for DMB on the surface of silica nanoparticles, has not been previously reported. Therefore, activated DoPAT chain transfer agent was grafted on the surface of nanoparticles by the initial reaction with 3-aminopropyldimethymethoxysilane onto the particles' surface, (DoPAT-g-SiO_2) (Scheme 3.2) followed by the reaction of activated DoPAT with the amino groups attached to the NP surface. The reaction of the inert n-octyldimethylmethoxysilane was conducted to import a more soluble interface to the NP surface via the n-octyl chains. The concentration of RAFT agent on the surface of nanoparticles was determined quantitatively by comparing the absorption at about 300 nm for the DoPAT anchored silica nanoparticles to a standard absorption curve made from known amounts of the free DoPAT. With this procedure the synthesis of DoPAT-*g*-SiO_2 at two densities of 85 mmol/g (0.35 chains/nm^2) and 34 mmol/g (0.15 chains/nm^2) was conducted, and used to study the SI-RAFT polymerization of DMB.

For the surface polymerization of DMB, DoPAT-g-SiO_2 particles need to be dispersed in a solvent medium that should be a polar-nonpolar mixture to simultaneously disperse the silica particles and later be able to dissolve the nonpolar high methyl content PDMB chains and to avoid any possible gelation

that might occur. Therefore, a mixture of tetrahydrofuran (THF) was used as a suitable polar solvent for the dispersion of silica particles combined with toluene as nonpolar solvent and excess monomer that also acts as a solvent for the PDMB chains. It was found that when the (THF:Toluene) ratio (v:v) was (1:1), gelation of the polymerization did not occur.

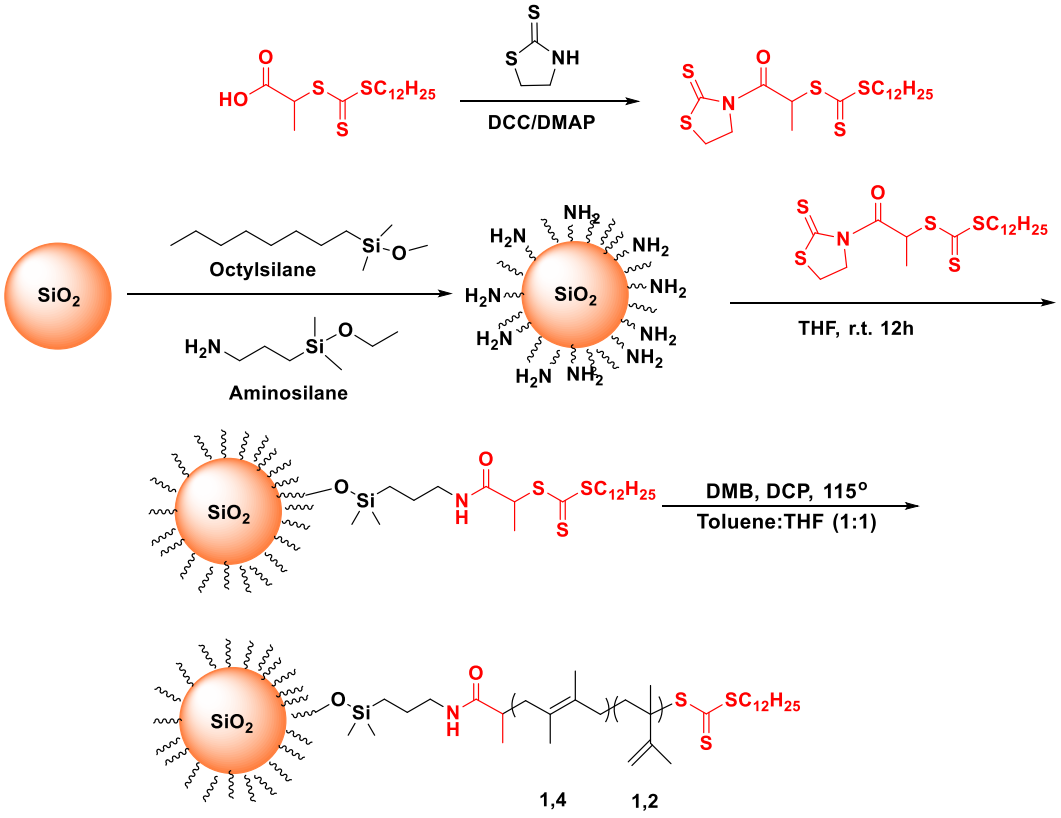

Scheme 3.2 Preparation of PDMB-*g*-SiO_2 NPs.

The SI-RAFT polymerizations of DMB were studied by using two different grafted RAFT agent densities of 85 mmol/g (0.36 chains/nm^2) and 34 mmol/g (0.15 chains/nm^2) to investigate the effect of grafting densities on the polymerization and were compared with the polymerization of free DoPAT. All

reactions were carried out under the same conditions using dicumyl peroxide as the initiator at 115° C and with the ratio between species of [monomer]:[CTA]:[initiator] of 600:1:0.1. The results of the kinetic studies for the SI-RAFT polymerization of DMB controlled by surface grafted RAFT agents are shown in Figure 3.3 (GPC data shown in Figure 3.5 and Table 3.5). The graphs show a linear relationship between monomer consumption and time for all cases over the range of conversion studied, which indicates a constant free radical concentration during the polymerization. The results also show the molecular weight increased linearly with monomer conversion for all polymerizations, measured molecular weights were in general agreement with the theoretical molecular weights, and molecular weight distributions were generally narrow (generally < 1.3). Nevertheless, the rates of the polymerizations controlled by surface grafted RAFT agents were apparently higher than the polymerization via free RAFT agent under identical conditions. From these results, we also observed that when grafted RAFT agents were present at higher graft density the polymerization rate was faster than low grafted RAFT density. This general trend is opposite that observed in the RAFT polymerization of chloroprene where the rate of polymerization was decreased with increasing RAFT agent density. In another comparison between the free and graft RAFT polymerization rates, DMB behaved similarly to isoprene where the free RAFT polymerization

rates were lower than grafted polymerization rates (Figure 3.6).[21,33] The chloroprene behavior that showed much higher rates than isoprene and DMB was ascribed to the differences in monomer reactivity because the chlorine atom

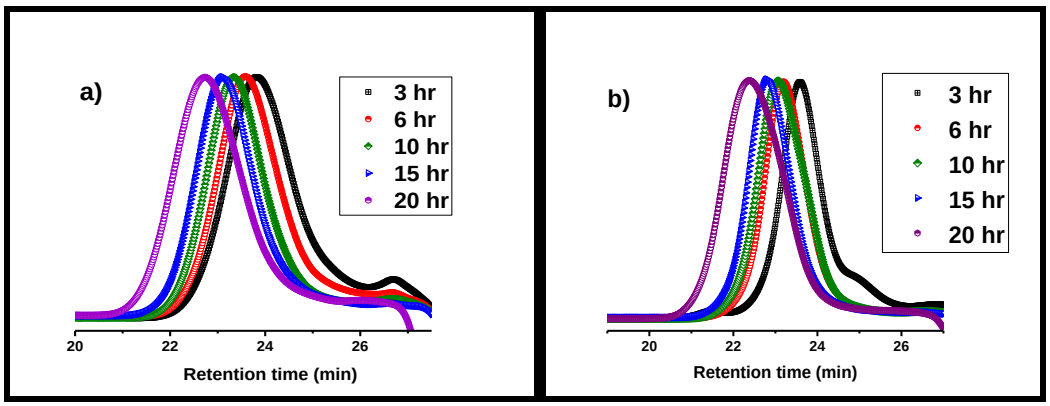

Figure 3.5 GPC traces of PDMB prepared from free RAFT-g-NPs polymerization a) 0.15 ch/nm^2, b) 0.36 ch/nm^2.

that is attached on the butadiene is electron withdrawing in nature and destabilizes the radical, thus making it comparatively more reactive. On the other hand, isoprene and DMB contain methyl groups that stabilize the radical on butadiene and will result in slower rates.[34–37] The second trend which is still not resolved is the difference between free RAFT and SI-RAFT rates because some monomers polymerize faster on particles and polymerization rates increase with increasing of grafting density.[29] Comparisons across many different monomers systems have not shown a clear trend to explain the varied behavior.

Table 3.5 The kinetic results for the RAFT-g-NPs polymerization of DMB [monomer]:[CTA]:[initiator] 600:1:0.1.

0.15 ch/nm^2					
Sample	Ln(M_o/M_t)	Theoretical Mn (kg/mol)	Mn (kg/mol)	PDI	Conversion %
3hr	0.087	3.5	7.3	1.36	8
6hr	0.14	5.7	8.9	1.31	13
10hr	0.17	7.9	11.1	1.31	16
15hr	0.21	8.9	12.7	1.36	19
20hr	0.24	10	16.5	1.43	20
0.36 ch/nm^2					
Sample	Ln(M_o/M_t)	Theoretical Mn (kg/mol)	Mn (kg/mol)	PDI	Conversion %
3hr	0.21	3.5	8.5	1.3	18.6
6hr	0.26	5.7	13	1.23	22.7
10hr	0.31	7.9	13.7	1.27	26.8
15hr	0.45	8.9	17.5	1.23	36.3
20hr	0.53	10	20.4	1.31	41.4

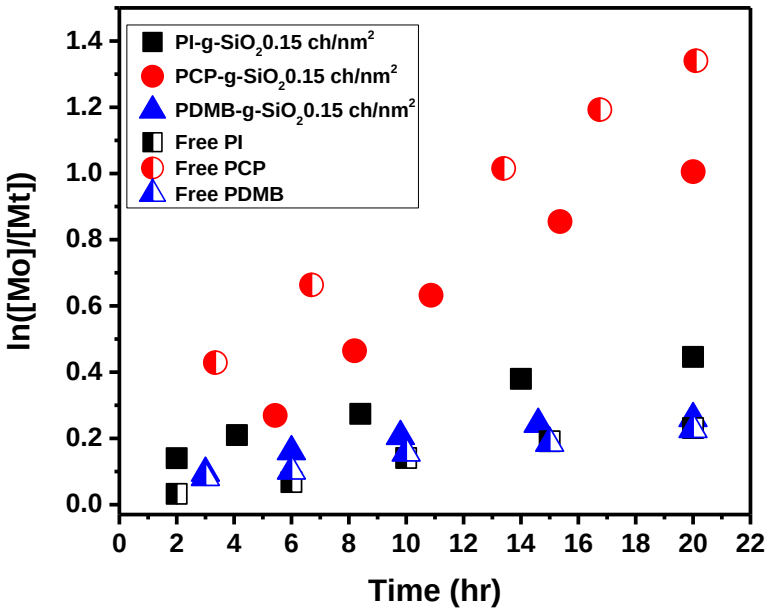

Figure 3.6 Rate of free RAFT polymerization and on 0.15 ch/nm^2 SiO_2 NPs of Isoprene, Chloroprene, and Dimethyl butadiene monomers.

Mechanical properties of matrix-free PDMB-*g*-SiO_2 NPs composites

The investigation of the mechanical properties of matrix-free PDMB grafted silica nanoparticle composites was done by preparing a series of nanocomposites from NPs with the two graft densities (0.15 ch/nm^2 and 0.02 ch/nm^2), and varying molecular weights of grafted polymer. The details of the samples are listed in Table 3.6. The PDMB-g-SiO_2 NPs were crosslinked as matrix-free composites by using dicumyl peroxide as crosslinking agent in solution and then the solvent was allowed to evaporate under vacuum. Dried samples were hot pressed at 160^{o}C for 25 min to obtain vulcanized rubber sheet of 0.4 mm thickness.

Table 3.6 Sample details of matrix-free PDMB-g-SiO_2 NPs composites

Sample name	Graft density (ch/nm^2)	Mn (kg/mol)	Silica Wt%	Tensile strength (MPa)	Elongation at break (mm/mm)	Hardness Shore °A
Unfilled	N/A	50k	0	0.62±0.004	0.32±0.04	51±2
24k	0.02	24k	67	1.90±0.31	0.047±0.001	95.5±1.5
42k	0.02	42k	60	3.52±0.31	0.82±0.21	88±2.5
94k	0.02	94k	49.6	3.07±0.45	1.69±0.26	75±2
35k	0.15	35k	41	1.30±0.32	0.72±0.15	80±1.5
46k	0.15	46k	26	0.85±0.08	0.57±0.11	76±1.5

Matrix-free nanocomposites have a dispersion advantage compared to traditional composites that are prepared by blending rubber directly with the nanoparticle. Traditional composite synthesis procedures require the mixing of particles with the polymer matrix, which introduces agglomeration of particles particularly with high nanoparticle loadings due to undesirable interface compatibility.[38–40] The grafted nanoparticles are separated from each other by the polymer brushes that were polymerized on the surface of these particles. Thus, good dispersion can be created and maintained in these systems.[28] As shown in Figure 3.7, good particle dispersion was achieved with both 42k PDMB-g-SiO_2 NPs 0.02 ch/nm^2, 60 silica wt%, and 46k PDMB-g-SiO_2 NPs 0.15 ch/nm^2, 26 silica wt%. There was no significant agglomeration of particles even at high silica loading. However, there was no well-defined organization of the nanoparticles

and d-spacing was not uniform, which is most likely due to the large size disparity of the core silica particles.[21]

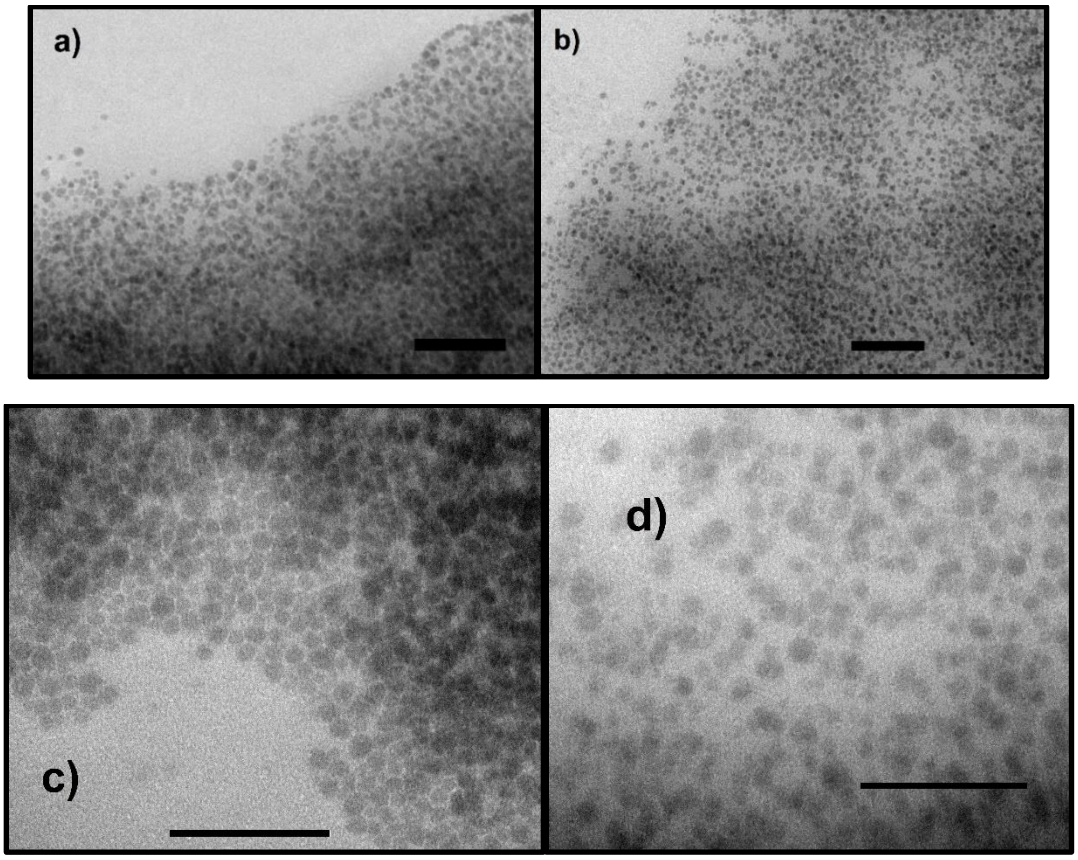

Figure 3.7 TEM image of a,c) 42k PDMB-g-SiO_2 NPs 0.02 ch/nm^2 60 silica wt%, b,d) 46k PDMB-g-SiO_2 NPs 0.15 ch/nm^2 26 silica wt% (all images are 200 nm scale bar)

To confirm the dispersion state of nanoparticles in matrix-free of the crosslinked samples, Small-angle X-ray scattering (SAXS) (Figure 3.8) was used to obtain more information. No agglomeration was detected from the X-ray scattering pattern at low q. The intensity of all the peaks was relatively weak, indicating a broad distribution of interparticle spacing. The location of the peak changed between the samples dependent upon the grafting density, for 0.02

ch/nm^2 the q value was approximately 0.04 A^{-1} which corresponds to a d spacing of ~15 nm, but for particles with 0.15 ch/nm^2 the q value was approximately 0.02 A^{-1} which corresponds to a d spacing of ~31 nm. The difference in a d spacing seems reasonable considering the low graft density particles have more space on the surface for chains to collapse, while the higher graft density chains are more extended would push the particles farther apart.

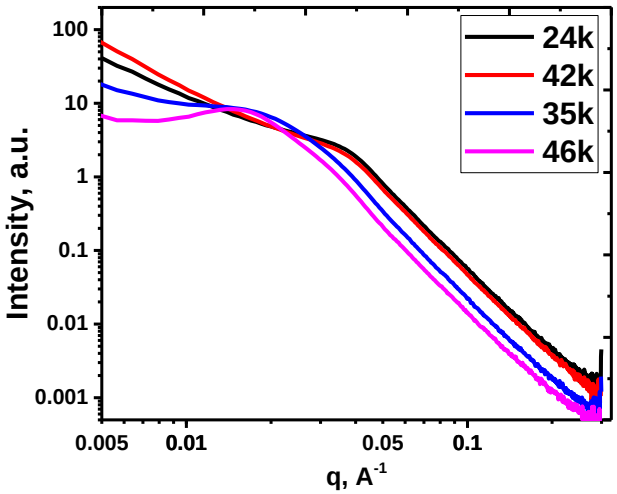

Figure 3.8 Representative small-angle X-ray scattering (SAXS) intensity curves for matrix-free PCP grafted silica nanocomposites.

At constant strain and frequency, dynamic mechanical behavior was measured (Figure 3.9) for the crosslinked silica nanocomposites and the crosslinked unfilled polymer. The glass transition temperature of the matrix-free composites was not altered compared with unfilled PDMB as observed in Figure 3.9 a. It is apparent the reduction of tan delta peak height increased with silica

loading, which may suggest a better reinforcing effect and stronger rubber-filler interaction at high silica loading.[41,42] As shown in Figure 3.9 b at low temperatures below the Tg, the effect of the silica on storage modulus is distinctly observed although the molecular chain segments are frozen in this region. In the rubbery plateau region above Tg, matrix-free silica composites also had higher storage modulus relative to the unfilled polymer. For all matrix-free composites, the storage modulus increasing silica loading.

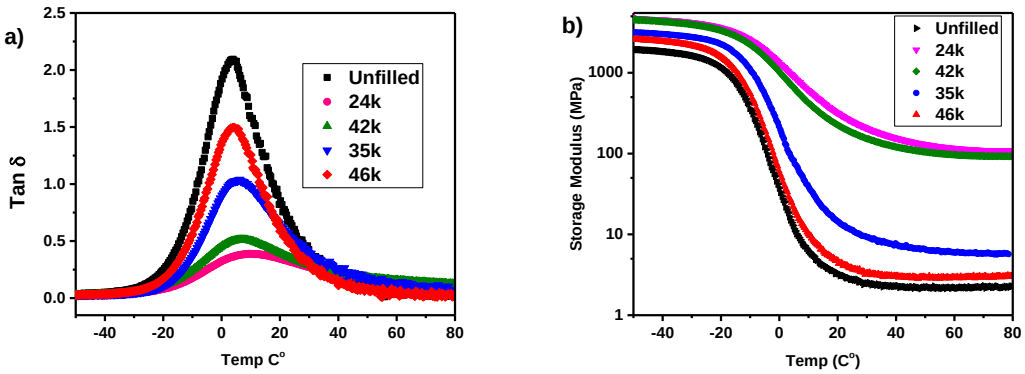

Figure 3.9 Temperature dependence of storage modulus and Tan delta of crosslinked unfilled and matrix-free PDMB silica nanocomposites.

The crosslinked matrix-free nanocomposite sheets were cut into dog-bones for standard mechanical property tests. It was found that the properties of the composites were directly related to the grafting density and silica loading of the nanocomposites. All the matrix-free composites had significantly improved tensile strength compared with unfilled PDMB (Figure 3.10). In addition to that, the tensile stress at break increased with silica loading and this general trend is

consistent with previous literature that tensile strength generally increases continuously with increasing inorganic filler loading. Matrix-free nanocomposite systems were tested at two graft densities, and the increase in molecular weight of the grafted polymers causes a decrease in silica loading at a fixed graft density. At low graft density (0.02 ch/nm^2), we observed a significant effect of chain molecular weight on the stress-strain behavior. The composite with 24k molecular weight chains was quite brittle and broke at ~4.7% elongation. At the same graft density, the composite with 42k molecular weight chains displayed clear yield behavior and failed at 82% elongation, indicating a much tougher material. We believe this is due to almost solely to a chain entanglement.

At higher chain densities (0.15 ch/nm^2), the 35k and 46k molecular weight grafts may be too crowded and at these intermediate chain lengths, are limited in their ability to entangle. Thus, lower tensile strengths were observed, although they still were improved as compared to the unfilled crosslinked polymer.

The final example in this data set is a low graft density sample (0.02 ch/nm^2) which had 94k molecular weight chains. This crosslinked sample displayed yield behavior, a high elongation at break (and toughness), and a high tensile stress at break. This is interpreted as a result maximizing chain

entanglement by the combination of high molecular weight chains and low graft density. [24,39,43]

Also, from Table 3.6 the results of hardness testing show good improvement on the final composites (Figure 3.10 b). The increase in silica loading led to an increase in the hardness of the surface, with a clear distinction between filled and unfilled composites. Overall, with the data set obtained this far, it appears that the hardness values appear to scale linearly with the silica content of the composites. Additional work would be needed to the test for the perhaps more subtle effects of chain density or chain length.

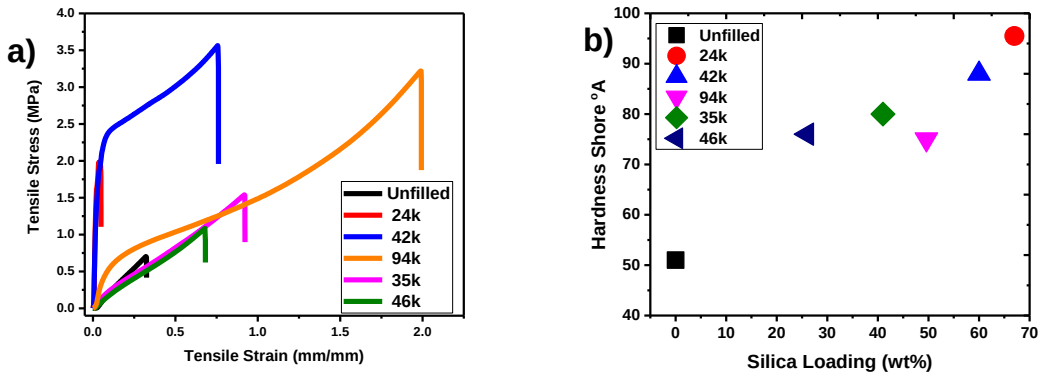

Figure 3.10 a) Stress-strain curves of crosslinked unfilled and filled nanocomposites, b) hardness of crosslinked unfilled and filled nanocomposites

3.5 Conclusion

A facile method was demonstrated for the polymerization of free dimethyl butadiene and dimethyl butadiene grafted on silica NPs using free RAFT and surface-initiated RAFT polymerization techniques, respectively. A high

temperature stable free chain transfer agent (DoPAT) was used to perform both free polymerization and SI-RAFT polymerization on the surface of silica particles with controllable graft densities. Controlled radical polymerizations were conducted to produce polymers with low dispersities and predictable molecular weights, and it was found that the surface anchored DoPAT showed excellent control over the surface graft polymerization of DMB. The microstructure of synthesized polymer was almost same ratios of (1,4) to (1,2) additions in both free and SI-RAFT polymerizations. Interestingly, the cis/trans ratios were different than the polymer prepared from anionic polymerization. The polymerization kinetics were studied, and it was found that the SI-RAFT polymerization rate was dependent on the graft density and generally faster than free polymerization mediated by free RAFT agent. Furthermore, when compared to previous studies DMB polymerization was found to have a similar rate as isoprene and much slower than chloroprene both free RAFT and SI-RAFT polymerizations. The PDMB-*g*-SiO_2 NPs were directly crosslinked to form matrix-free nanocomposites that showed good particle dispersion and improved mechanical properties compared to unfilled PDMB. These strong, tough composite materials could be useful in many applications that require these improved properties.

3.6 References

(1) Wolf, H.; Ralph, W. *Rubber - A Story of Glory and Greed*; New York, **1936**.

(2) Griesbaum, K.; Behr, A.; Biedenkapp, D.; Voges, H.-W.; Garbe, D.; Paetz, C.; Collin, G.; Mayer, D.; Hoke, H. *Ullmann's Encycl. Ind. Chem*. 1 **2000**, *18* (2), 133–189.

(3) Harp, S. L. A *World History of Rubber: Empire, Industry, and the Everyday*; **2016**.

(4) Morton, M.; Gibbs, W. E. *J. Polym. Sci. Part A Gen. Pap.* **1963**, *1* (8), 2679–2695.

(5) Kyriakides, L. P. *J. Am. Chem. Soc*. **1914**, *36* (5), 987–1005.

(6) YEN, T. F. *J. Polym. Sci.* **1958**, *35* (129), 533–543.

(7) YEN, T. F. *J. Polym. Sci*. **1959**, *38* (133), 652–656.

(8) Schrock, R.; McLain, S.; Sancho, *J. Pure Appl. Chem.* **1980**, *52* (3), 729–732.

(9) Wreford, S. S.; Fischer, M. B.; Datta, S. *J. Organometal. Chem*. **1980**, *188*, 353–366.

(10) Cataldo, F.; Ragni, P.; Ursini, O.; Angelini, G. *Radiat. Phys. Chem*. **2008**, *77* (8), 941–948.

(11) Wendell, C. B. A *study of 2,3-dimethyl butadiene-1,3 and related compounds*, University of Massachusetts Amherst, PhD Thesis, **1933**.

(12) Ying, W. Bin; Jang, J. U.; Lee, M. W.; Yang, H. S.; Moon, D. S.; Lee, K. J.; Lee, B. *Polym. (United Kingdom)* **2016**, *101*, 158–167.

(13) Blondin, D.; Regis, J.; Prud'homme, J. *Macromolecules* **1974**, *7* (2), 187–189.

(14) Uemura, T.; Nakanishi, R.; Mochizuki, S.; Murata, Y.; Kitagawa, S. *Chem. Commun*. **2015**, *51* (48), 9892–9895.

(15) Cordoneanu, A.; Baird, M. C. *Macromolecules* **2004**, *37* (18), 6744–6747.

(16) Moad, G. *Macromol. Chem. Phys*. **2014**, *215* (1), 9–26.

(17) Wei, R.; Luo, Y.; Zeng, W.; Wang, F.; Xu, S. *Ind. Eng. Chem. Res*. **2012**, *51*, 15530–15535.

(18) Faraji, S.; Yardim, M. F.; Can, D. S.; Sarac, A. S. *J. Appl. Polym. Sci*. **2017**, *134* (2), 1–10.

(19) Merza, K. S.; Al-Attabi, H. D.; Abbas, Z. M.; Yusr, H. A. *Green Sustain. Chem.* **2012**, *2* (February), 26–28.

(20) Natarajan, B.; Neely, T.; Rungta, A.; Benicewicz, B. C.; Schadler, L. S. *Macromolecules* **2013**, *46* (12), 4909–4918.

(21) Zheng, Y.; Abbas, Z. M.; Sarkar, A.; Marsh, Z.; Stefik, M.; Benicewicz, B. C. *Polymer (Guildf)*. **2018**, *135*, 193–199.

(22) Huang, Y.; Zheng, Y.; Sarkar, A.; Xu, Y.; Stefik, M.; Benicewicz, B. C. *Macromolecules* **2017**, *50* (12), 4742–4753.

(23) Kumar, S. K.; Benicewicz, B. C.; Vaia, R. A.; Winey, K. I. *Macromolecules* **2017**, *50* (3), 714–731.

(24) Poochai, C.; Pae-on, P.; Pongpayoon, T. *Int. Sch. Sci. Res. Innov*. **2010**, *4* (5), 969–973.

(25) Akcora, P.; Liu, H.; Kumar, S. K.; Moll, J.; Li, Y.; Benicewicz, B. C.; Schadler, L. S.; Acehan, D.; Panagiotopoulos, A. Z.; Pryamitsyn, V.; Ganesan, V.; Ilavsky, J.; Thiyagarajan, P.; Colby, R. H.; Douglas, J. F. *Nat. Mater*. **2009**, *8* (4), 354–359.

(26) Stefik, M.; Guldin, S.; Vignolini, S.; Wiesner, U.; Steiner, U. *Chem. Soc. Rev.* **2015**, *44* (15), 5076–5091.

(27) Zhao, D.; Di Nicola, M.; Khani, M. M.; Jestin, J.; Benicewicz, B. C.; Kumar, S. K. *ACS Macro Lett.* **2016**, *5* (7), 790–795.

(28) Li, Y.; Krentz, T. M.; Wang, L.; Benicewicz, B. C.; Schadler, L. S. *Appl. Mater. Sci.* **2014**, *6* (9), 6005–6021.

(29) Li, C.; Han, J.; Ryu, C. Y.; Benicewicz, B. C. *Macromolecules* **2006**, *39* (9), 3175–3183.

(30) Chiang, W.-L.; Hsieh, H. C.-C.; Tsiang, R. C.-C. *J. Polym. Res.* **1998**, *5* (4), 227–232.

(31) Moad, G. *Polym. Int.* **2017**, *66* (1), 26–41.

(32) Keddie, D. J.; Moad, G.; Rizzardo, E.; Thang, S. H. *Macromolecules* **2012**, *45* (13), 5321–5342.

(33) Khani, M. M.; Abbas, Z. M.; Benicewicz, B. C. *J. Polym. Sci. Part A Polym. Chem*. **2017**, 1–9.

(34) Poutsma, M. L. *J. Org. Chem*. **2011**, *76* (1), 270–276.

(35) Fellows, C. M.; Senogles, E. *Eur. Polym. J*. **2003**, *39* (7), 1509–1513.

(36) Bamford, C. H.; Jenkiins, A. D.; Johnston, R. *Trans. Faraday Soc*. **1958**, *55*, 418–432.

(37) Bamford, C. H.; Jenkins, a. D. *Trans. Faraday Soc*. **1963**, *59* (2), 530.

(38) Kapgate, B. P.; Das, C.; Das, A.; Basu, D.; Wiessner, S.; Reuter, U.; Heinrich, G. *J. Appl. Polym. Sci*. **2016**, *133* (30), 1–10.

(39) Bansod, N. D.; Kapgate, B. P.; Das, C.; Basu, D.; Debnath, S. C.; Roy, K.; Wiessner, S. *RSC Adv.* **2015**, *5* (66), 53559–53568.

(40) Hooper, J. B.; Schweizer, K. S. *Macromolecules* **2006**, *39* (15), 5133–5142.

(41) Stojanovic, D.; Orlovic, A.; Glisic, S. B.; Markovic, S.; Radmilovic, V.; Uskokovic, P. S.; Aleksic, R. *J. Supercrit. Fluids* **2010**, *52* (3), 276–284.

(42) Kumnuantip, C.; Sombatsompop, N. *Mater. Lett*. **2003**, *57* (21), 3167–3174.

(43) Sae-oui, P.; Sirisinha, C.; Thepsuwan, U.; Hatthapanit, K. *Eur. Polym. J.* **2007**, *43* (1), 185–193.

CHAPTER 4

REINFORCEMENT OF POLYCHLOROPRENE BY GRAFTED SILICA NANOPARTICLES

4.1 Abstract

Reversible addition-fragmentation chain transfer polymerization of chloroprene on the surface of silica nanoparticles was performed to obtain polychloroprene-grafted-silica nanoparticles (PCP-g-SiO_2 NPs). These particles were dispersed in a commercial polychloroprene matrix to obtain PCP nanocomposites with different silica core loadings (1, 5, 10, and 25 wt%). Two different chain graft densities were studied ("low," 0.022 ch/nm^2 and "high," 0.21 ch/nm^2) as a function of the grafted polymer molecular mass. The cured samples showed significant improvement in the mechanical properties of the PCP rubber nanocomposites as compared to the unfilled PCP as measured by standard tensile and dynamic mechanical analysis even with low silica content. The mechanical properties of the nanocomposites were notably enhanced when the graft density was low and molecular masses were high. The interaction between the rubber and SiO_2 NPs was explored by FTIR. The dispersion of nanoparticles was investigated by transmission electron microscopy (TEM), and Small-Angle X-ray Scattering (SAXS).

4.2 Introduction

Mechanical reinforcement of rubber materials by inorganic fillers has been practiced for many years.[1–5] Carbon black and metal oxides are the most popular

types of fillers that have been used in rubber nanocomposites.[6–10] One of the most common strategies employed for enhancing the dispersion of the inorganic fillers particles in the polymer is to enhance their miscibility with the polymer matrix, and these interactions between the inorganic fillers and polymeric matrix exert a strong influence on the properties of the final composite.[11] One of the leading research areas in using inorganic fillers in rubbery matrices has been to lower the phase separation of the inorganic particles.[12] Many early attempts used modified fillers containing some organic functional groups that were miscible or could react with the matrix to minimize the agglomeration of the fillers. More recent efforts have carefully examined many molecular variables such as graft chain density, particle loading and ligand choice which can influence the composite properties.[13–15] The reinforcements of the rubber materials have been focused on the improvement of stiffness, modulus, rupture energy, tear strength, tensile strength, cracking resistance, fatigue resistance, and abrasion resistance.[16]

A critical aspect of the presence of a filler is the strength of interaction between a chemically grafted filler particle and the matrix.[17] The major factors that control the reinforcing mechanism of inorganic fillers in rubber matrices are the dispersion into the matrix and the interaction between rubber and fillers.[18] Various functional groups have been used to passivate the surface of the inorganic fillers including silanes, phosphonates, amines, hydroxides, and alkyl

groups. However, many of the previous studies still resulted in agglomeration and aggregation of the fillers due to particle-matrix incompatibility.[19,20]

Polychloroprene (PCP) was discovered by Dupont (1931) and has been widely used in the rubber industry.[21] It can be vulcanized with sulfur, organic peroxides and metal oxides to produce sheets and films with good elasticity, perspiration, resistance to oil and various solvents, excellent weatherability, and excellent thermal and thermoxidative stability.[22] It is particularly noted for its durability when exposed to multiple degradation modes.

In this work, silica nanoparticles with grafted PCP chains were used as hybrid fillers in PCP matrices to improve the composite properties. Strong rubber-filler interactions lead to increased strength in rubber composites. A bound rubber model was suggested in several reports where tightly and loosely bound rubber, surrounding the filler particles, had been shown to act as an additional crosslink mechanism in the rubber matrix.[19,23] Bound rubber represents the bonds of rubber chains to the inorganic particles being strong enough to persist in the final composite.[7,23] However, most studies focus on the use of small surface functional groups to enhance the interactions. Our previous work has shown that the molecular weight and graft density of grafted chains can also be used to control the dispersion of nanoparticles in polymer matrices,

as well as the strength of interactions.[25-27] To expand on this concept in the current study, we explored two different polymer graft densities, four silica loading levels (1, 5, 10, 25 wt%) and a broad range of grafted molecular weights (34.8-161 kg/mol). The use of these grafted nanoparticles in cured composites showed improvements for filled samples even at low silica loadings (1 wt%). Furthermore, the high grafted molecular weights (161 kg/mol and 134 kg/mol) enhanced the final composite properties more than low grafted molecular weights (38 kg/mol and 34.8 kg/mol), and the low graft densities (0.022 ch/nm^2) were better than the high graft densities (0.21 ch/nm^2).

4.3 Materials and Methods:

Materials. Chloroprene monomer was prepared through dehydrochlorination of 3,4-dichloro-1-butene purchased from TCI America.[16,28] The RAFT agent 2-methyl-2-(dodecylsulfanylthiocarbonyl)sulfanyl] propanoic acid (MDSS) (97%) was purchased from Strem Chemicals and used as received. Spherical silica nanoparticles (SiO_2) with a diameter of 14 ± 4 nm were purchased from Nissan Chemical Co. Tetrahydrofuran (THF) (HPLC grade, Fisher), aminopropyldimethylethoxysilane (APS), octyldimethylethoxysilane (ODMES) and octadecyldimethylethoxysilane (C18) were purchased from Gelest (95%) and used as received. 2.2'-Azobisisobutyronitrile (AIBN) was purified by

recrystallization from methanol and dissolved in THF to make a 10mM solution. PCP 150K was purchased from Sp2 polymers. All other reagents were used as received.

Synthesis of alkyl silane-grafted-SiO_2 (C18 NPs). A solution (10 mL) of colloidal silica particles (30 wt % in methyl isobutyl ketone) was added to a 250 mL round bottom (r.b.) flask equipped with a condenser and diluted with 30 mL of THF. Octadecyldimethylethoxysilane (C18) (1 g, 2.92 mmol) was added to the mixture and refluxed in a 75 °C oil bath for 12 hours under flowing nitrogen. The reaction was then cooled to room temperature (r.t.) and precipitated in methanol (120mL). The particles were recollected by centrifugation (5000 rpm) and dispersed in THF using sonication (5 min) and precipitated in methanol again. The C18-functionalized particles were then dispersed in 40 mL of THF.

Synthesis of Chloroprene Monomer. For the synthesis of chloroprene monomer, NaOH (16 g, 0.404 mol) and PTC (4.35 g, 0.0134 mol) in 65 ml of water were charged to a 250 mL three-necked round bottom flask. A condenser was fitted, and the mixture was stirred and heated. At 55° C, 3,4-dichloro-1-butene (25 g, 0.2 mol) was added dropwise over five minutes. Heating was continued at 60-75 °C for two hours and the product distilled as a hazy liquid. Drying over $MgSO_4$ yielded a clear, colorless liquid. Chloroprene monomer is self-polymerizing

under ambient conditions and was stabilized by adding 0.1% (w/w) phenothiazine stabilizer to the dried product and the solution purged with nitrogen. Yield 74%. ^{1}H NMR (400 MHz, $CDCl_3$) δ 5.04 (2H, m, C**H**$_2$=CH), 5.34 (2H, dd, C**H**$_2$=CCl), 6.32 (1H, t, CCl-C**H**,). HRMS (EI) (m/z) calcd. for C_4H_5Cl: 88.0080; found: 88.0091.

Activation of 2-Methyl-2-[(dodecylsulfanylthiocarbonyl) sulfanyl]propanoic acid (MDSS). The procedure for the activation of MDSS is given below, similar to that previously reported.[3] MDSS (2 g, 5.49 mmol), N,N'-dicyclohexylcarbodiimide (1.24 g, 6.03 mmol) and 2-mercaptothiazoline (0.718 g, 6.03 mmol) were dissolved in dichloromethane (40 mL) in a 100 mL r.b. flask under a nitrogen stream. After 10 min at r.t., a solution of 4-dimethylaminopyridine (0.067 g, 0.549 mmol) dissolved in dichloromethane (2 mL) was added to the mixture and the nitrogen flow was removed. After 5 h at r.t., the mixture was filtered, and the solvent evaporated using a rotary evaporator. The product was purified by column purification using a silica column with 5:4 ethyl acetate:hexane. Yields are usually greater than 80%, m.p. 34-34˚C, ^{1}H NMR (400 MHz, $CDCl_3$) δ 3.21 (2H, t, S-C**H**$_2$-$(CH2)_{10}$-CH_3), 1.6 (6H, s, C-(C**H**$_3$)$_2$), 1.19-1.31 (16H, t, -(C**H**$_2$)$_8$-CH_3), 1.58 (2H, m, C**H**$_2$-$(CH_2)_8$-CH_3), 2.06 (2H, m, -C**H**$_2$-CH_2-$(CH_2)_8$-CH_3) 0.81 (3H, t, SCH_2-$(CH2)_{10}$-C**H**$_3$), 3.51 (2H, t, N-C**H**$_2$-CH_2-S), 3.91 (2H, t, S-C**H**$_2$-CH_2-N) GS-MS: 464.11, Elemental Analysis: calcd: C,

51.57; H, 7.57; N, 3.01; O, 3.43; S, 34.41, found: C, 53.08; H, 7.68; N, 2.67; O, 3.76; S, 32.41.

Synthesis of MDSS-g-SiO_2. A solution (10 mL) of silica nanoparticles (30 wt % in methyl isobutyl ketone) was added to a 100 mL r.b. flask and diluted with 15 mL of THF. Octyldimethylethoxysilane (ODMES) (0.3 mL, 1.21 mmol) was added to the mixture and refluxed in a 75°C oil bath for 12 hours under flowing nitrogen. The reaction was cooled to r.t. and precipitated in hexanes (120mL). The particles were recollected by centrifugation and dispersed in THF (20 ml) using sonication and precipitated in hexanes again. The ODMES-functionalized particles were dissolved in THF (20 mL), combined with 3-aminopropyldimethylethoxysilane (0.3 mL, 1.59 mmol) and the mixture was refluxed in a 75°C oil bath for 3 hours under flowing nitrogen. The reaction was then cooled to r.t. and precipitated in hexanes (120mL). The particles were recollected by centrifugation and dispersed in THF using sonication and precipitated in hexanes again. The amine-functionalized particles were dispersed in 40 mL of THF for further reaction. Then 0.2 g (0.4 mmol) of activated MDSS was added dropwise to a THF solution of the amine functionalized silica nanoparticles (40 mL, 6 g) at r.t. After complete addition, the solution was stirred overnight. The reaction mixture was then precipitated into 400mL of hexanes. The particles were recollected by centrifugation at 3000 rpm for 8 min. The

particles were redispersed in 30 mL THF and precipitated in hexanes. This dissolution-precipitation procedure was repeated 2 more times until the supernatant layer after centrifugation was colorless. The yellow MDSS-anchored silica nanoparticles were dried under vacuum at r.t. and analyzed using UV analysis to determine the chain density using a calibration curve constructed from standard solutions of free MDSS.[29–31]

Procedures of surface-initiated RAFT polymerization of chloroprene. The polymerization of chloroprene (1g) with MDSS-g-SiO_2 as the RAFT agent (0.22g 0.21ch/nm^2), AIBN (114ul from 10 mM stock solution) with reaction ratio [1000:1:0.1, (monomer: CTA: initiator)] and THF (3ml) were added and mixed well in a Schlenk tube. The mixture was degassed by three freeze-pump-thaw cycles, filled with nitrogen, and the Schlenk flask was placed in an oil bath at 60°C for 48 hours. The resulting PCP grafted particles were precipitated into a large amount of methanol and centrifuged at 8,000 rpm for 10 min and redispersed in THF. After cleaving the chains from the silica NPs, the molecular weight of the grafted chains was 38 kg/mol. Different molecular weights were synthesized by varying the [monomer: CTA: initiator] ratio and time.[32]

Procedure for cleaving grafted polymer from particles. PCP-g-SiO_2 particles (20 mg) were dissolved in 2mL of THF. Aqueous HF (49%, 0.2 mL) was added, and

the solution was stirred overnight at r.t. The solution was poured into a PTFE Petri dish and allowed to stand in a fume hood overnight to evaporate the volatiles. The recollected PCP was then subjected to GPC analyses.

Nanocomposite preparation. 1g of PCP matrix was dissolved in 30mL of THF and mixed with different loadings of core SiO_2 NP (1, 5, 10, and 25 wt%). Thermogravimetric analysis was used to estimate the neat weight of grafted PCP on SiO_2 NP, then the needed free PCP weight of matrix was added to match projected silica loadings.

Curing process of PCP nanocomposites. A solvent mixing technique was used to cure the PCP by adding curing agents. The chloroprene polymer was cured using zinc oxide (5phr), magnesium oxide (2phr), N-phenylnaphthalen-2-amine (2phr), stearic acid (0.5phr), and 2-mercaptothiazoline (0.5phr) in THF. After evaporating the solvent samples were hot pressed at 160° for 25 minutes to obtain vulcanized rubber sheet of 0.4 mm thickness.[33]

Characterization Techniques

Molecular weights. Molecular weights (Mn) and dispersities (*Đ*) were determined using a Varian 290 LC gel permeation chromatography (GPC) with a 390 LC multidetector unit, and three Styragel columns. The columns consisted of HR1, HR3, and HR4 in the effective molecular weight ranges of 100-5000, 500-

30000, and 5000-500000, respectively. THF was used as eluent at 30°C and the flow rate was adjusted to 1.0mL/min. Molecular weights were calibrated with poly(styrene) standards obtained from Polymer Laboratories.

FTIR Spectroscopy. FTIR spectra of the prepared rubber samples were recorded in attenuated total reflectance mode (ATR) using a BioRad Excalibur FTS3000 spectrometer. All measurements were recorded in the scan range of 400 cm^{-1} – 4000 cm^{-1}.

Transmission Electron Microscopy. The Transmission Electron Microscopy (TEM) was performed on a Hitachi H8000 TEM at an accelerating voltage of 200 kV. The samples were prepared by cryoultramicrotomy sectioning of crosslinked samples in a solution of H_2O:DMSO 30:70, then placed on copper grids. The image was acquired in bright field mode using on objective aperture and a XYZ detector.

Dynamic Mechanical Analysis. Dynamic mechanical analysis was performed with an Eplexor 2000N dynamic measurement system (TA, ARES-RSA3) using a constant frequency of 10 Hz in a temperature range -80 ^{o}C to 80 ^{o}C. The analysis was done in tension mode. For the measurement of the complex modulus, E*, a static load of 1% pre-strain was applied and the samples oscillated to a dynamic

load of 0.5% strain. Measurements were done with a heating rate of 3° C/min under nitrogen flow.

Strain amplitude sweep test. In the strain sweep test, the frequency is set at a constant 1 rad s^{-1} while the strain is swept from 0.01% to 100% at 25 °C. Samples were cut into square shapes with dimensions of 16.5 x 8 mm with 0.4mm thickness.

Stress-Strain Analysis. Tensile tests of samples were carried out using an Instron 5543A material testing machine with crosshead speed 20 mm/min (ASTM D412, ISO 527). Samples were cut into standard dumbbell shapes with neck cross-section dimensions of 5 x 22 mm with 0.4mm thickness. At least five measurements were recorded, and the average values were reported.

Swelling Measurements. Swelling of the PCP composites was accomplished by soaking the cured sheet of rubber in toluene for seven days at r.t. During the seven days, the toluene was changed daily using fresh toluene. The rubber sheets were removed after seven days and residual solvent on the surface was removed using lab wipes. The weights of the sheets were measured using an analytical balance directly after removal from the residual solvent. The degree of swelling (Q) was determined by the following eq.[34]

$$Q\ (\%) = \frac{Ws - Wo}{Wo} * 100 \qquad (1)$$

Where, Ws is the weight of the sample after swelling and Wo is the weight of sample the before swelling.

Crosslink density. The crosslink density is the number of effectively elastic chains per unit volume, and can be obtained using the Flory-Rehner eq.[35,36]

$$v = -[\ln(1 - Vr) + Vr + \chi Vr^2]/Vt(Vr^{\frac{1}{3}} - \left(\frac{Vr}{2}\right)) \qquad (2)$$

Where Vr is the volume fraction of rubber in the swollen state, Vt is the molar volume of toluene (106.2), χ is the effective interaction parameter (CR-toluene), which is (0.342) for the CR-toluene system. All reported values were the average of five test samples after immersion in toluene at 22 °C for one week, and the solvent was replaced daily.

Small-Angle X-ray Scattering (SAXS). X-ray experiments were conducted using a SAXS Lab Ganesha instrument at the South Carolina SAXS Collaborative. A Xenocs GeniX3D microfocus source was used with a Cu target to generate a monochromic beam with a 0.154 nm wavelength. The instrument was calibrated using National Institute of Standards and Technology (NIST) reference material 640c silicon powder with the peak position at 2θ=28.44° where 2θ is the total scattering angle. A Pilatus 300 K detector (Dectris) was used to collect the two-dimensional (2D) scattering patterns. All SAXS data were acquired with an X-ray flux of ~4.1 M and ~21.4 M photons/s incident upon the samples. All data were

acquired by 10-15 minutes measurements. Transmission SAXS was measured normal to sample substrates to observe the purely in-plane morphology. These 2D images were azimuthally integrated to yield the scattering vector and intensity.

Energy-dispersive X-ray spectroscopy. (EDS): EDS spectra were collected using a FEI Talos F200X S-TEM Microscope operating at an accelerating voltage of 200 kV and equipped with a Bruker super-X EDS system with 4 symmetric silicon drift detectors (SDD). Images were collected using STEM high-angle annular dark field (HAADF) imaging on microtomed slices 60 nm thick. The corresponding EDS data was collected in two steps – a spectral scan (3 minutes) for determining the elements present by measuring the Kα and Lα electron energies and mapping (7 minutes) to determine the distribution within the area of interest. All scans were done with either a magnification of 28500x or 40000x.

4.4 Results and Discussion

Generally, all fillers that disperse in a rubber interact and play a a significant role in the mechanical properties of the elastomeric composites. Our previous work showed that we could controllably polymerize chloroprene from the surface of silica NPs and preliminary mechanical properties were reported on samples made at a single chain density using matrix free composites only.[3] In

this work, a more detailed study was conducted using PCP-g-SiO_2 NPs (PCP-g-NPs) in an industrial rubber to prepare silica-filled rubber composites to study the effect of SiO_2 NPs on the reinforcement of the rubber composites. This was done at four different loadings and dispersing SiO_2 NPs grafted with different PCP molecular weight brushes into a commercial PCP matrix. A series of composites were prepared using SiO_2 NPs grafted only with short octadecyl chains (C18), ODDMMS-g-SiO_2, to avoid self-agglomeration, and PCP grafted SiO_2 NPs using two different graft densities of (0.21 ch/nm^2) and (0.022 ch/nm^2) with a broad range of molecular weights (34.8-161 kg/mol) of grafted PCP. All samples were dispersed in a fixed weight ratio of the industrial matrix with a 150 kg/mol molecular weight. The details of the samples are listed in Table 4.1.

Table 4.1 Sample details and properties of cured PCP nanocomposites

Sample name	Mn (kg/mol) *	Graft density (ch/nm^2)	Silica** loading (Wt %)	Tensile strength (MPa)	Elongation at Break	Degree of Swelling (%)	Crosslink Density ($v*10^4$ mol/cc)
PCP Unfilled	150	---	0	2.25 ± 1.10	5.27 ± 1.11	491 ± 5	0.518 ± 0.008
C18 -1	0	---	1	2.60 ± 0.73	4.90 ± 1.02	486 ± 9	0.579 ± 0.019
38k-1	38	0.21	1	2.61 ± 0.05	5.81 ± 1.07	481 ± 11	0.590 ± 0.023
73k-1	73	0.21	1	3.37 ±1.05	6.26 ±0.53	461 ± 7	0.634 ± 0.017
161k-1	161	0.21	1	4.74 ±0.73	8.76 ±0.8	442 ± 12	0.683 ± 0.033
C18-5	0	---	5	3.21 ± 0.85	6.30 ± 0.31	462 ± 3	0.585 ± 0.007
38k-5	38	0.21	5	4.62 ±0.77	7.50 ±1.17	445 ± 4	0.627 ± 0.006
73k-5	73	0.21	5	4.27 ±1.67	7.52 ±1.89	429 ± 15	0.693 ± 0.025
161k-5	161	0.21	5	5.96 ±0.51	10.78 ±0.3	411 ± 2	0.717 ± 0.006

34.8k-5	34.8	0.022	5	7.35 ±1.54	7.21 ±0.57	438 ± 15	0.643 ± 0.039
134k-5	134	0.022	5	7.45 ±2.81	7.35 ±1.97	407 ± 5	0.737 ± 0.008
C18-10	0	---	10	4.36 ± 1.01	6.90 ± 0.97	429 ± 12	0.613 ± 0.046
38k-10	38	0.21	10	4.68 ±0.44	8.29 ±0.39	400 ± 3	0.678 ± 0.009
73k-10	73	0.21	10	5.57 ±1.07	10.26 ±1.01	389 ± 11	0.724 ± 0.051
161k-10	161	0.21	10	6.94 ±1.01	12.86 ±1.3	341 ± 6	0.914 ± 0.015
34.8k-10	34.8	0.022	10	6.68 ±1.05	6.75 ±1.0	381 ± 4	0.739 ± 0.013
134k-10	134	0.022	10	7.83 ±1.15	8.80 ± 0.83	361 ± 11	0.812 ± 0.042
C18-25	0	---	25	4.95 ± 1.95	9.23 ± 0.43	311 ± 6	0.665 ± 0.021
34.8k-25	34.8	0.022	25	7.92 ± 1.40	9.40 ± 0.64	225 ± 7	1.149 ± 0.063
134k-25	134	0.022	25	8.90 ± 1.25	9.51 ± 0.38	166 ± 10	1.912 ± 0.188

* All composites dispersed in 150 kg/mol PCP

** Silica loading calculated to total polymer plus silica

The PCP grafted silica NPs were prepared by the surface-initiated RAFT polymerization of chloroprene. After polymerization, the particles were purified using centrifugation to remove small amounts of free PCP chains.[3] NMR analysis showed that the polymer contained 71% 1,4-trans, 23% cis, 1.3% 1,2-additions and 4.7% 3,4-additions, similar to that found in normal free radical polymerization.[37,38] Chloroprene rubbers are often vulcanized using a mixture of metal oxides. In this work, a common recipe was used comprising zinc oxide, magnesium oxide, 2-mercaptothiazoline (accelerator), stearic acid (stabilizer), and N-phenylnaphthalen-2-amine. The rubber can be vulcanized in the presence of only zinc oxide, but the use of magnesium oxide is necessary to avoid burning or charring originating from the dehydrochlorination reaction. Under such

conditions, the dehydrochlorination reaction of the tertiary allylic positions will occur first, and once the tertiary allylic chlorines (1,2-units) are consumed, the less reactive 3,4- and 1,4-units that will undergo dehydrochlorination.[36] Overall, this method has been reported to produce cured rubbers with high flexibility and dimensional stability. [19,33,40]

FT-IR spectroscopy was performed to analyze the unfilled and filled rubber. The spectrum of the filled sample shows additional peaks in the range 1100-1000 cm^{-1} (Si-O-Si) derived from the silica nanoparticles.[41] In addition to this, peaks are observed at 1120 cm^{-1} (C-N) and 1570 cm^{-1} (N-H) which are related to the APS grafted on the SiO_2 NPs.[42] Specifically, bands at 640 cm^{-1} and 820 cm^{-1} correspond to carbon to chlorine bond (C-Cl) of the PCP. The remainder of the bands can be attributed to the PCP rubber; at 1300-1433 cm^{-1} for (CH_2) bands, the asymmetric (CH) appears at 2750-2900 cm^{-1}, the alkene band is observed at 1660 cm^{-1} (C=C), and a band at 3010 cm^{-1} for (=CH). Finally, the wide-stretching band at 3200-3500 cm^{-1} is due to silanol (-OH)(Figure 4.1)(Table 4.2).[37]

Thermal gravimetric analysis (TGA) was used to confirm the RAFT agent attachment and graft polymerization of chloroprene from the surface of the NPs (Figure 4.2). The small weight loss observed for the RAFT agent grafted NPs is representative of

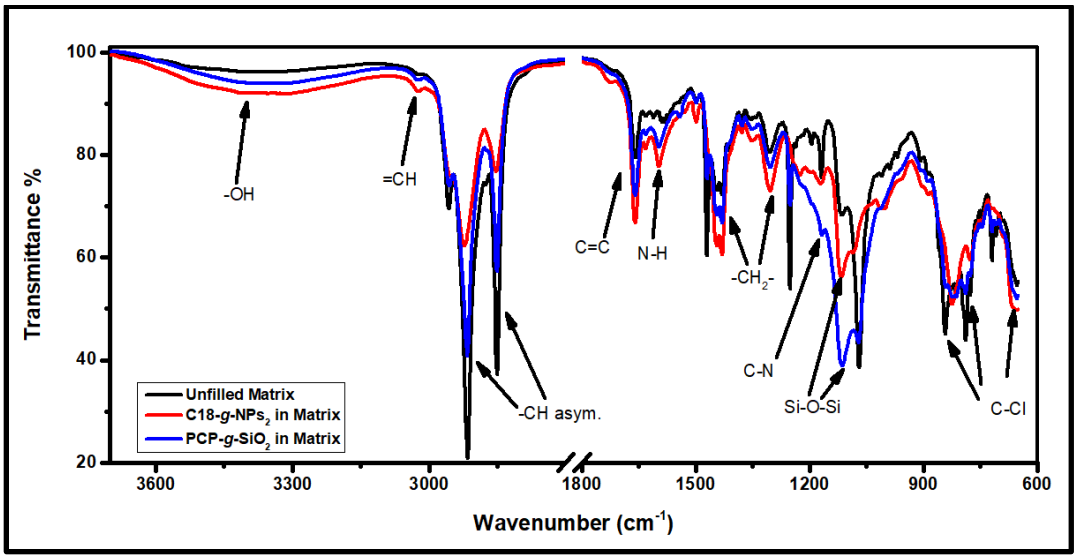

Figure 4.1 FTIR spectra of the unfilled, C18 NPs, and PCP-g-SiO_2

Table 4.2 Absorption Peaks in FTIR Spectra

Peaks	Wavenumber cm^{-1}
C-Cl ms*	640-820
Si-O-Si ms	1100
C-N w	1120
-CH_2- m, vs	1300-1433
-NH- ms	1570
C=C s	1660
-CH asymmetric vs	2750-2900
=CH w	3010
-OH ms	3200-3500

* vs., very strong; s, strong; ms, medium strong; m, medium; w, weak.

the weight loss for the grafted RAFT agent and the nanoparticles surfactant stabilizer. The TGA weight loss result (red line) for a 34.8k-g-NP sample is also consistent with the calculated value for this chain density. Finally, weight loss

for the composite (blue line) containing dispersed grafted PCP in commercial PCP matrix for the 25 wt % silica core is in agreement with the calculations when considering the additional metal oxide curing agents.

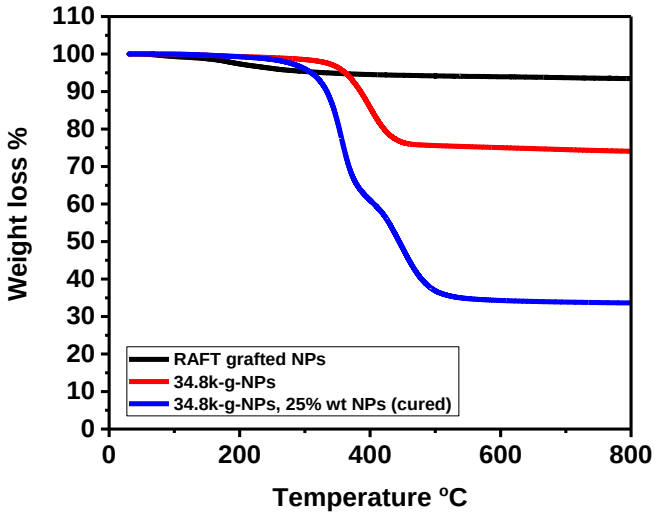

Figure 4.2 TGA results for RAFT agent attached NPs (black line), 34.8k-g-NPs 0.022 ch/nm^2 (red line) and 25 wt% cured composites (blue line).

Mechanical properties of the cured composites were evaluated using conventional stress-strain measurements (Figure 4.3). The increase in modulus for silica reinforced elastomers can be predicted using the Guth-Gold equation,[43]

$$\frac{Ec}{Eo} = 1 + 2.5\varphi + 14.1\varphi^2 \qquad (3)$$

Where, Ec and Eo are the tensile moduli of the filled and unfilled composites, respectively. Ec/Eo is termed as the modulus enhancement and φ is the calculated volume fraction of silica in the filled composite.

Table 4.3 Calculations of modulus enhancement (Ec/Eo) of filled composites

Sample name	1st	2nd	3rd	4th	5th	Average	St.Dev.	Modulus improvement
PCP Unfilled	0.97785	0.90203	0.7774	0.78524	0.82254	0.853	0.09	1.00
C18 -1	1.053	0.753	0.6987	0.954	0.987	0.889	0.15	1.04
38k-1	0.89252	1.254	0.70088	1.19434	0.678	0.944	0.27	1.11
73k-1	0.70205	1.108	1.104	0.9672	0.820116	0.940	0.178	1.10
161k-1	0.876541	0.8965	1.29874	1.3547	0.9543	1.076	0.231	1.26
C18-5	0.88697	1.3002	0.89654	1.099434	0.80235	0.997	0.202	1.17
38k-5	0.89976	1.03956	0.97882	1.19956	1.06956	1.037	0.111	1.22
73k-5	0.98871	0.98707	1.014616	1.26616	1.17616	1.087	0.127	1.27
161k-5	1.19568	1.27988	1.142558	1.23363	1.32563	1.235	0.071	1.45
34.8k-5	1.27533	1.0268	1.9582	1.0024	1.30063	1.313	0.386	1.54
134k-5	1.785	1.563	1.245	1.346	1.109	1.410	0.267	1.65
C18-10	1.120	1.154	0.965	0.855	1.095	1.038	0.125	1.22
38k-10	1.437	1.024	1.065	1.755	0.875	1.231	0.359	1.44
73k-10	1.456	1.366	1.205	1.154	0.987	1.234	0.184	1.45
161k-10	1.207	1.094	1.423	1.279	1.506	1.302	0.165	1.53
34.8k-10	1.52364	1.5485	1.1025	1.8452	1.025	1.409	0.341	1.65
134k-10	1.62974	1.20567	1.6541	1.3068	1.7023	1.500	0.227	1.76
C18-25	1.1984	0.9564	0.83124	1.2795	1.16785	1.087	0.186	1.27
34.8k-25	1.86432	2.3454	1.396	1.1139	1.03286	1.550	0.551	1.82
134k-25	1.703265	1.806547	2.05124	1.30454	1.2345	1.620	0.345	1.90

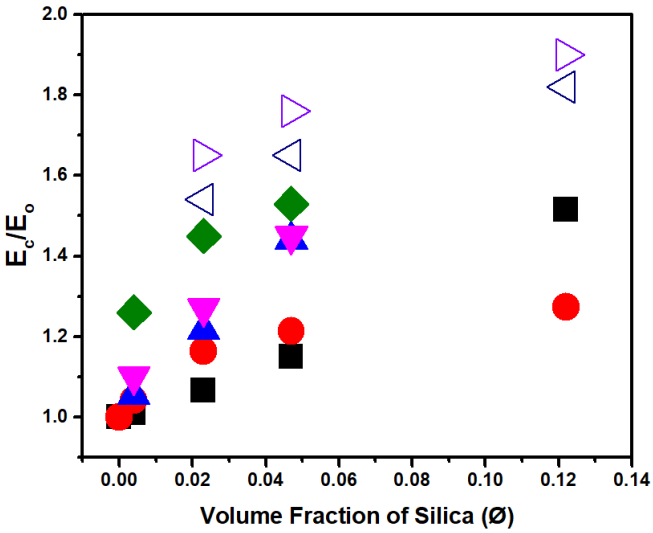

Figure 4.3 Modulus enhancement (Ec/Eo) of filled composites (volume fraction, φ) for both predicted (■) and experimental samples ●, C18-SiO_2; ▲,38k-high density; ▼,73k-high density; ◆,161k-high density; ◅,34.8k-low density; ▻, 134k-low density.

The experimental data for the modulus enhancement (Ec/Eo) were higher than those predicted by the Guth-Gold equation for all of the polymer grafted nanocomposite films. The C18 composite films showed little or minor modulus enhancement, or in the case of the highest loading level tested, a decrease as compared to the theoretical prediction. This suggests that the treatment of silica with grafted chains that can entangle with matrix chains significantly contribute to composite modulus enhancements, beyond the simple creation of a hydrophobic surface layer. Interestingly, samples with lower graft density (unfilled symbols) and high molecular weights of the grafted polymer (e.g., 134k-g-0.022 ch/nm^2) showed much greater improvements in the tensile modulus

compared to the unfilled composite and the high graft density filled composites (filled symbols).[44] This also supports the chain entanglement hypothesis as a major contributory factor in improving composite mechanical properties as the long low-density chains will be more efficient in entangling with matrix chains than densely grafted chains . Generally, the strength of the rubber filler interaction appears enhanced by the grafted polymer chains on the silica surface, which results in effectively increasing the filler volume fraction.[6,7,18]

Figure 4.4 shows the stress-strain data for the unfilled polymer and filled composites with different molecular weights of grafted PCP and loading of Silica nanoparticles.

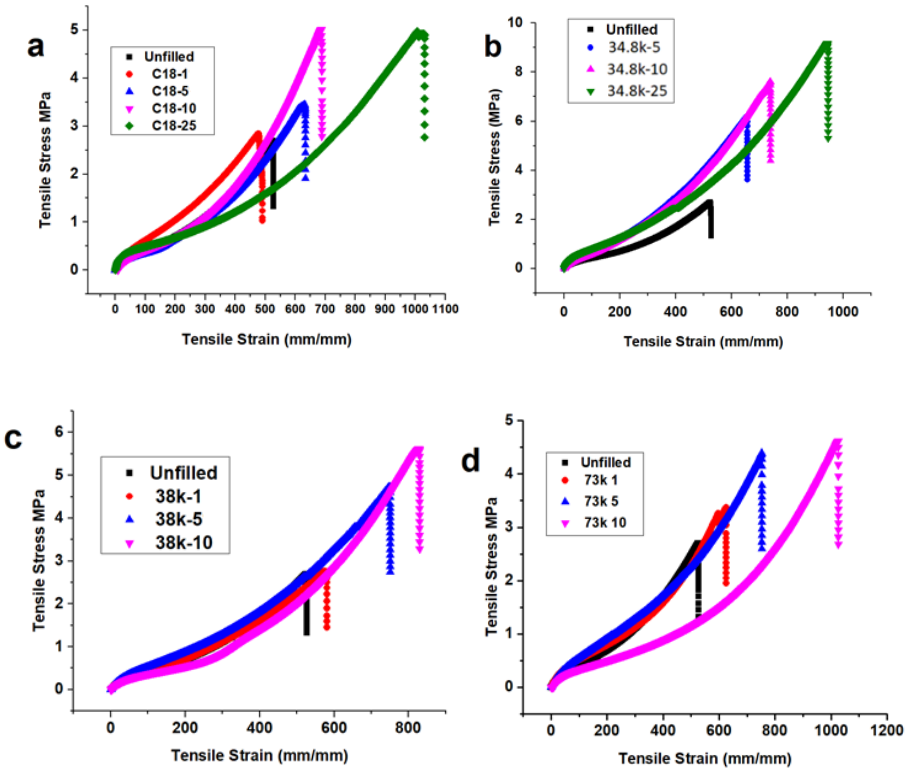

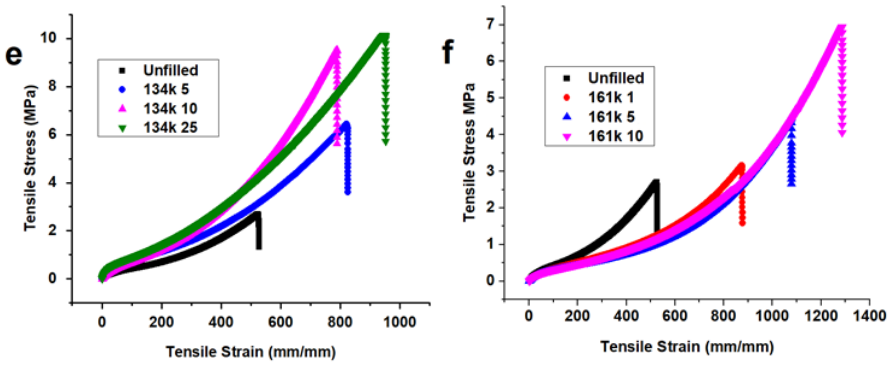

Figure 4.4 Stress-strain diagram of unfilled and filled composites with increasing in silica loading and grafted molecular weight (a), C18-SiO_2; (b),34.8k-low density; (c), 38k-high density; (d), 73k-high density; (e), 134k-low density; (f),161k-high density.

A more comprehensive analysis of the stress-strain data for the composites is shown in Figure 4.5. For reference, the unfilled, crosslinked PCP properties are plotted as the 0% silica loading using the molecular weight of the resin before crosslinking and the C18-SiO_2 grafted particle composites are plotted as the zero value M_n data. The results show the general expected trend of higher mechanical properties with higher loading levels of silica nanoparticles.

The comparison between the C18-SiO_2 grafted nanocomposite properties and the polymer grafted nanocomposite properties is valuable in pointing to the importance of chain entanglement effects. The C18 grafted chains are effective in creating a hydrophobic layer on the NPs and assisting in dispersing the NPs in the matrix but do not contribute to chain entanglement effects with the matrix polymer. The data for long-chain grafted NPs shows that the mechanical properties were improved across all experimental graft variables and specifically

when chain entanglement was most enhanced. These results agree with previous results of NP grafted composites for glassy polymers and general concepts that address the bound layer effect in filled rubbers.[19,22–25,45]

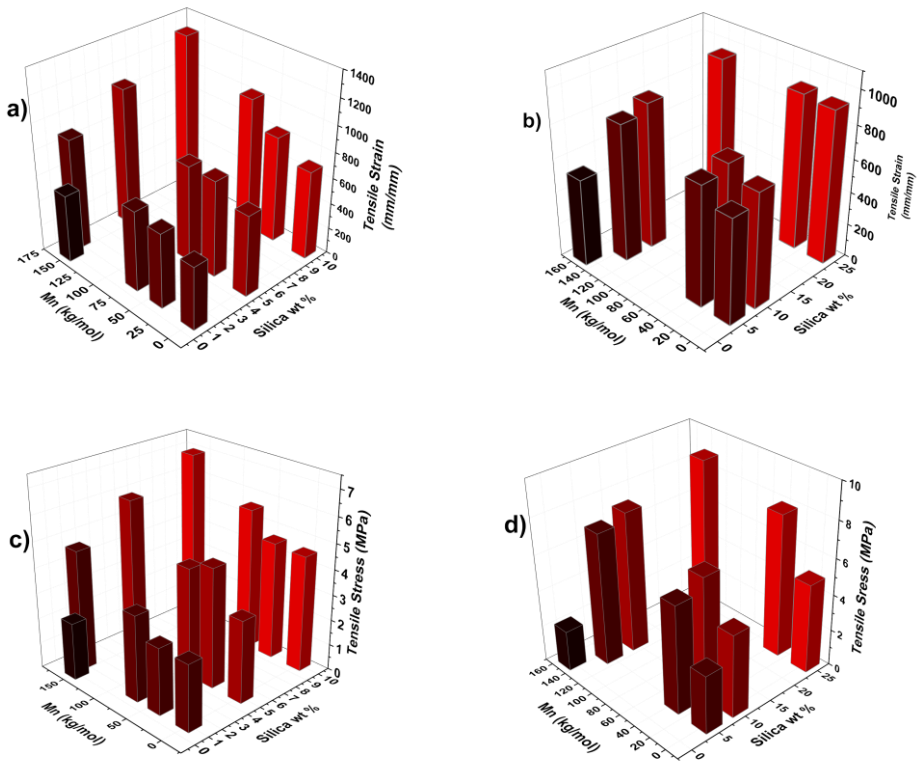

Figure 4.5 a) Strain diagram of unfilled polymer and filled composites with different silica loadings and grafted molecular weights of 0.21 ch/nm^2 NPs, b) strain diagram of unfilled polymer and filled composites with different silica loadings and grafted molecular weights of 0.022 ch/nm^2 NPs, c) stress diagram of unfilled polymer and filled composites with different silica loadings and grafted molecular weights of 0.21 ch/nm^2 NPs, d) stress diagram of unfilled polymer and filled composites with different silica loadings and grafted molecular weights of 0.022 ch/nm^2 NPs.

The importance of graft density and its effects on chain entanglement are also evident from the current study. For example, we can compare the data for 10 wt% silica loaded composites at graft densities of 0.21 ch/nm^2 and 0.022 ch/nm^2

with similar molecular weights of grafted chains (161k and 134k, respectively). The stress-at-break for these samples is 6.94 MPa and 7.83 MPa, suggesting that the difference in graft density and its effect on chain entanglement are an important variable of the grafting architecture. For NPs with low graft densities, higher particle loading levels can be attained since the weight percent of grafted chains is smaller than with high graft densities. Thus, further increases in mechanical properties (both tensile strength and modulus, e.g., Figure 4.5) were observed at higher silica loading levels for the low graft density NP filled composites.

The effect of PCP-g-NPs on the dynamic mechanical properties of 1, 5, 10, and 25 wt% silica filled nanocomposites is shown in Figure 4.6. The storage moduli (E') in the rubbery plateau region showed a continual increase with increasing silica loading. However, the molecular weight of the grafted chains also played an important role in the storage modulus. At each of the different chain densities, the storage modulus showed an increase with increasing graft molecular weight. For both chain densities, the highest grafted molecular weights (134k and 161k) yielded the highest values for the storage modulus, as well as the highest values for effective crosslink density. The effects of graft density were also observed at lower molecular weights. Comparison of the samples with 38k grafted chains (high graft density) and 34.8k (low graft density)

show that the composites using the 34.8k grafted PCP grafted nanoparticles gave higher room temperature storage moduli at all loading levels. We attribute this to the enhanced chain entanglement of the matrix chains with the low graft density grafted chains that have more space for the matrix chains to penetrate between grafted chains.[2] It should be mentioned that the C18 NP composite samples showed a significant drop in E', particularly noticeable at the higher loading levels. This decrease is likely due to the C18 chains, which have a melting point ~18-20 °C. Thus, the grafted short ligands would not be expected to contribute to a stable entangled state and rubber-silica interaction with the matrix chains at these temperatures. [44-46] A single loss peak was observed for all of the polymer grafted NP composites which were approximately the same as the unfilled crosslinked rubber, also indicating a fairly continuous interface-matrix region. [47]

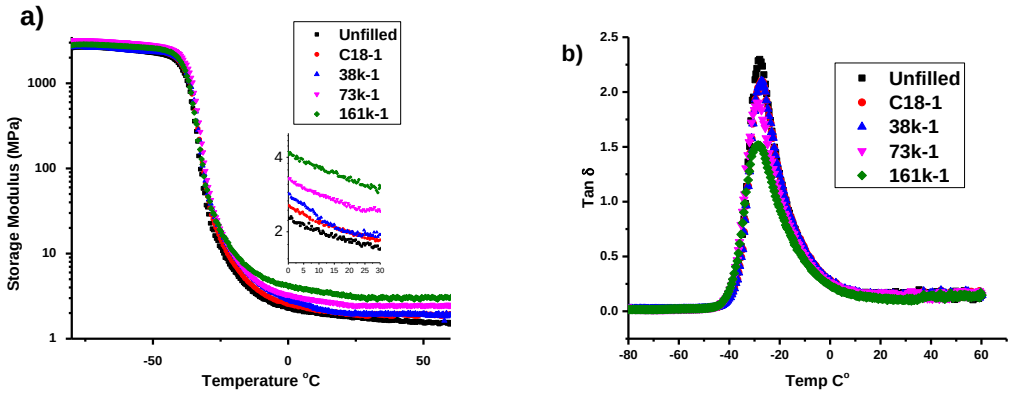

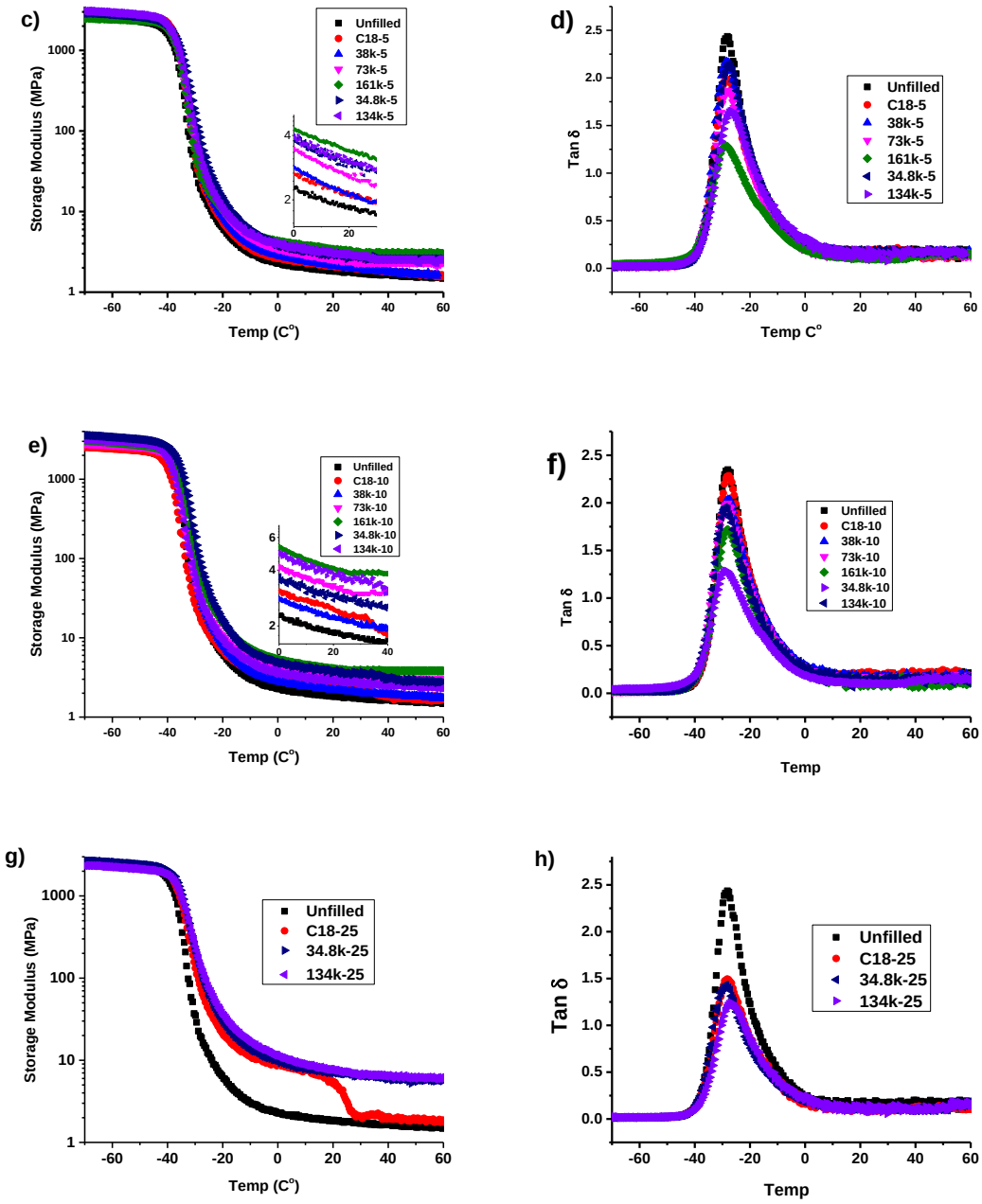

Figure 4.6 a, c, e, and g) Storage moduli of unfilled polymer and NP filled composites with different silica loadings and grafted molecular weights at 0.022 and 0.21 ch/nm^2. b, d, f, and h) tan δ of unfilled polymer and NP filled composites with different silica loadings and grafted molecular weights at 0.022 and 0.21 ch/nm^2.

The effect of PCP-g-NPs on the dynamic mechanical properties of storage modulus of 1, 5, 10, and 25 wt% silica filled nanocomposites is shown in Figure

4.6 (a, c, e, and g). The graphs show an increase in storage modulus with increasing silica loading. However, the graft density is also playing a significant role. The low graft density samples show a larger increase in storage modulus compared to the high graft density samples, because in low graft density the matrix chains have more space to penetrate between grafted chains and this will increase the crosslinking between the matrix and grafted polymer.[2] This conclusion is consistent with the stress-strain data that was plotted in Figure 4.3. It should be mentioned that the C18 NPs samples show two peaks of (Tg) in the DMA analysis and it is apparent in the 25 wt% sample. This second peak is due to the C18 chains, which have a melting point approximately 18-20^{o} C. Therefore, this grafted ligand will not maintain chain entanglement with the matrix chains.[48]

Consequently, raising the percent of grafted PCP will also lead to an increase in the crosslink density for the nanocomposites, which in turn contributes to storage modulus enhancement. This result agreed with the highest tensile modulus (25 wt%) and shown in the stress-strain study. Previously, (Das et al. 2015) worked on controlling the growth of silica in a natural rubber/chloroprene rubber blend by a solution sol-gel method, and the DMA analysis had two observed Tg peaks that relate to both rubber blends. For all composites in this work, the Tg was not altered from the Tg of the unfilled nanocomposites, as observed in the tan δ vs. temperature plot in Figure 4.6 (b, d,

h, and f). However, the reduction of the tan δ peak height increased with silica loading, which suggests a better reinforcing effect and stronger rubber-filler interaction at high silica loading.[49]

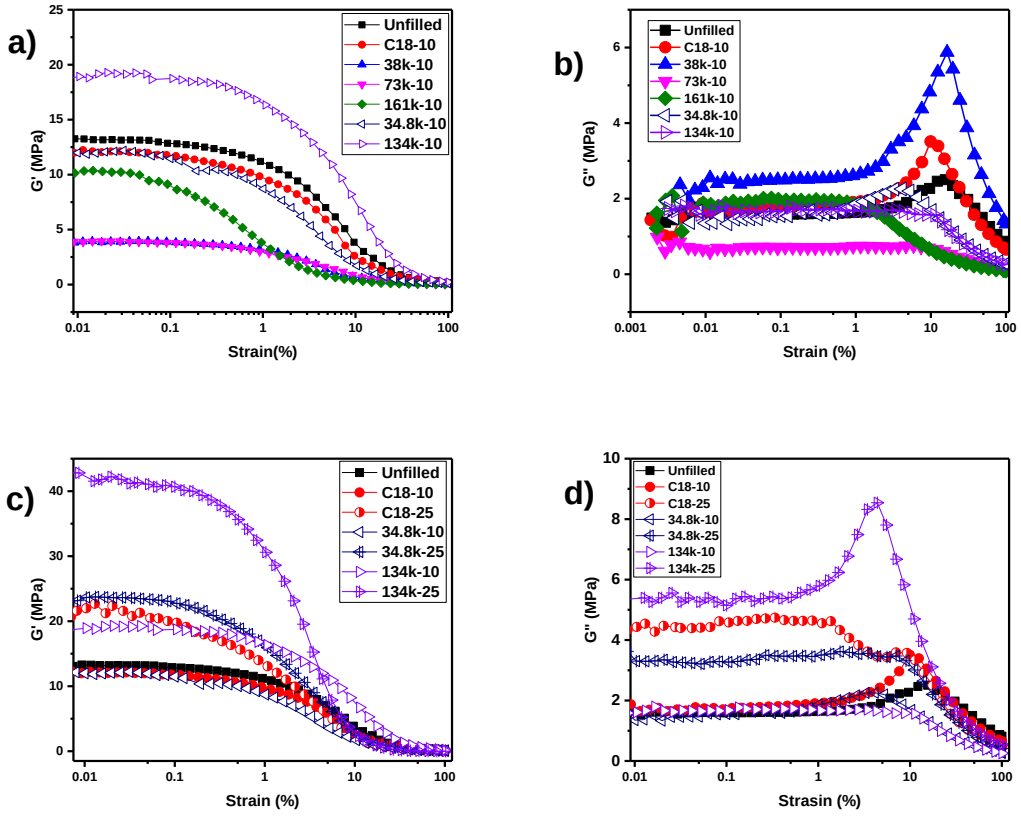

Figure 4.7 a) Storage modulus versus strain amplitude sweep of unfilled and 10% SiO_2 loading samples. b) Loss modulus versus strain amplitude sweep of unfilled and 10% SiO_2 loading samples. c) Storage modulus versus strain amplitude sweep of unfilled, 10%, 25% SiO_2 loading samples. d) Loss modulus versus strain amplitude sweep of unfilled, 10%, and 25% SiO_2 loading samples.

The Payne effect is known as a filler network disruption by deformation; displacement of the particles with increasing dynamic strain amplitude causes a substantial decrease in the storage modulus and a peak in the loss modulus. This

behavior is shown in Figure 4.7 for polychloroprene rubber containing various levels of silica loading. Unfilled matrix does not show this strain dependence of their dynamic properties as much as filled matrices.[45]

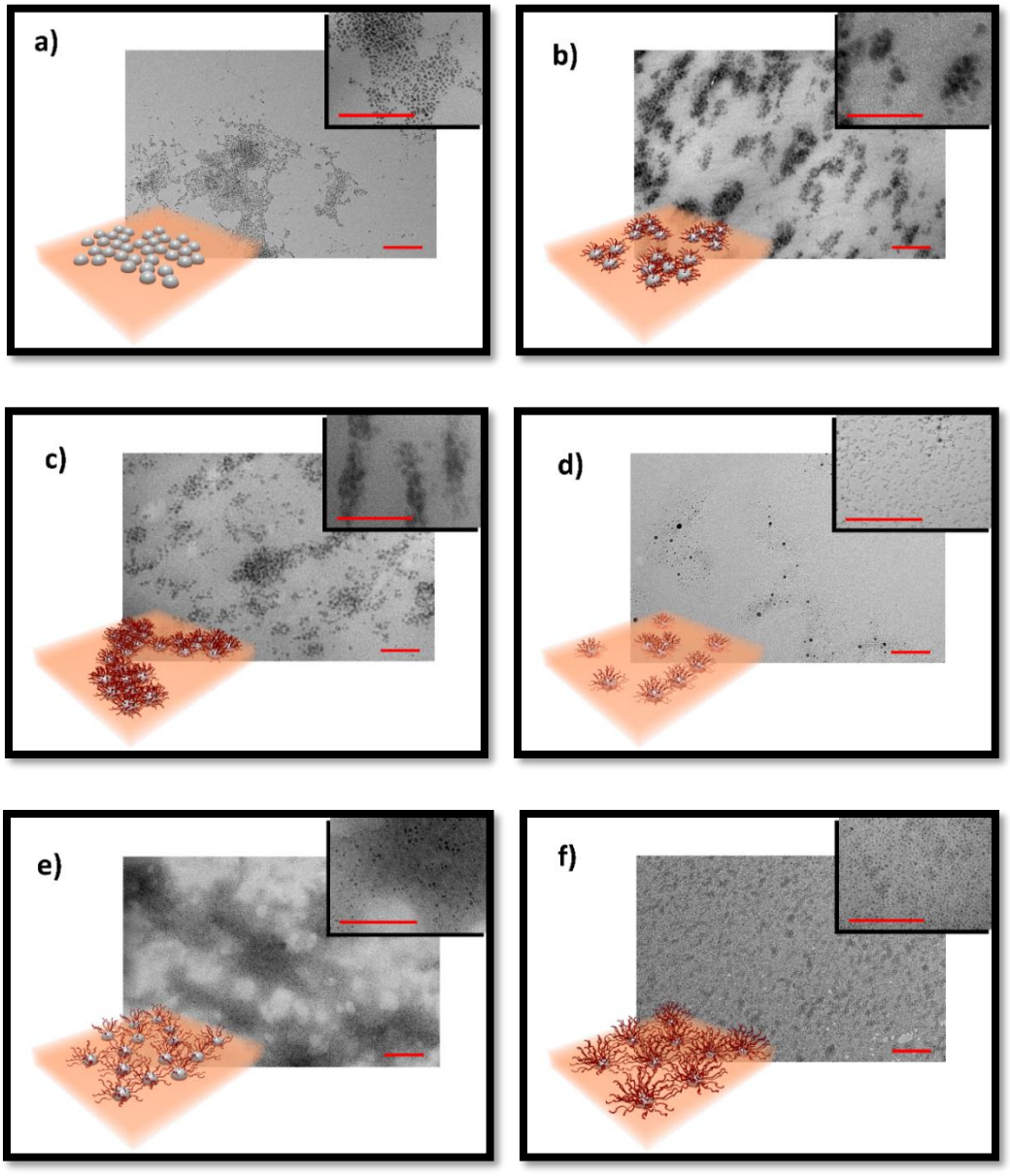

Figure 4.8 a) TEM images of PCP nanocomposites with 10 wt% SiO_2 loading, a) C18 NPs, b) 34.8k-g-SiO_2 at 0.022 ch/nm^2, c) 38k-g-SiO_2 at 0.21 ch/nm^2, d) 73k-g-SiO_2 at 0.21 ch/nm^2, e) 134k-g-SiO_2 at 0.022 ch/nm^2, f) 161k-g-SiO_2 at 0.21 ch/nm^2 (scale bar for all images is 200 nm).

TEM micrographs were acquired to study the dispersion state of the silica NPs in the PCP nanocomposites. Figure 4.8 shows the results for 10% silica loading levels of the grafted NPs for all the molecular weights and graft densities. The short C18 grafted NPs (Figure 4.8 a) showed the highest level of agglomeration. At the low polymer molecular weights, clustering was observed in both the 34.8k (0.022 ch/nm^2) and 38k (0.21 ch/nm^2) grafted NP samples (Figure 4.8 b and c) due to the incompatibility between the short chains of grafted polymer and longer matrix chains. At the next higher molecular weight, the 73k-g-SiO_2 filled sample (Figure 4.8 d) showed improved dispersion with just a moderate amount of clustering. At the highest graft molecular weights, the 134k and 161k grafted NPs (Figure 4.8 e and f)were dispersed much more effectively due to the improved compatibility and entanglement with matrix chains, consistent with the increase in mechanical properties.[12,34]

Small-angle X-ray scattering (SAXS) measurements were performed to compare ensemble measurements with localized TEM observations. Kratky plots were used to highlight subtle changes to the scattering patterns (Figure 4.9). As expected, the SAXS profile of the purely PCP film was monotonic without features corresponding to different material phases. The SAXS profile for PCP with 10 wt% of C18 SiO_2-NP loaded films (10 wt% C18 NPs) were like pure PCP with a distinct peak near q= 1.96 nm^{-1}, corresponding to a 3.2 nm correlation. The

correlation length is consistent with the interparticle separation for agglomerates observed in Figure 4.8a. For all nanocomposites examined, the addition of grafted PCP chains expanded the interparticle separation. Going from the 34.8K to the 38K-g-SiO_2-NP films led to a shifted peak/inflection point, consistent with the longer chains enhancing the interparticle separation. Subsequent samples with longer grafted chains and higher chain density (73, 126, 161 kg/mol at 0.2ch/nm^2) exhibited similar inflection points, attributed to similar interparticle correlations, albeit within an inherently polydisperse system. As the molecular weight of the grafted PCP was increased, the scattering intensity slightly decreased, suggestive of reduced extent of nanoparticle aggregation as also observed by TEM. This reduced intensity of the scattering feature paired and minor shifts to lower-q suggest a reduced extent of aggregation with an expanding interparticle spacing within aggregates. These observations are consistent with TEM imaging in Figure 4.8.[50] Trends were also noted for the effect of chain density on the state of dispersion: a sample with a high molar mass of 134kg/mol and low chain density (0.022 ch/nm^2) exhibited a more pronounced peak of scattering intensity, suggestive of particle aggregation and consistent with TEM data in Figure 4.8e. These findings highlight the important roles of having both sufficiently high grafted chain density and high molar mass grafted chains to promote particle dispersion.

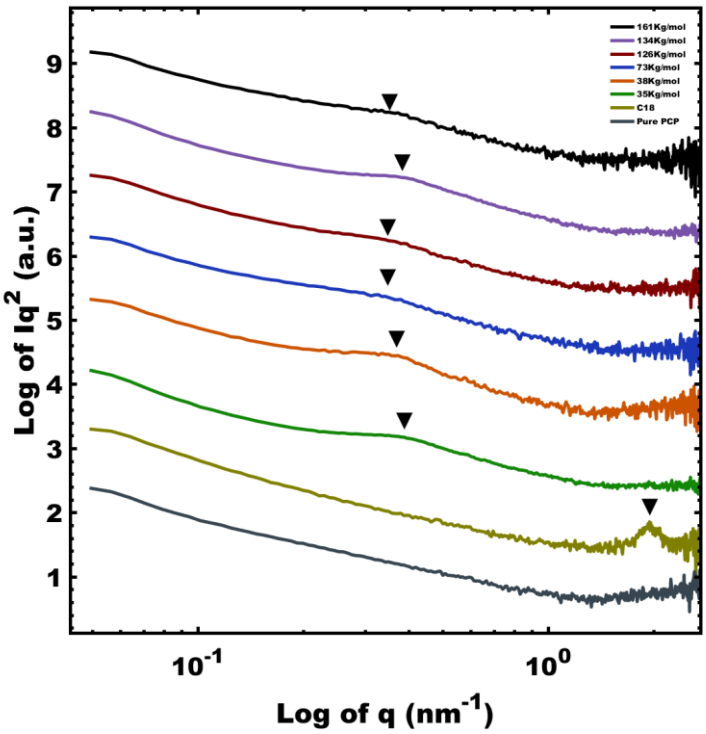

Figure 4.9 The 38, 73, 129, and 161kg/mol samples have a chain density of 0.2ch/nm^2 while the 34.8 and 134kg/mol have a chain density of 0.022 ch/nm^2. The data were offset vertically for clarity.

To establish the existence of bound rubber over silica surface and the study the unexpected behavior of Payne effect, scanning electron microscopy equipped with energy dispersive X-ray spectroscopy (SEM-EDS) was performed for a selected sample and the results are shown in Figure 4.10. It is evident here that the silica NPs were distributed through the rubber matrix. It can also be seen that the silica particles appear to be brighter compared to zinc oxide which appears agglomerated in the TEM images. This indicates the presence of

individual silica particles and suggests that the PCP chains are entangled to the matrix.

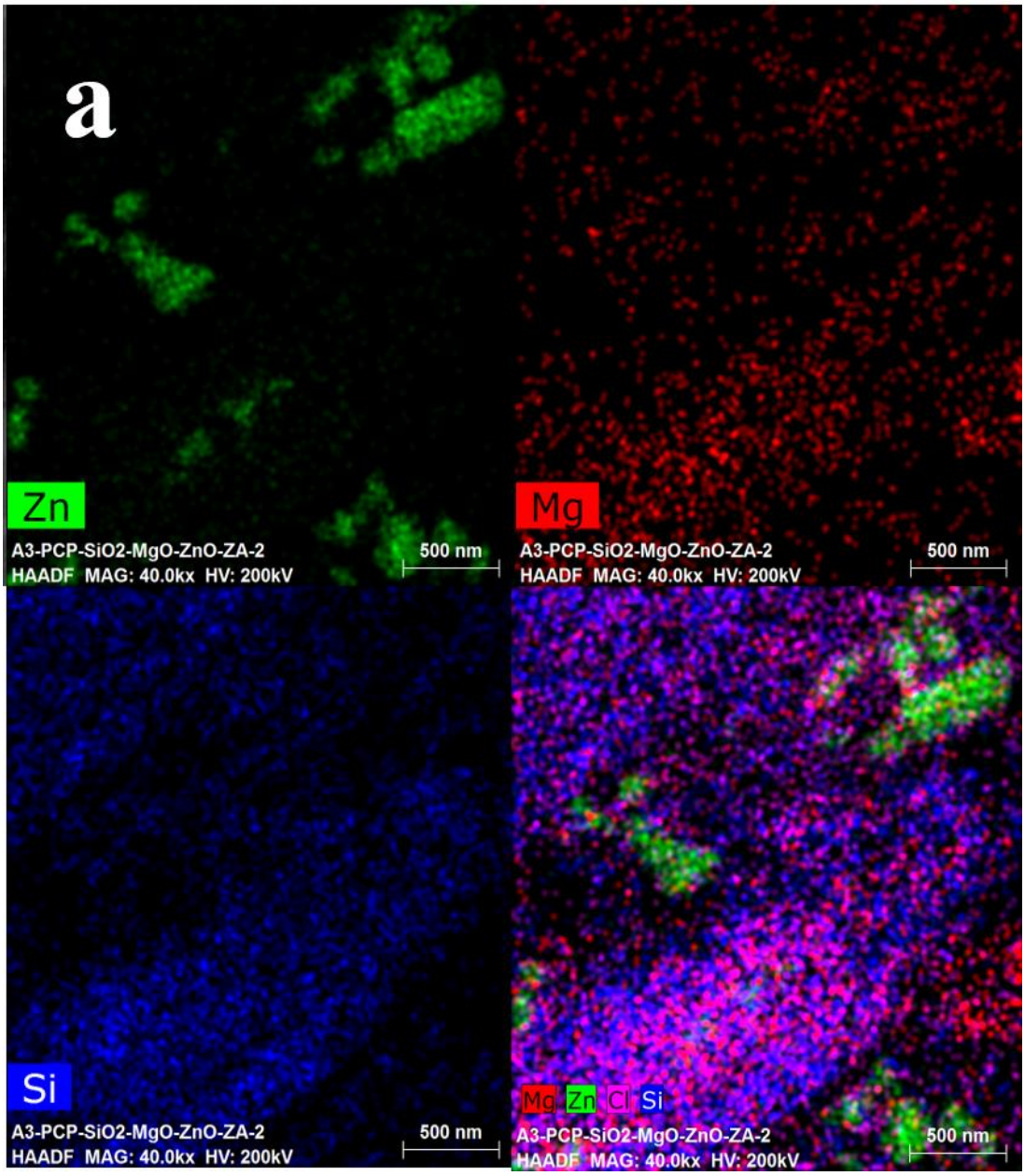

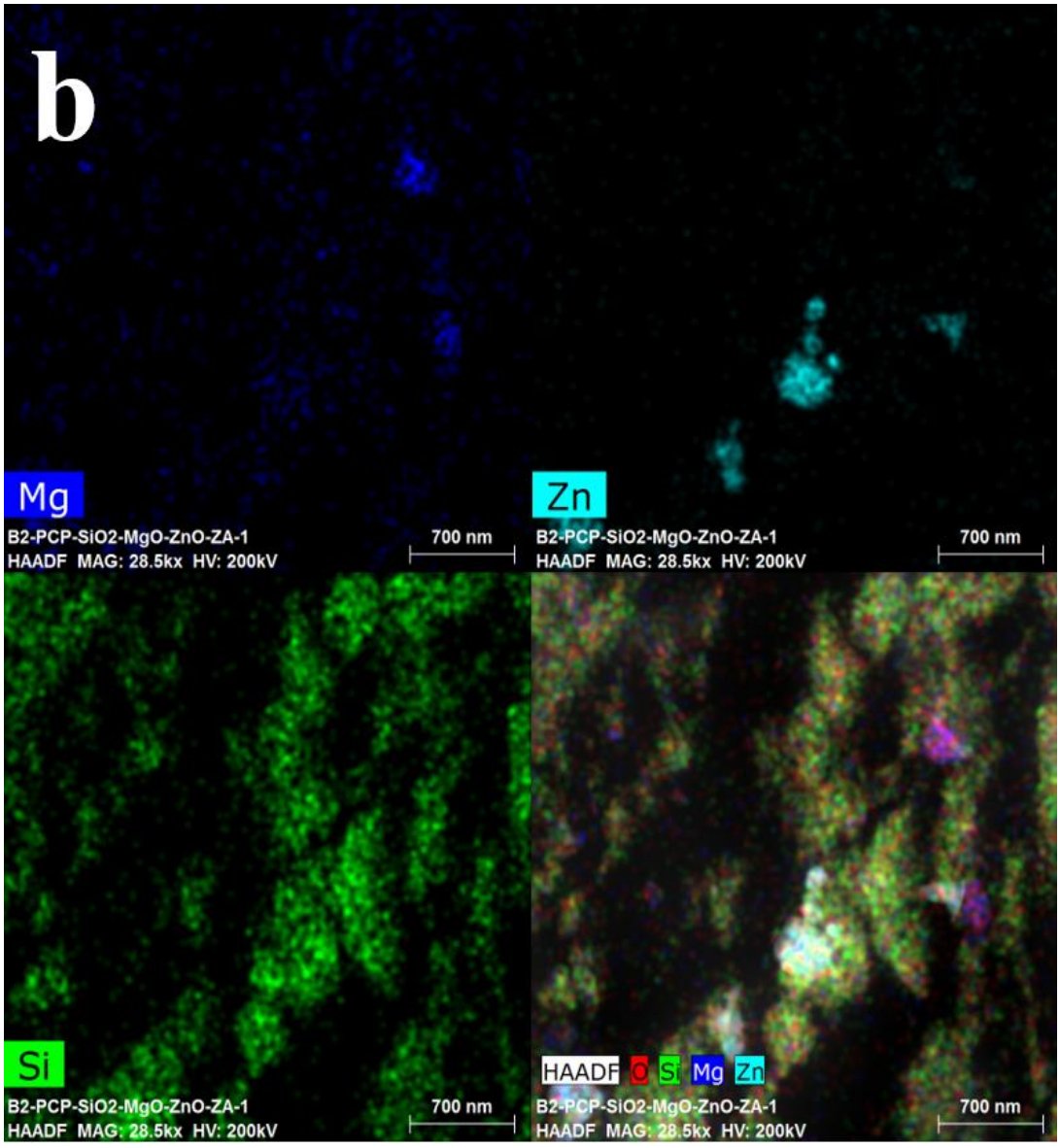

Figure 4.10 (a) SEM-EDS image of 134k-10 (b) SEM-EDS image of 34.8k-25

4.5 Conclusion

A study on the reinforcement of polychloroprene (PCP) was performed using PCP grafted silica nanoparticles, prepared by the polymerization of chloroprene from the surface of silica via surface-initiated RAFT polymerization. The results were compared to short C18 grafted NPs, which was used to create a

hydrophobic layer on the silica. Comparatively, the cured composites with the C18 grafted NPs showed lower mechanical properties and poor dispersion in the PCP matrix. Samples with grafted PCP showed higher mechanical properties and better dispersion due to the improved interactions and chain entanglement of the matrix with the grafted polymer chains. Two different graft densities were studied representing the low and high graft density regimes. The cured composites with low graft density NPs exhibited greater enhancement and at lower grafted molecular weights due to the penetration of matrix chains into the polymer brushes. The mechanical properties generally improved by increasing the silica loading from 1 to 25 wt%. The modified rubber produces a strong nanocomposite which will be useful in many applications. The control and variation of grafted molecular weight and chain density of grafted polymer could be a very effective technique to convey improved nanocomposite properties for practical applications.

4.6 References

(1) Faraji, S.; Yardim, M. F.; Can, D. S.; Sarac, A. S. *J. Appl. Polym. Sci.* **2017**, *134* (2), 1–10.

(2) Huang, Y.; Zheng, Y.; Sarkar, A.; Xu, Y.; Stefik, M.; Benicewicz, B. C. *Macromolecules* **2017**, *50* (12), 4742–4753.

(3) Zheng, Y.; Abbas, Z. M.; Sarkar, A.; Marsh, Z.; Stefik, M.; Benicewicz, B. C. *Polymer (Guildf).* **2018**, *135*, 193–199.

(4) Zhao, D.; Di Nicola, M.; Khani, M. M.; Jestin, J.; Benicewicz, B. C.; Kumar, S. K. *ACS Macro Lett.* **2016**, *5* (7), 790–795.

(5) Hosler, D.; Burkett, S. L.; Tarkanian, M. *J. Science*. **1999**, *284* (5422), 1988–1991.

(6) Othman, A. bin; Gregory, M. J. *J Nat Rubb Res* **1988**, *3* (1), 7–20.

(7) Qu, M.; Deng, F.; Kalkhoran, S. M.; Gouldstone, A.; Robisson, A.; Van Vliet, K. *J. Soft Matter* **2011**, *7* (3), 1066.

(8) MUTER, M. A.; MUGAR, Q. K. *J. Nat. Sci. Res*. **2014**, *4* (24), 60–73.

(9) Merza, K. S.; Al-Attabi, H. D.; Abbas, Z. M.; Yusr, H. A. *Green Sustain. Chem*. **2012**, *2* (February), 26–28.

(10) Mao, Y.; Li, S.; Ploehn, H. J. *J. Appl. Polym. Sci*. **2017**, *134* (27), 1–11.

(11) Bhattacharya, S. N.; Kamal, M. R.; Gupta, R. K. *Polymeric Nanocomposites Theory and Practice; Carl Hanser Publishers:* Munich, **2007**. p 53

(12) Hooper, J. B.; Schweizer, K. S. *Macromolecules* **2006**, *39* (15), 5133–5142.

(13) Moll, J. F.; Akcora, P.; Rungta, A.; Gong, S.; Colby, R. H.; Benicewicz, B. C.; Kumar, S. K. *Macromolecules* **2011**, *44* (18), 7473–7477.

(14) Li, C.; Benicewicz, B. C. *Macromolecules* **2005**, *38* (14), 5929–5936.

(15) Li, C.; Han, J.; Ryu, C. Y.; Benicewicz, B. C. *Macromolecules* **2006**, *39*, 3175–3183.

(16) Polmanteer, K. E. *Rubber Chemistry and Technology*. **1975**, pp 795–809.

(17) Heinrich, G.; Kluppel, M.; Vilgis, T. A. *Curr. Opin. Solid State Mater. Sci*. **2002**, *6*, 195–203.

(18) Maillard, D.; Kumar, S. K.; Fragneaud, B.; Kysar, J. W.; Rungta, A.; Benicewicz, B. C.; Deng, H.; Brinson, L. C.; Douglas, J. F. *Nano Lett.* **2012**, *12* (8), 3909–3914.

(19) Kapgate, B. P.; Das, C.; Das, A.; Basu, D.; Wiessner, S.; Reuter, U.; Heinrich, G. J. *Appl. Polym. Sci*. **2016**, *133* (30), 1–10.

(20) Tunnicliffe, L. B.; Busfiel, J. J. C. *Adv. Polym. Sci*. **2016**, *275*, 71–102.

(21) Carothers, W. H.; Williams, I.; Collins, A. M.; Kirby, J. E. J. *Am. Chem. Soc*. **1931**, *53* (11), 4203–4225.

(22) Scagliusi, S. R.; Araújo, S. G.; Landini, L.; Lugão, A. B. *Int. Nucl. Atl. Conf. Rio Janeiro, RJ, Brazil* **2009**, *41* (35).

(23) Dannenberg, E. M. *Rubber Chem. Technol*. **1986**, *59* (3), 512–524.

(24) Xu, H.; Song, Y.; Jia, E.; Zheng, Q. J. *Appl. Polym. Sci*. **2018**, *135* (22), 63–67.

(25) Kumar, S. K.; Jouault, N.; Benicewicz, B.; Neely, T. *Macromolecules* **2013**, *46* (9), 3199–3214.

(26) Natarajan, B.; Neely, T.; Rungta, A.; Benicewicz, B. C.; Schadler, L. S. *Macromolecules* **2013**, *46* (12), 4909–4918.

(27) Akcora, P.; Liu, H.; Kumar, S. K.; Moll, J.; Li, Y.; Benicewicz, B. C.; Schadler, L. S.; Acehan, D.; Panagiotopoulos, A. Z.; Pryamitsyn, V.; Ganesan, V.; Ilavsky, J.; Thiyagarajan, P.; Colby, R. H.; Douglas, J. F. *Nat. Mater*. **2009**, *8* (4), 354–359.

(28) Koiry, B. P.; Moukwa, M.; Singha, N. K. *J. Fluor. Chem*. **2013**, *153*, 137–142.

(29) Khani, M. M.; Abbas, Z. M.; Benicewicz, B. C. *J. Polym. Sci. Part A Polym. Chem*. **2017**, 1–9.

(30) Kumar, S. K.; Benicewicz, B. C.; Vaia, R. A.; Winey, K. I. *Macromolecules* **2017**, *50* (3), 714–731.

(31) Li, C.; Han, J.; Ryu, C. Y.; Benicewicz, B. C. *Macromolecules* **2006**, *39* (9), 3175–3183.

(32) Benicewicz, B.; Wang, L.; Mohammadkhani, M. Butadiene-derived polymers grafted nanoparticles and their methods of manufacture and use, U.S. Patent 9, 249, 250, February 6, **2016.**

(33) Datta, R. N. Rubber Curing Systems; Rapra Technology Limited: Shropshire, **2002**; *Vol. 12.*

(34) Sperling, L. H.; Sperling, L. H. Introduction to Physical Polymer Science., 4th Edditi.; A JOHN WILEY & SONS, INC. PUBLICATION: New Jersey, **2015**.

(35) Ibarra, L.; Chamorro, C. *J. Appl. Polym. Sci.* **1991**, *43* (10), 1805–1819.

(36) Valentín, J. L.; Carretero-González, J.; Mora-Barrantes, I.; Chassé, W.; Saalwächter, K. *Macromolecules* **2008**, *41* (13), 4717–4729.

(37) Arjunan, V.; Subramanian, S.; Mohan, S. *Turkish J. Chem*. **2003**, *27* (4), 423–431.

(38) Moad, G. *Polym. Int*. **2017**, *66* (1), 26–41.

(39) Desai, H.; Hendrikse, K. G.; Woolard, C. D. *J. Applied Polym. Sci*. **2007**, *105*, 865–876.

(40) Chokanandsombat, Y.; Sirisinha, C. *J. Appl. Polym. Sci.* **2013**, *128* (4), 2533–2540.

(41) Lippincott, E. R.; Vanvalkenburg, a.; Weir, C. E.; Bunting, E. N. *J. Res. Natl. Bur. Stand. (1934).* **1958**, *61* (1), 61.

(42) Parida, K. M.; Mallick, S.; Sahoo, P. C.; Rana, S. K. *Appl. Catal. A Gen*. **2010**, *381* (1–2), 226–232.

(43) Guth, E. *J. Appl. Phys.* **1945**, *16* (1), 20–25.

(44) Tao, P.; Li, Y.; Rungta, A.; Viswanath, A.; Gao, J.; Benicewicz, B. C.; Siegel, R. W.; Schadler, L. S. *J. Mater. Chem*. **2011**, *21* (46), 18623.

(45) Roland C. M. *Ref. Modul. Mater. Sci. Mater. Eng*. **2016**, 2475–2480.

(46) Torres, J. M.; Stafford, C. M.; Vogt, B. D. *Polymer (Guildf).* **2010**, *51* (18), 4211–4217.

(47) Robertson, C. G.; Lin, C. J.; Bogoslovov, R. B.; Rackaitis, M.; Sadhukhan, P.; Quinn, J. D.; Roland, C. M. *Rubber Chem. Technol*. **2011**, *84* (4), 507–519.

(48) Das, A.; Costa, F. R.; Wagenknecht, U.; Heinrich, G. *Eur. Polym. J*. **2008**, *44* (11), 3456–3465.

(49) Bansod, N. D.; Kapgate, B. P.; Das, C.; Basu, D.; Debnath, S. C.; Roy, K.; Wiessner, S. *RSC Adv*. **2015**, *5* (66), 53559–53568.

(50) Baeza, G. P.; Genix, A. C.; Degrandcourt, C.; Petitjean, L.; Gummel, J.; Couty, M.; Oberdisse, J. *Macromolecules* **2013**, *46* (1), 317–329.

CHAPTER 5

POLYISOPRENE GRAFTED SILICA NANOPARTICLES FOR RUBBER REINFORCEMENT OF CIS AND TRANS POLYISOPRENE MATRICES

5.1 Abstract

Silica-polyisoprene nanocomposites (PIP-*g*-SiO_2) have been synthesized by surface-initiated reversible addition-fragmentation chain transfer polymerization (SI-RAFT) and the properties of these materials were studied. The PIP-*g*-SiO_2 were used to be prepare rubbery nanocomposites that are useful for exploring new surface interactions between silica nanofillers and rubbery materials. Attempts to scale-up the SI-RAFT reaction have been successful and detailed mechanical property studies have been conducted to estimate the possibility of these new grafted polymers on improving rubbery composite properties. These grafted particles were dispersed in a commercial polyisoprene matrix to obtain PIP nanocomposites with different silica loadings (20, 40, and 60 wt %). The cured samples showed superior mechanical properties compared to PIP rubber nanocomposites measured by hardness, tensile and dynamic mechanical analysis even with low silica content. Mechanical studies demonstrated that the nanocomposites exhibited notable enhancements when low graft density was combined with high molecular mass. The interactions between rubber and SiO_2 NPs were explored by FTIR. The dispersion of particles was investigated by transmission electron microscopy (TEM), and Small-Angle X-ray Scattering (SAXS).

5.2 Introduction

The process of polymer composites blending have been developed to produce products that result from mixing two or more components with polymer to enhance properties.[1] Rubber nanocomposites are one example of these materials that has very important applications in industry.[2,3] Tremendous efforts have been made to investigate the effect of inorganic fillers in rubbery materials and how they interact with functionalized polymers such as grafted polymers or grafted functional groups.[4] The reinforcements of the rubber have been studied with regards to improvements in stiffness, modulus, rupture energy, tear strength, tensile strength, hardness, fatigue resistance, and abrasion resistance for the final rubber film.[5] The elongation at break (%) gradually decreases with increasing filler loading and this reduction of elongation at break is due to stiffening of the polymer matrix by the filler.[6] Dynamic mechanical analysis (DMA) of the storage modulus is often used to probe the reinforcement effect from the inorganic fillers, as the interaction between rubber and fillers may decrease the chain mobility and result in an increase in storage modulus.[7,8] In addition to that, surface hardness plays one of the most important roles in evaluating the improvement of mechanical properties of any materials especially by increasing the inorganic filler content.[9]

Rubber nanocomposites have already been synthesized through polymer-grafted particles due to the easy attachment and precise control over the grafting techniques.[10–12] Since the first report on the application of surface-initiated reversible addition fragmentation chain transfer radical polymerization (SI-RAFT) to modify silica nanoparticles using a surface-anchored RAFT agent by Benicewicz et al., this SI-RAFT technique has been used in the modification of nanoparticles with a wide range of polymers.[13–16]

One of the important classes of rubbery materials is polyisoprene, which has been widely used in industry with different kinds of blends for reinforcement purposes.[5,17] Anionic, cationic, and radical polymerizations have prepared isoprene polymers with both cis and trans configurations.[18–20] Anionic polymerization produces polymer with narrow dispersity (Đ); however, it is not compatible with electrophilic and acidic functional groups and is very sensitive to moisture and contamination.[21] Cis-1,4-polyisoprene is the most popular form of isoprene rubber due to its importance in tire industry and is also known as natural rubber (NR). In addition, trans-1,4-polyisoprene (TPI) is also used for many applications different from NR products. It can be semi-crystalline, so the properties and structure of TPI crystals were studied very well individually or in blends with NR.[22] There has been some work on controlled radical polymerization (CRP) of isoprene by RAFT and nitroxide-mediated

polymerization (NMP). Perrier et al. and Wooly et al. have independently reported RAFT polymerization of isoprene in bulk using a stable trithiocarbonate RAFT agent in high temperatures.[23,24] Isoprene polymer contains double bonds in the polymer backbone which allows for further functionalization or chemical modifications, especially vulcanization.[22,25]

Surface polymerization of isoprene by free radical polymerization and from the surface of silica nanoparticles via RAFT was reported by Benicewicz et al.[10] The polymer produced from this process is a mixture of 23% cis and 75% trans for both free and grafted polymerizations. To the best of our knowledge, mechanical properties of surface-tethered polyisoprene have not been investigated. In this work, we report an in-depth investigation of the surface-initiated RAFT polymerization of isoprene on silica nanoparticles and their dispersion and properties in polyisoprene matrices. The polyisoprene grafted nanoparticles are dispersed and cured to produce composites using both cis and trans PIP (it's important to mention the trans used here is also polymerized via RAFT, so it will have %75 trans content). The final composites showed improvements for filled silica samples (up to 60 wt %). Moreover, this work showed good enhancement of final mechanical properties even with low molecular weights of grafted polymer.

5.3 Materials and Methods

Materials. Isoprene was obtained from TCI America and was purified by passage over a neutral alumina prior to use. Cis-polyisoprene was purchased from Sigma Aldrich. The RAFT agent 4-cyano-4-(dodecylsulfanylthiocarbonyl) sulfanylpentanoic acid (DOPAT) (97%) and 2-methyl-2[(dodecylsulfanylthiocarbonyl) sulfanyl] propanoic acid (MDSS) (97%) were purchased from Strem Chemicals and used as received. Spherical SiO_2 nanoparticles with a diameter of 14 ± 4 nm were purchased from Nissan Chemical Co. Tetrahydrofuran (THF) (HPLC grade, Fisher), dicumyl peroxide (Acros, 99%), and 3-aminopropyldimethylethoxysilane (Gelest, 95%) were used as received.

Free polymerization of isoprene. Isoprene (5 g, 73 mmol), DOPAT (30 mg, 74 μmol) and dicumyl peroxide initiator (4 mg, 14.3 μmol) with a ratio between species of [monomer]:[CTA]:[initiator] = 1000:1:0.2 were added to a Schlenk tube. The mixture was degassed by three freeze-pump-thaw cycles, filled with nitrogen, and then the sealed Schlenk tube was placed in an oil bath set at 120 °C. The polymerization was stopped by quenching in ice water. Molecular weights were measured using gel permeation chromatography (GPC) in THF which was calibrated with poly(methyl methacrylate) standards.

Synthesis of DOPAT-g-SiO_2. A solution (20 mL) of colloidal silica particles (30 wt % in methyl isobutyl ketone) was added to a two-necked round bottom flask and diluted with 110 mL of THF. Dimethylmethoxy-n-octylsilane (0.16 mL) was added to improve dispersibility along with 3-aminopropyldimethylethoxysilane (0.06 mL, 0.32 mmol) and the mixture was heated at reflux in a 75 °C oil bath for 5 hours under nitrogen protection. The reaction was then cooled to room temperature and precipitated in a large amount of hexanes (500 mL). The particles were recovered by centrifugation and dispersed in THF using sonication, then precipitated in hexanes again. The amine-functionalized particles were dispersed in 40 mL of THF for further reaction. Then 0.2 g (0.5 mmol, 1.5 eq) of activated DOPAT was prepared and added dropwise to a THF solution of the amine functionalized silica nanoparticles (40 mL, 6 g) at room temperature.[26] After complete addition, the solution was stirred overnight. The reaction mixture was precipitated into a large amount of hexanes (400 mL). The particles were recovered by centrifugation at 3000 rpm for 8 min. The particles were redispersed in 30 mL THF and precipitated in hexanes. This dissolution–precipitation procedure was repeated 2 more times until the supernatant layer after centrifugation was colorless. The yellow DOPAT-anchored silica nanoparticles were dried at room temperature and analyzed

using UV analysis to determine the chain density using a calibration curve constructed from standard solutions of free DOPAT.

Surface-initiated RAFT polymerization of isoprene. Isoprene (1.22 g, 17.8 mmol), DOPAT-g-silica NPs with surface density of 41.9 μmol/g (0.17 chs/nm^2) (80 mg, 3.27 μmol), THF (2 ml) and dicumyl peroxide initiator (0.67 mmol) with a ratio between species of [monomer]:[CTA]:[initiator] = 5000:1:0.2 were added to a Schlenk tube. The particles were dispersed into the solution via sonication for 1 min and subsequently the mixture was degassed by three freeze-pump-thaw cycles, filled with nitrogen, and then the sealed Schlenk tube was placed in an oil bath set at 120 °C for various intervals. The polymerization was stopped by quenching in ice water. The resultant polymer grafted particles were then precipitated into a large amount of isopropanol and centrifuged at 8,000 rpm for 12 min and the particles were dispersed back into THF.

Nanocomposite preparation. Thermogravimetric analysis was used to determine the weight of grafted PIP on SiO_2 NP. Then the needed free PIP weight of matrix was calculated to match silica loadings desired in the final nanocomposite. The calculated PIP matrix was dissolved in 30mL of THF and mixed with different loadings of grafted NPs to obtain the final content of core SiO_2 NP (20, 40, and 60 wt %).

Curing process of PIP nanocomposites. A solvent mixing technique was used to prepare the PIP and curing agents in THF. The isoprene polymer (100eq) was cured using dicumyl peroxide (10eq), all equivalents are PHR (Parts per Hundred Rubber). After evaporating the solvent samples were hot pressed at 160° for 25 minutes to obtain vulcanized rubber sheet of 0.4 mm thickness.[27,28]

Characterization Techniques

Molecular weights. Molecular weights (Mn) and dispersities (*Đ*) were determined using a Varian 290 LC gel permeation chromatography (GPC) with a 390 LC multidetector unit, and three Styragel columns. The columns consisted of HR1, HR3, and HR4 in the effective molecular weight ranges of 100-5000, 500-30000, and 5000-500000, respectively. THF was used as eluent at 30°C and the flow rate was adjusted to 1.0mL/min. Molecular weights were calibrated with poly(styrene) standards obtained from Polymer Laboratories.

Nuclear Magnetic Resonance Spectroscopy. ^{1}H NMR (Bruker Avance III-HD 400 MHz) were conducted using $CDCl_3$ as solvent.

Differential scanning calorimetry (DSC). DSC was conducted using a TA Q2000 DSC (TA Instruments) under a nitrogen atmosphere at a heating rate of 10 °C/ min from −85 to 180° C.

Transmission Electron Microscopy. The Transmission Electron Microscopy (TEM) was performed on a FEI Talos 120C TEM at an accelerating voltage of 80 kV at NYU Langone's Microscopy Laboratory. The samples were prepared by cryo-ultramicrotomy sectioning of crosslinked samples with a Leica EM FCS cryo-ultramicrotome. Sections were cut at -80 °C with thicknesses of 100 nm at 2 mm/s and placed on a formvar coated copper grid. The grids were transferred and stored under LN2 prior to imaging. Images were acquired in bright field mode using an objective aperture with a Gatan OneView digital camera at a variety of magnifications across the samples.

Dynamic Mechanical Analysis. Dynamic mechanical analysis was performed with an Eplexor 2000N dynamic measurement system (TA, ARES-RSA3) using a constant frequency of 10 Hz in a temperature range -80^{o} C to 50^{o} C. The analysis was done in the tension mode. For the measurement of the complex modulus, E*, a static load of 1% pre-strain was applied and then the samples oscillated to a dynamic load of 0.5% strain. Measurements were done at a heating rate of 3 ^{o}C/min under nitrogen flow.

Stress-Strain Analysis. Tensile tests of dumbbell-shaped samples were carried out using the material testing machine (Instron 5543A) with crosshead speed 40 mm/min (ISO 527).

Hardness Test. Hardness of PIP cured specimens was measured using a durometer with Shore A scale (Cogenix Wallace, Surrey) as per ASTM D2240.

Thermal Aging: Thermal aging was conducted on the obtained reinforced elastomeric materials, and was performed in an air circulating oven operated at 100 °C for 72 h and 168 h.

Small-Angle X-ray Scattering (SAXS). Scattering experiments were conducted using a SAXS Lab Ganesha at the South Carolina SAXS Collaborative. A Xenocs GeniX3D microfocus source was used with a Cu target to generate a monochromic beam with a 0.154 nm wavelength. The instrument was calibrated using National Institute of Standards and Technology (NIST) reference material 640c silicon powder with the peak position at $2\theta=28.44^{\circ}$ where 2θ is the total scattering angle. A Pilatus 300K detector (Dectris) was used to collect the two-dimensional (2D) scattering patterns. All SAXS data were acquired with an X-ray flux of 4.1 M photons/s incident upon the samples with a sample detector distance of 1502.1 mm. All WAXS measurements were acquired with an X-ray flux of 36.3 M photons/s with a sample detector distance of 112.1 mm. SAXS measurements were conducted for 1200 s while WAXS measurements were conducted for 600 s, both were with a transmission geometry. The resulting 2D

images were azimuthally integrated and transmission-corrected to yield the scattering vector and absolute scattering intensity

5.4 Results and Discussion

The process of adding fillers to polymeric materials often improves the mechanical properties of the polymer matrix. This reinforcement is correlated to the properties of the interphase and depends on the nature of the interactions between polymer and reinforcing filler.[6] In this work, PIP is grafted to silica nanoparticles (PIP-*g*-SiO_2 NPs) and mixed with an industrial rubber to prepare silica-filled rubber composites to study the effect of SiO_2 NPs on the reinforcement of the rubber composites. Cis and trans PIP matrices were used to mix with the grafted PIP NPs at different loadings of SiO_2 NPs. A series of composites were prepared, and the NPs were dispersed in a fixed weight ratio of polymer matrices. The details of the samples are listed in Table 5.1

Table 5.1 Composition and mechanical properties of PIP-*g*-SiO_2 NPs nanocomposites

Sample name	Mn kg/mol	Graft density ch/nm²	Silica wt %	Grafted PIP %*	Free PIP% **	Tensile strength (MPa)	Elongation at break (mm/mm)	Hardness Shore A	Young's Modulus (MPa)
Free PIP Cis (FC)	40k	---	0	00	100	0.32±0.03	0.11±0.081	43±2	3.32±0.02

Free PIP 75% Trans (FT)	52k	---	0	00	100	0.41±0.06	0.13±0.012	47±1.5	4.01±0.01
20 g-Silica in Cis (20C)	35k	0.035	20	8.75	91.25	1.03±0.024	0.42±0.012	76±3	4.19±0.90
20 Bare Silica in Cis (20BC)	---	---	20	00	100	0.54±0.13	0.19±0.06	72±2.5	3.79±0.66
20 g-Silica in 75% Trans (20T)	35k	0.035	20	8.75	91.25	1.13±0.28	0.80±0.31	79.5±1	3.51±0.41
20 Bare Silica in 75% Trans (20BT)	---	---	20	00	100	0.35±0.24	1.10±0.17	72.5±1	0.49±0.05
40 g-Silica in Cis (40C)	35k	0.035	40	26.67	73.33	1.30±0.34	2.47±0.04	86.5±2	6.54±0.89
40 g-Silica in 75% Trans (40T)	35k	0.035	40	26.67	73.33	1.64±0.21	3.13±0.45	88±3	4.59±1.82
60 g-Silica in Cis (60C)	35k	0.035	60	45	55	4.48±0.73	2.79±0.53	90±1	6.51±0.31
60 Bare Silica in Cis (60BC)	---	---	60	00	100	2.95±1.36	1.59±0.62	86±1.5	3.54±1.12
60 g-Silica in 75% Trans (60T)	35k	0.035	60	45	55	9.07±1.67	3.76±0.28	90.5±1.5	3.55±0.07
60 Bare Silica in 75% Trans (60BT)	---		60	00	100	5.10±0.81	2.18±0.72	90±1.5	3.22±0.24
Matrix Free (MF) 75% Trans	35k	0.035	75	100	00	8.84±0.13	1.25±0.21	96±2	124.7±12.8

* The percent of grafted polymer to the total weight of polymer in composite

**The percent of free polymer to the total weight of polymer in composite

NMR characterization of PIP free and grafted on silica NPs was conducted using 400 ^{1}H NMR to study the configurational composition of the final polymer chain. The total content of 1,4 addition was around 95% between cis and trans and the remaining 5% was 1,2 and 3,4 addition.[29] To recognize the difference between the 1,4 cis and trans content the chemical shift of two methyl groups are not completely equivalent and the total percent of cis and trans are shown in Figures 5.1, 5.2, and Table 5.2.[30] The chemical shift of methyl group of 1,4 cis PIP is 1.6 ppm, but it is 1.5 ppm for 1,4 trans PIP.

Table 5.2 Overall configurational composition of the PIP polymer via RAFT polymerization.

Linkage	%
1,4 trans addition	75
1,4 cis addition	20
1,2 addition	1.3
3,4 addition	3.7

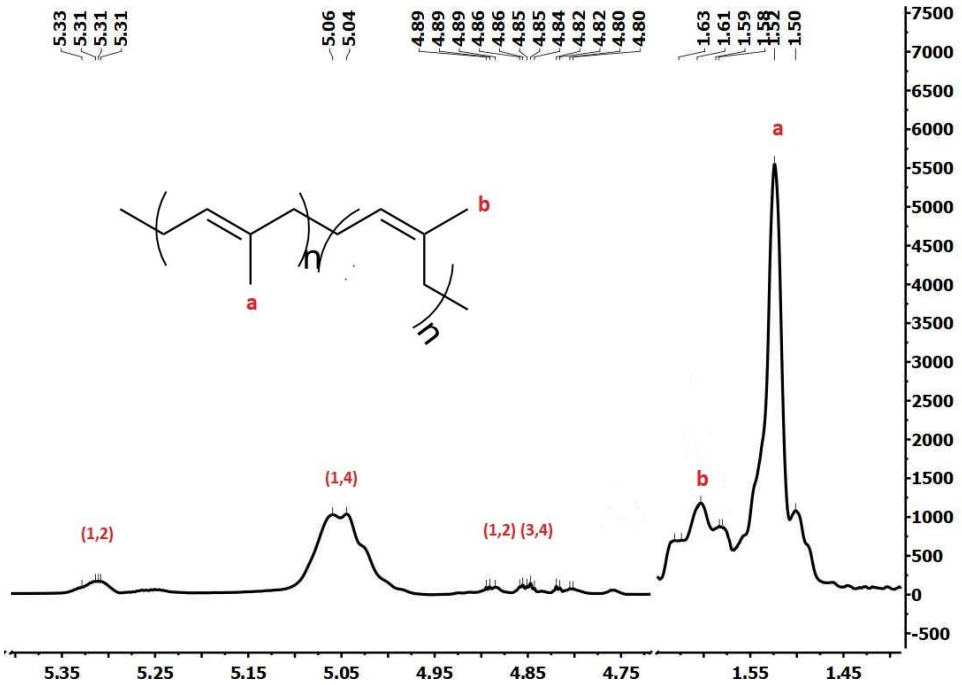

Figure 5.1 400-MHz ^{1}H NMR spectra of free PIP

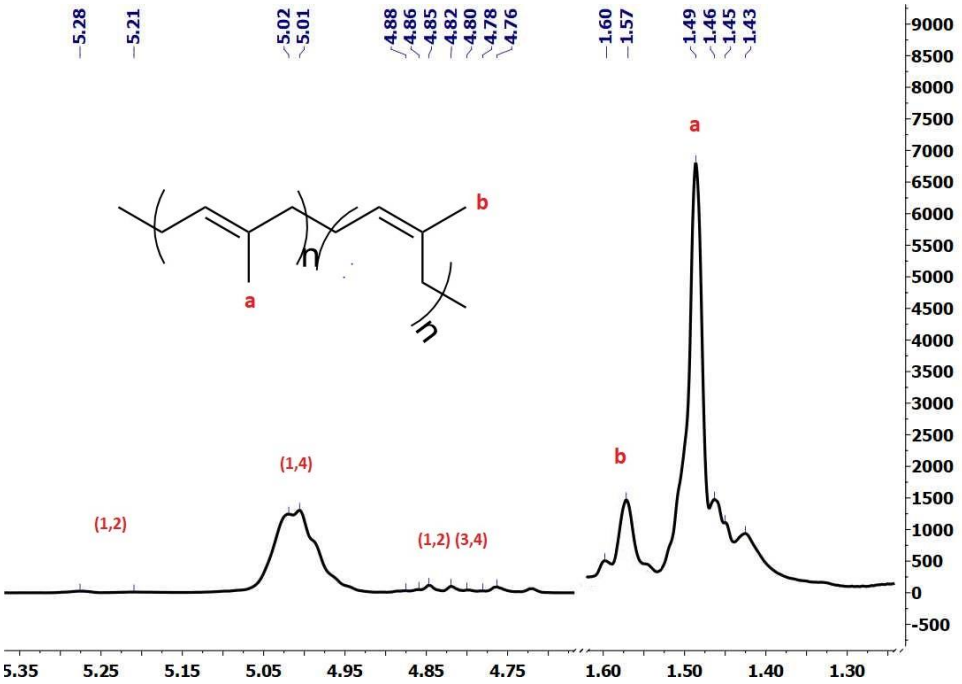

Figure 5.2 400-MHz ^{1}H NMR spectra of grafted PIP

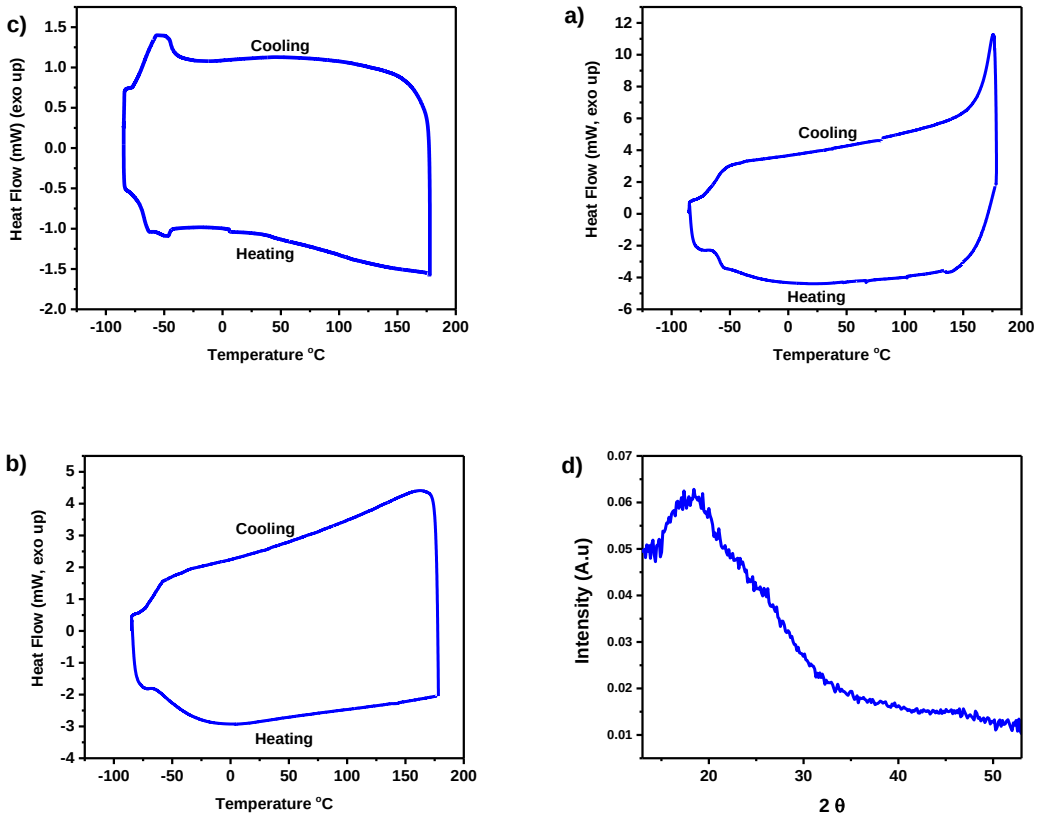

Figure 5.3 a) DSC curve of uncured 75% trans-free PIP as a function of temperature from -85 to 170 °C, b) DSC curve of uncured 75% trans-free PIP as a function of temperature from -85 to 170 °C, c) DSC curve of matrix free as a function of temperature from -85 to 170°C, d) X-ray diffraction spectra of 40-g-Silica in 75% Trans (40T) composite.

Trans -1,4-polyisoprene (TPI) is a semi-crystalline polymer. Previous work done by Boochathum et al. showed that carbon-carbon crosslinks were observed to reduce the crystallinity of NR and TPI.[22] For the present work, dicumyl peroxide was used as the curing agent. It's well known crystallinity is one of the most important parameters that affect many physical and chemical properties of polymers, including 75% trans-PIP.[31] Figures 5.3-a and b, show the DSC's of both uncured and cured free 75% trans-PIP, and Figure 5.3-c shows cured trans PIP-*g*-

NPs' of 40% wt of silica. All showed no evidence of crystallization in either the heating or cooling cycles even with a high content of TPI.[32] Furthermore, the WAXS data were plotted using Bragg's law between (2Θ) and intensity and are shown in Figure 5.3-d, for a sample of mixed TPI grafted NPs and free TPI. There was no evidence of crystallinity in the composite similar to that expected for NR and its composites.[33–35]

In general, the state of inorganic filler dispersion and interactions with rubber matrix is the influence that contributes to improving the mechanical properties of the elastomeric composites. Therefore, the morphology of the PIP composites at 20 % wt silica loading was studied by TEM. Figure 5.4 shows the presence of large spherically shaped silica particle aggregates in the PIP matrix filled with untreated silica. Some particles with spherical structure with a dimension of few nm can be found. The size of the individual SiO_2 particles is 15 nm, whereas the large silica aggregates are of 200–1000 nm size in the trans-PIP matrix. However, a reduction in the agglomeration as well as in the size of clusters is observed in the cis-PIP matrix. Contrary to this finding, the grafted silica NPs showed a huge reduction in the agglomeration in both matrices. In grafted NP nanocomposites, smaller clusters were observed (100-200 nm) in the trans-PIP matrix. Remarkably, a reduction in cluster size and agglomeration much more noticeable in the cis-PIP matrix system, where the distribution of

silica particles was found to be more uniform. We believe that the better dispersion of the trans-PIP grafted NPs in the cis-PIP matrix was affected by the relative molecular weights of the grafted polymer (35k g/mol) and cis-PIP matrix (40k g/mol), despite the different in polymer configurations. The larger agglomerations observed in the trans-PIP grafted NPs in the trans-PIP matrix can be ascribed to the larger mis-match in molecular weights (35k g/mol vs. 52k g/mol, respectively). We have shown previously that the ratio of grafted chain length to matrix chain length plays a major role in determining the dispersion state in polymer nanocomposites, and thus their properties.[16]

Small-angle X-ray scattering (SAXS) was used to obtain more information on the particle dispersion state of the crosslinked samples (Figure 5.5). No agglomeration was detected from the X-ray scattering pattern at low q.[11] The intensity of all the peaks were relatively weak, indicating a broad distribution of interparticle spacing. The location of the peak did not change much between the crosslinked samples, which corresponded to a d spacing approximately between 16-19 nm, which seems reasonable considering the grafted PIP molecular weight of 35k with low grafting density. However, the bare particles tested with 20 % wt did not show any agglomeration below 200 nm, but the d-spacing curve was lower than grafted samples. 20BT sample showed severe agglomeration under TEM while 20CB showed severe clusters under TEM with sizes more than 100nm

and neither could be detected by SAXS. The 40, 60 % wt, and matrix free samples all showed the same peak position. It was also observed that all grafted and bare particles did not show the agglomeration.

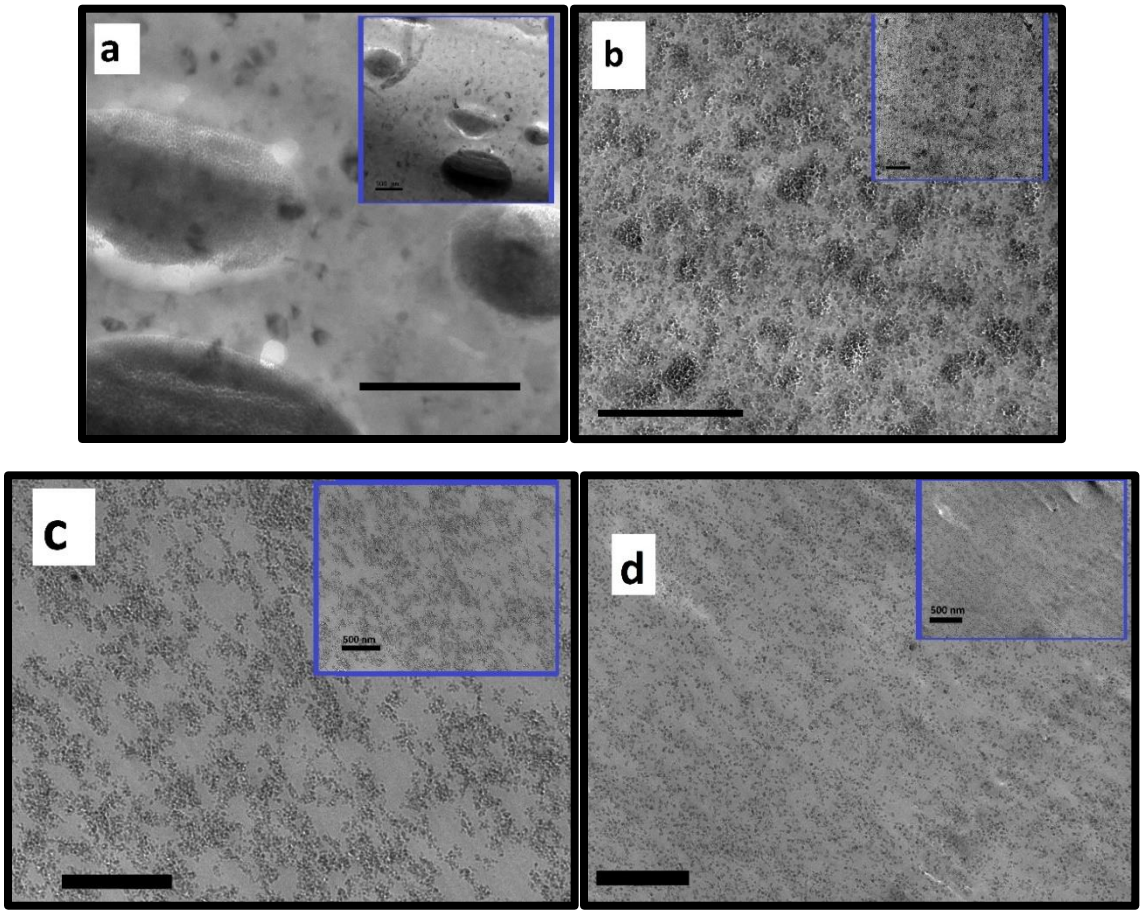

Figure 5.4 a) TEM images of PIP nanocomposites with 20 % wt SiO_2 loading, a) bare NPs in trans-PIP matrix, b) bare NPs in cis-PIP matrix, c) 35k-g-SiO_2 (0.035 ch/nm^2) in trans-PIP matrix, d) 35k-g-SiO_2 (0.035 ch/nm^2) in cis-PIP matrix, (scale bar in all images 500 nm).

The reinforcement effect expected by silica in rubber nanocomposites was investigated through the application of the modified Guth-Gold equation, which describes the enhancement in Young's modulus of the composites and is shown in Figure 5.6.[37]

$$\frac{Ec}{Eo} = 1 + 2.5\varphi + 14.1\varphi^2 \ldots\ldots\ldots\ldots (1)$$

Where E_c and E_o are the tensile modulus of the filled and unfilled composites respectively. E_c/E_o is termed as the modulus enhancement and φ is the calculated volume fraction of silica in the filled composite. The mechanical properties of all nanocomposites were improved by increasing the silica loading in both matrices compared to unfilled and bare NPs samples. By using the calculations of volume fraction of silica in the nanocomposite the expected plotted data for every composite was obtained using the calculated values in modified Guth-Gold equation. Next, experimental data was taken from the stress-strain curve and divided by the Young's modulus of the unfilled rubber individually for cis-PIP and trans-PIP. The values for each set are plotted against the corresponding volume fraction of silica. The experimental data of modulus enhancement (E_c/E_o) were close to the expected data for cis-PIP nanocomposites, while the trans-PIP matrix was all lower than that of theoretical expectations. Consequently, the silica volume fraction φ is about 0.076, 0.18, and 0.33 for each set of samples (20, 40, 60 % wt), respectively, and 0.5 for the matrix free sample. This shows that the treatment of silica enhances the Young's modulus of the cis-PIP composites only, while the influence of PIP-g-SiO_2 samples are much greater than that of bare NPs in both matrices. Surprisingly, the modulus of matrix free

sample was 6 times greater than expected due to the high entanglement of the grafted polymer in addition to the high silica loading.

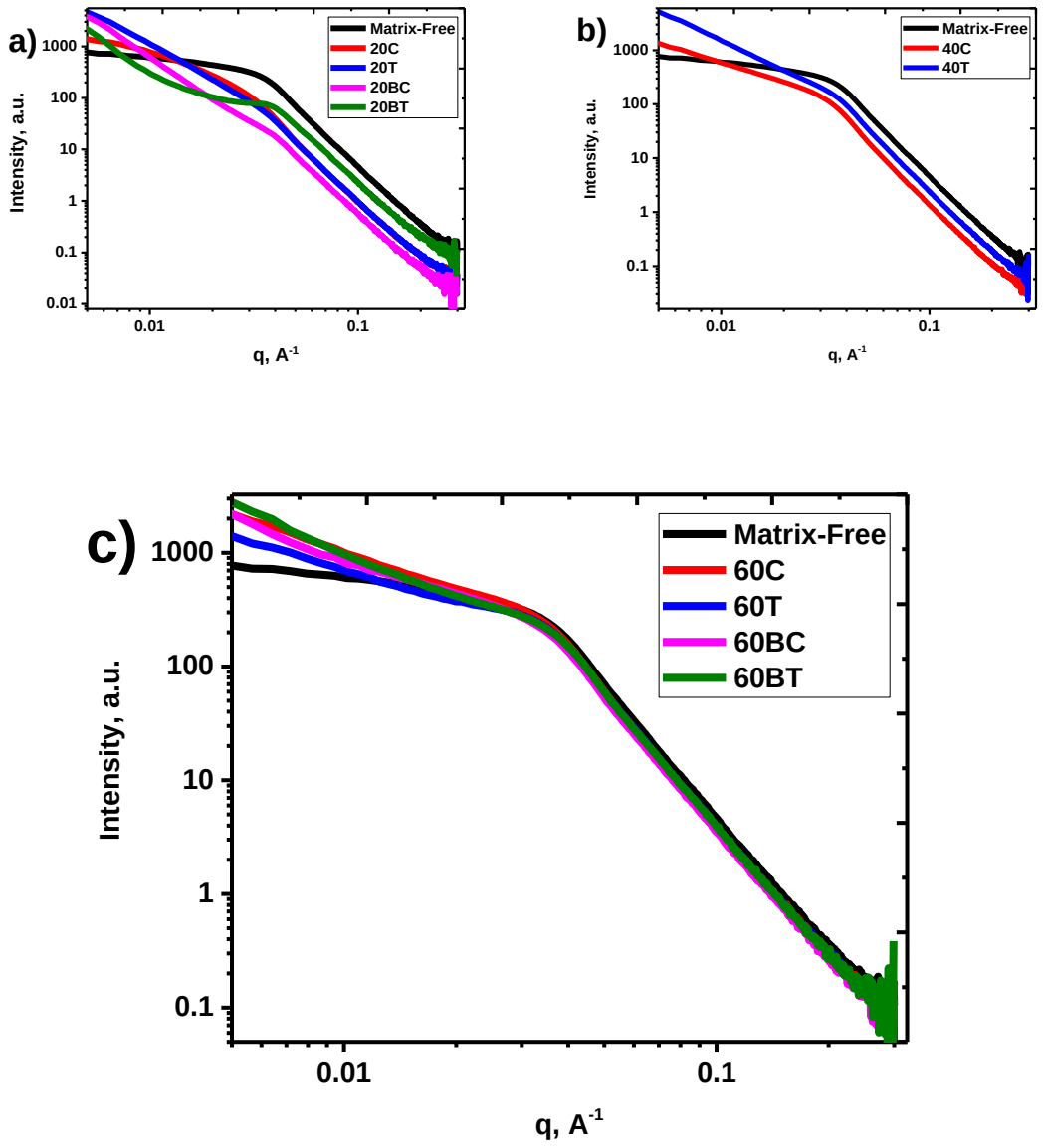

Figure 5.5 Representative small-angle X-ray scattering (SAXS) intensity curves for matrix- free PIP and in matrix nanocomposites.

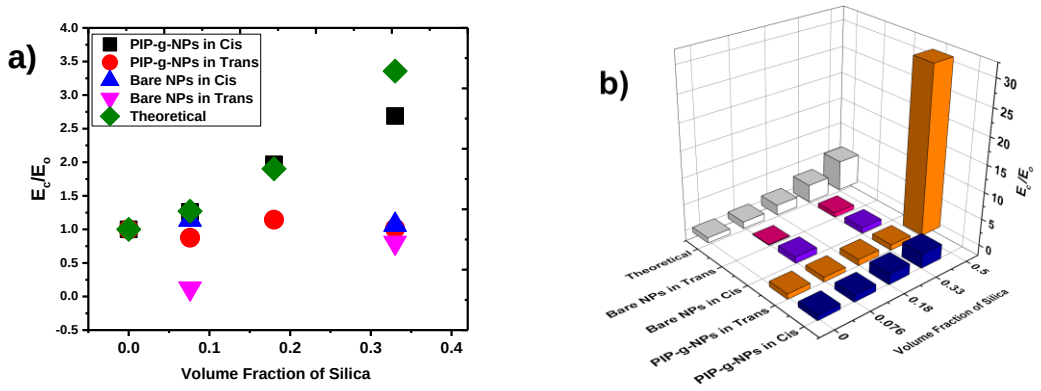

Figure 5.6 Plots of modulus enhancement (Ec/Eo) versus volume fraction (φ) for both theoretical and experimental results for each sample.

The tensile strength and elongation at break of the inorganic fillers effect on different PIP properties of the NP filled systems were analyzed for the matrix free, cis-PIP and trans-PIP matrix blends. Figure 5 (a, b, and c) shows that the tensile strength of the matrix free sample was severed times greater than the free polymers. This outcome was expected since higher silica loading usually leads to higher tensile strength.[26] In addition, the nanoparticle grafted polymer with no free matrix should be highly entangled. The addition of the PIP-g-SiO_2 to the cis-PIP and trans-PIP matrices improves the properties proportionally with the increase in silica loading as compared to the free polymer.[17] The grafted NP filled composites also showed improved properties as compared to the filled composites using ungrafted base silica, even at identical core silica loading levels of 20, 40 and 60 wt%. In addition to the individual stress-strain curves shown in Figure 5.7 (a,b and c), the comparisons for elongation-at break and tensile stress for all samples are analyzed in Figure 5.7 (d and e).[38] One more characteristic

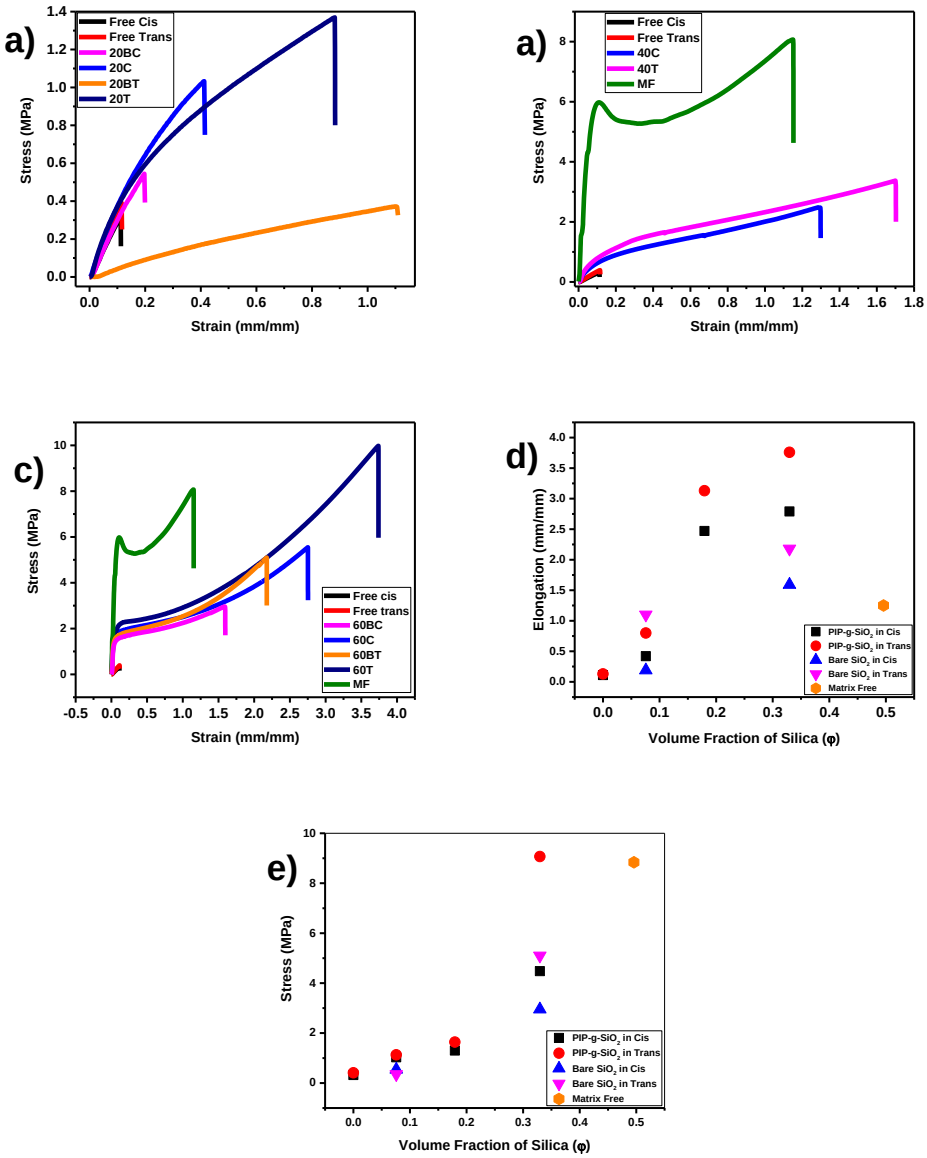

Figure 5.7 a) Stress-strain curves of unfilled and filled composites with 20 wt% silica loading. b) Stress-strain curves of unfilled and filled composites with 40 wt% silica loading. c) Stress-strain curves of unfilled and filled composites with 60 wt% silica loading. d) Elongation at break vs silica volume fraction for all the samples. e) Tensile stress vs silica volume fraction for all the samples.

important to mention is the matrix compatibility to the grafted polymer. For the trans-PIP matrix, the grafted PIP and matrix PIP were both made via RAFT polymerization, and the microstructure of chains was almost identical. When this

characteristic is selectively compared at all the loadings levels, the grafted trans-PIP NPs in trans-PIP matrix always produced high elongation at break and tensile stress than the grafted trans-PIP in cis-PIP matrices. An unexpected property was observed in the behavior of the matrix free composite which exhibited a very high yield point and stress at break. In contrast, the samples containing free polymer matrix showed higher elasticity and lower yield points. Only the 60 % g silica in trans sample showed higher stress at break than the matrix free sample.

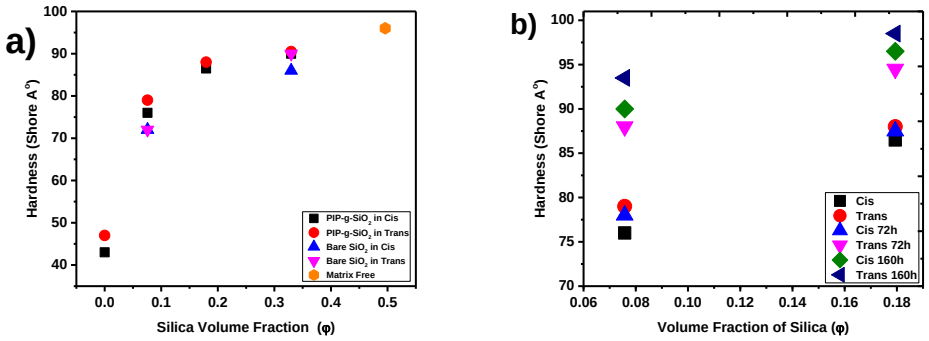

Figure 5.8 a) Hardness vs silica volume fraction for all the samples. b) hardness of 20 wt% and 40 wt% samples after aging at 100°C for 72 h and 160h

Figure 5.8 (a) shows the results of hardness testing, which generally show an increase in surface hardness with an increase of silica loading in the composites.[39] The improvement was expected due to the presence of the silica nanoparticles. However, the trans-PIP samples showed higher values than the cis-PIP matrix samples. Two sets of samples (20 and 40 wt%) were tested for the

effects of thermal aging shown in Figure 5.8(b). A change in the hardness values increased with increasing silica loading, which can be attributed the loss of the crosslinking network upon thermal aging. The reversion process led to make the rubber physically weaker and losing the mechanical performance of the rubbery material.[40]

Dynamic mechanical behavior (DMA) of the PIP nanocomposites were studied from (-80 to 50° C) at constant strain and frequency. The DMA results support the general reinforcement character of the NPs filled systems, as observed in the stress–strain study. Figure 5.9 (a, b) show the temperature dependence of storage modulus (E′) and exhibit an increase in storage modulus in both the glassy and the rubbery plateau regions of the filled composites relative to the unfilled matrices which scaled with the filler loading level.[17,39] A comparison has can be made between storage modulus of both matrices at 25° C. Figure 5.9 (c) shows the general trends in the storage modulus with increasing silica volume fraction. This effect was enhanced by compatibility of the grafted trans-PIP chains with the trans-PIP matrix as compared to the grafted trans-PIP chains with cis-PIP matrix.

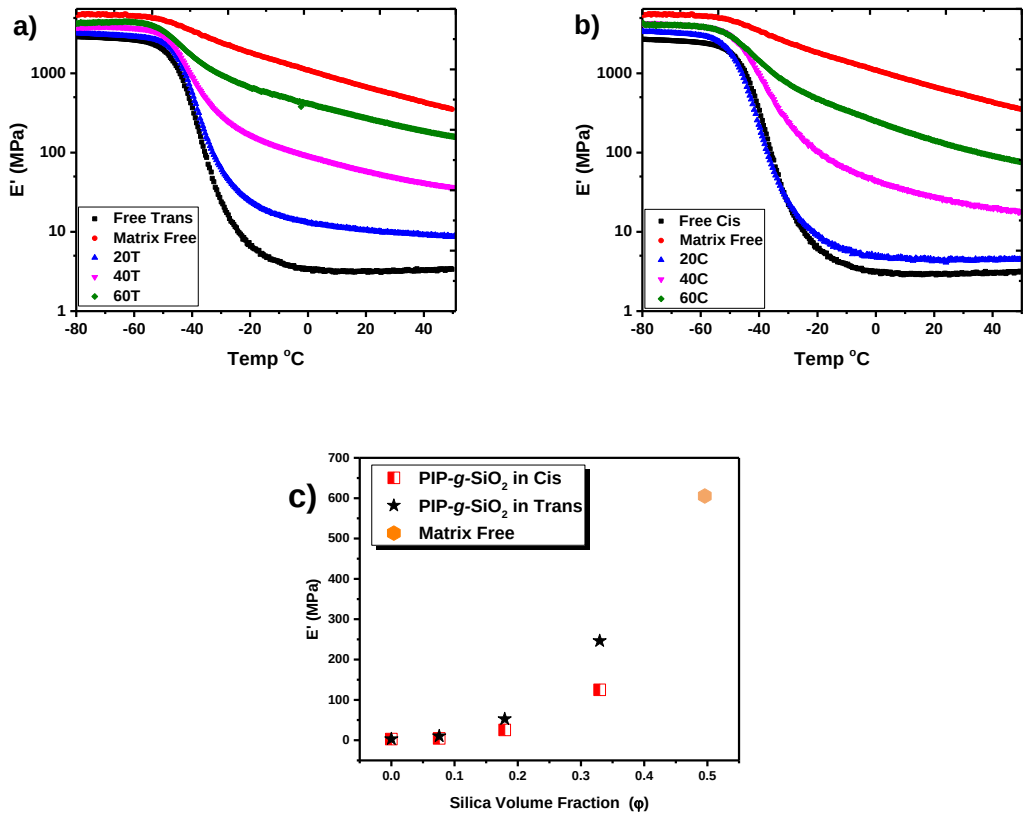

Figure 5.9 a, b) Storage modulus diagram of unfilled and filled composites with increasing in silica loading in both cis and trans matrices. c) Storage modulus at 25°C.

It's well known that the more free volume of polymer, the more easily polymer chains can move and with different physical conformations.[41] Therefore, damping properties of the materials which are related to the free volume change are investigated also for PIP samples through examination of both matrices by dynamic mechanical analysis to calculate the height and width of tan δ curves. The tan δ values decrease when the free volume change becomes smaller. In the transition region from glassy to rubbery phase, the increase of particle volume fraction will reduce the height of tan δ peaks which is observed for both sets of

samples shown in Figure 5.10 (a and b). Additionally, it could be expected that

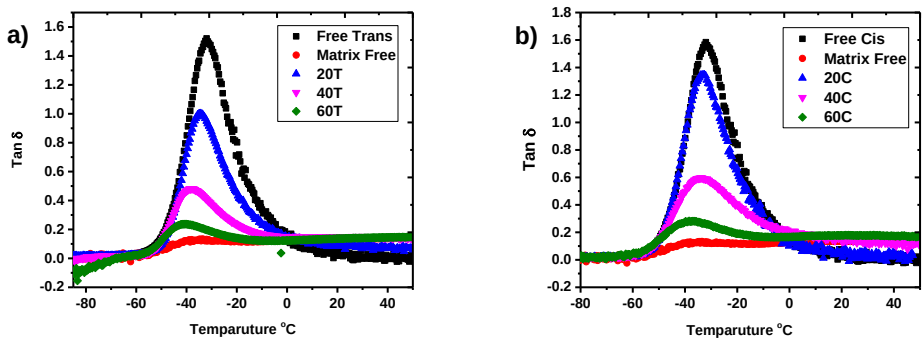

Figure 5.10 a, and b) Tan δ diagram of unfilled and filled composites with increasing in silica loading in both cis and trans matrices.

confining the rubber segment movement by anchoring them to rigid particle surfaces through the grafted polymer will decrease the free volume of the final composite. Thus, in the extreme limit where all chains are anchored to the NPs, the matrix free sample showed the smallest tan δ peak due to high entanglement with high loading and very low free volume.[39] The shifting of T_g to lower temperature and broader peak width could be attributed to the different dispersion state of the inorganic particles, could create many different environments and mobilities for the chain segments. Thus, the energy needed to mobilize the polymer chains will be broader, resulting in a broader distribution of tan δ values.[42]

5.5 Conclusion

The present study was designed to investigate the influence of PIP grafted silica nanoparticles as inorganic fillers on the properties of elastomer based on cis-PIP and trans-PIP matrices. Even though TPI is reported as a semi crystalline polymer, no evidence of crystallinity was detected in the cured samples and we concluded that the crosslinking destroyed any crystallinity that might have been present prior crosslinking. NMR studies showed the PIP produced by the RAFT polymerization of isoprene was 95% 1,4 addition with approximately 75% trans content. The dispersion state of the grafted NPs in both cis-PIP and trans-PIP was controlled by two main factors, the ratio of grafted chain length to the matrix chain length and the compatibility of the grafted trans-PIP isomer with the trans-PIP matrix. Generally, the mechanical properties increased with the silica loading level and showed the largest increases when particles were well dispersed, and the two factors mentioned above were optimized for compatibility and chain entanglement. In all cases, the grafted NP composites were improved compared to the ungrafted bare silica composites, even when compared an identical core silica loading levels. The matrix free grafted NP composites showed exceptional mechanical properties and could be useful in specialty applications. These strong, tough composite materials could be useful in many applications that require improved properties over conventional silica rubbers.

5.6 References

(1) *Handbook of Composites from Renewable Materials Volume 8: Nanocomposites: Advanced Applications*; Thakur, V. K., Thakur, M. K., Kessler, M. R., Eds.; John Wiley & Sons, Incorporated, 2017.

(2) Wolf, H.; Ralph, W. *Rubber - A Story of Glory and Greed*; New York, 1936.

(3) Harp, S. L. *A World History of Rubber: Empire, Industry, and the Everyday*; 2016.

(4) Heinrich, G.; Kluppel, M.; Vilgis, T. A. *Curr. Opin. Solid State Mater. Sci.* **2002**, *6*, 195–203.

(5) Polmanteer, K. E. *Rubber Chemistry and Technology*. 1975, pp 795–809.

(6) Samaržija-Jovanović, S.; Jovanović, V.; Marković, G.; Zeković, I.; Marinović-Cincović, M. *Sci. World J.* **2014**, *2014*, 9.

(7) Liu, X.; Wang, T.; Chow, L. C.; Yang, M.; Mitchell, J. W. *Int. J. Polym. Sci.* **2014**, *2014*, 1–8.

(8) Baboo, M.; Dixit, M.; Sharma, K.; Saxena, N. S. *Int. J. Polym. Mater.* **2009**, *58* (12), 636–646.

(9) *Handbook of Composites from Renewable Materials Volume 7: Nanocomposites: Science and Fundamentals*; Thakur, V. K., Thakur, M. K., Kessler, M. R., Eds.; John Wiley & Sons, Incorporated, 2017.

(10) Khani, M. M.; Abbas, Z. M.; Benicewicz, B. C. *J. Polym. Sci. Part A Polym. Chem.* **2017**, 1–9.

(11) Zheng, Y.; Abbas, Z. M.; Sarkar, A.; Marsh, Z.; Stefik, M.; Benicewicz, B. C. *Polymer (Guildf).* **2018**, *135*, 193–199.

(12) Perrier, S.; Takolpuckdee, P.; Mars, C. A. *Macromolecules* **2005**, *38* (6), 2033–2036.

(13) Benicewicz, B.; Wang, L.; Mohammadkhani, M. Butadiene-derived polymers grafted nanoparticles and their methods of manufacture and use, U.S. Patent 9, 249, 250, February 6, **2016**.

(14) Li, C.; Benicewicz, B. C. *Macromolecules* **2005**, *38* (14), 5929–5936.

(15) Moad, G. *Polym. Int.* **2017**, *66* (1), 26–41.

(16) Akcora, P.; Liu, H.; Kumar, S. K.; Moll, J.; Li, Y.; Benicewicz, B. C.; Schadler, L. S.; Acehan, D.; Panagiotopoulos, A. Z.; Pryamitsyn, V.; Ganesan, V.; Ilavsky, J.; Thiyagarajan, P.; Colby, R. H.; Douglas, J. F. *Nat. Mater.* **2009**, *8* (4), 354–359.

(17) Kumar, V.; Hanel, T.; Giannini, L.; Galimberti, M.; Giese, U. *KGK Kautschuk Gummi Kunststoffe* **2014**, *67* (10), 38–46.

(18) Janeczek, H. *J. Polym. Sci. Part A Polym. Chem.* **2006**, *44* (3), 1086–1092.

(19) Nazhat, S. N.; Parker, S.; Riggs, P. D.; Braden, M. *Biomaterials* **2001**, *22* (15), 2087–2093.

(20) Nazhat, S. N.; Parker, S.; Patel, M. P.; Braden, M. *Biomaterials* **2001**, *22* (17), 2411–2416.

(21) Fetters, L. J. *J. Res. Notional Bur. Stand. - A. Phys. Chem.* **1966**, *70A* (5), 421–433.

(22) Boochathum, P.; Chiewnawin, S. *Eur. Polym. J.* **2001**, *37* (3), 429–434.

(23) GERMACK, D. S.; WOOLEY, K. L. *J. Polym. Sci. Part a-Polymer Chem.* **2007**, *45*, 4100–4108.

(24) Jitchum, V.; Perrier, S. *Macromolecules* **2007**, *40* (5), 1408–1412.

(25) Tutorsky, I. A.; Shumanov, L. A.; Dogadkin, B. A. *Polymer (Guildf).* **1968**, *9*, 413–418.

(26) Huang, Y.; Zheng, Y.; Sarkar, A.; Xu, Y.; Stefik, M.; Benicewicz, B. C. *Macromolecules* **2017**, *50* (12), 4742–4753.

(27) Rajan, R.; Varghese, S.; George, K. E. *Prog. Rubber, Plast. Recycl. Technol.* **2012**, *28* (4), 201–220.

(28) Boochathum, P.; Prajudtake, W. *Eur. Polym. J.* **2001**, *37*, 417–427.

(29) Sato, H.; Tanaka, Y. *J. Polym. Sci. Polym. Chem. Ed.* **1979**, *17* (11), 3551–3558.

(30) Chen, H. Y. *Anal. Chem.* **1962**, *34* (13), 1793–1795.

(31) Kavesh, S.; Schultz, J. M. *Polym. Eng. Sci.* **1969**, *9* (6).

(32) Anandakumaran, K.; Kuo, C. C.; Mukherji, S.; Woodward, A. E. *J. Polym. Sci.* **1982**, *20*, 1669–1676.

(33) Zhou, W.; Meng, L.; Lu, J.; Wang, Z.; Zhang, W.; Huang, N.; Chen, L.; Li, L. *Soft Matter* **2015**, *11* (25), 5044–5052.

(34) Rabiej, S.; Wlochowicz, A. *Die Angew. Makromol. Chemie* **1990**, *175* (1), 81–97.

(35) Venkatanarasimhan, S.; Dhamodharan, R. *Polym. Bull.* **2015**, *72* (9), 2311–2330.

(36) Rahman, I. A.; Jafarzadeh, M.; Sipaut, C. S. *Ceram. Int.* **2009**, *35* (5), 1883–1888.

(37) Guth, E. *J. Appl. Phys.* **1945**, *16* (1), 20–25.

(38) Maillard, D.; Kumar, S. K.; Fragneaud, B.; Kysar, J. W.; Rungta, A.; Benicewicz, B. C.; Deng, H.; Brinson, L. C.; Douglas, J. F. *Nano Lett.* **2012**, *12* (8), 3909–3914.

(39) Kapgate, B. P.; Das, C.; Basu, D.; Das, A.; Heinrich, G. *J. Elastomers Plast.* **2015**, *47* (3), 248–261.

(40) Sathi, S. G.; Jang, J. Y.; Jeong, K. U.; Nah, C. *J. Appl. Polym. Sci.* **2016**, *133* (42), 1–14.

(41) Vallée, R. A. L.; Cotlet, M.; Van Der Auweraer, M.; Hofkens, J.; Müllen, K.; De Schryver, F. C. *J. Am. Chem. Soc.* **2004**, *126* (8), 2296–2297.

(42) Jovanović, V.; Budinski-Simendić, J.; Milić, J.; Aroguz, A.; Ristić, I.; Prendzov, S.; Korugic-Karasz, L. *ACS Symp. Ser.* **2010**, *1061*, 167–193.

CHAPTER 6

CONCLUSION AND FUTURE WORK

6.1 Conclusion

Reversible addition-fragmentation chain transfer (RAFT) polymerization was used for the grafting of polydienes chains to the surface of silica nanoparticles to allow for the control over the nanoparticle dispersion, grafted brush entanglement, brush graft density, and brush molecular weight, thus controlling the interface between the particles and the polymer matrix. The interface between silica and a rubber matrix was controlled via the development the grafted rubbery polymeric chains on 15 nm silica surfaces to obtain dispersed NPs in polymer nanocomposites. We studied the chemistry of surface-initiated RAFT polymerization of several 1,3-diene monomers derivatives grafted from silica NPs. Trithiocarbonate RAFT agents were used to be attached to the surface of silica NPs with controlled graft density, and controlled radical polymerizations were conducted to produce a surface grafted polymer of predetermined molecular weight and relatively narrow PDI. The polymerization kinetics were studied, and it was found that the grafting-from polymerization rate was dependent on the graft density. The experiments revealed that the SI-RAFT polymerization of isoprene from particles proceeded with a higher rate when compared to polymerization mediated by free RAFT agent and proceeded at higher rates as the surface density of the RAFT agent increased. However, this behavior was reversed for chloroprene, i.e., the polymerization was slower on

particles than free RAFT agent mediate polymerization and proceeded at slower rates as the surface density of the RAFT agent increased. Polymer grafted silica NPs were directly crosslinked to form matrix-free nanocomposites that showed uniform particle dispersion and improved mechanical properties than unfilled crosslinked polymer. These strong, sturdy composite materials could be useful in many applications. The molecular weight of polymer chains was also shown to be crucial in the dispersion of particles throughout the matrix-free nanocomposite. Also, the matrix-free composite SAXS data showed that as the molecular weight of the grafted chains on silica particles was increased the d-spacing between particles also increased. Nanocomposites with high silica loading exhibit higher tensile stress and storage modulus but occurred with a decrease in the final composite elongation. Also, the dispersion of particles was analyzed by TEM and displayed a good state of dispersion for the particles.

The polymerization of 2,3-dimethyl butadiene, DMB, was also done as part of investigations of diene-type monomers, and its behavior was similar to isoprene as the polymerization rate mediated by free RAFT agent was higher than the polymerization rate on silica nanoparticles. Matrix-free nanocomposites were prepared by curing the grafted chains and showed good improvement as compared to the unfilled crosslinked matrix. The dispersion of nanoparticles was

also studied by TEM and SAXS which was influenced by polymer molecular weight and chain density of the grafted polymer.

The PCP-g- SiO2 NPs were disperse a in commercially available PCP matrix. Significant improvements were revealed from mechanical studies on the crosslinked composites. Dynamic mechanical analysis showed increases in the storage modulus in the rubbery state for the silica filled samples compared with the unfilled crosslinked matrix. In addition to the mechanical testing results, TEM and SAXS results suggested that excellent nanoparticle dispersion could be achieved with the proper grafting characteristics. Partial nanoparticle aggregation existed with low molecular weight grafted chains due to phase separation. Also, the low graft density particles showed a lower level of dispersion due to core-core attractions, which could be potentially improved by using a bimodal polymer grafting architecture.

PIP-g-SiO2 NPs were also dispersed in commercially available cis-PIP, and a PIP matrix synthesized by free RAFT polymerization (75% trans). The difference in the mechanical properties was apparent due to miscibility of grafted polymer with the trans-PIP matrix because of the similarity of the macrostructure of grafted and matrix polymeric chains. Thus, the tensile stress, strength and storage modulus were all higher in composites made using the trans-PIP matrix.

The particle dispersion was shown by TEM and SAXS to be approximately equivalent for both the cis-PIP and trans-PIP matrices.

6.2 Future Work

Publications concerned with the mechanism of surface-initiated RAFT polymerization of diene monomers is limited. The behavior of polymerizations mediated by free RAFT and SI-RAFT with different densities could be further studied and compared with RAFT polymerizations of styrenic and acrylic monomers to investigate the widely varying polymerization rates between free RAFT and SI-RAFT polymerizations. One suggestion for the future work is to investigate the RAFT polymerization of other substituted diene monomers to understand the mechanism of their RAFT polymerization. A more detailed study of the effects of electron donating and withdrawing groups of dienes on the polymerization rate and the radical stability of the RAFT agent could be valuable.

In addition to that, the grafted polydiene have a lot of potential in reinforced rubber nanocomposites where the dispersion and the compatibility of nanoparticles are essential factors in achieving targeted properties. However, most of the industrial rubber materials are high molecular weight polymers. Different molecular weights should be synthesized by varying the polymerization conditions to accomplish the desired matching between the

grafted polymer, and these matrices, since based on previous findings brush molecular weight needs to be matched with the matrix molecular weight. This is a challenge that can be addressed in the future for more practical applications.

The silica surface influences particle agglomeration due to the particle-particle interaction. Moreover, due to enhanced chain entanglement and better mechanical properties when using low graft density brushes, bimodal architectures with short brushes and high graft density should be explored as this could eliminate particle-particle interaction to achieve better dispersion. However, the mechanical properties of PCP showed an unexpected behavior of the Payne effect due to multiple factors that influence the nanocomposite entanglement but were complicated by the particulates present in the curing additives. For future direction, Payne effect studies could be repeated with a non-metal oxide curing process to investigate the real effects of grafted NPs on rubber nanocomposites.

Post-modification of the diene polymers, via hydrogenation of the grafted polymers can produce polyolefin grafted nanoparticles. The hydrogenation of substituted diene polymers will provide a variety of substituted olefins grafted onto NPs. The controlled radical polymerization of different monomers in sequence could lead to AB block copolymers with mono and disubstituted

dienes. Such rubbery block copolymers (both olefinic and hydrogenated) appear to be almost completely unexpected in the literature